

# Quantum phase transitions in the shapes of atomic nuclei

Pavel Cejnar

*Institute of Particle and Nuclear Physics, Faculty of Mathematics and Physics, Charles University, V Holešovičkách 2, 180 00 Prague, Czech Republic*

Jan Jolie

*Institute of Nuclear Physics, University of Cologne, Zùlpicher Strasse 77, 50937 Cologne, Germany*

Richard F. Casten

*Wright Nuclear Structure Laboratory, Yale University, New Haven, Connecticut 06520, USA*

(Published 5 August 2010)

Signatures of criticality in the evolution of the nuclear ground-state shapes across the  $N \times Z$  plane are discussed. Attention is paid to specific data indicating sudden structural changes in various isotopic and isotonic chains of medium-mass and heavy even-even nuclei, as well as to diverse theoretical aspects of the models used to describe these changes. The interacting boson model and the geometric collective model, in particular, are discussed in detail, the former providing global predictions for the evolution of collective observables in nuclei between closed shells and the latter yielding a parameter-efficient description of nuclei at the critical points of shape transitions. Some issues related to the mechanism of first- and second-order quantum phase transitions in general many-body systems are also outlined.

DOI: [10.1103/RevModPhys.82.2155](https://doi.org/10.1103/RevModPhys.82.2155)

PACS number(s): 21.60.Ev, 21.60.Fw, 21.10.Re, 64.70.Tg

## CONTENTS

I. Introduction	2155	C. Quasidynamical symmetries	2184
II. Evolution of Nuclear Structure	2156	V. Shape Transitions in the Geometric Models	2186
A. Theoretical underpinning	2157	A. Critical-point solutions	2186
B. Empirical observables	2158	1. The X(5) critical-point solution	2187
1. Energies of $2_1^+$ and $4_1^+$ states	2158	2. Empirical manifestations of X(5)	2189
2. $E2$ transition strengths	2161	3. The E(5) critical-point solution	2193
3. Two-neutron separation energies	2161	4. Other critical-point solutions	2194
4. Other observables	2162	5. Extension to odd- $A$ nuclei	2194
C. Microscopic considerations	2163	B. Calculations away from critical points	2195
III. Models for Shape Transitions	2166	VI. Further Developments	2196
A. Geometric collective model	2166	A. Extensions of models	2197
1. Bohr Hamiltonian and its phase structure	2166	1. Simple treatment of triaxial shapes	2197
2. Separable and quasiseparable potentials	2168	2. Nonquadrupole degrees of freedom	2198
B. Interacting boson model	2169	3. Coupled boson-boson and boson-fermion systems	2199
1. Dynamical symmetries and forms of the Hamiltonian	2170	B. Mechanism of critical phenomena	2202
2. Coherent state formalism and phase transitions	2172	1. Critical-point scaling properties	2202
3. Mapping nuclei onto the symmetry triangle	2174	2. Relation to thermal phase transitions	2203
C. Fermionic approaches	2175	C. Quantum phase transitions for excited states	2205
1. Phenomenological fermion models	2175	VII. Summary	2206
2. Microscopic calculations	2176	Acknowledgments	2207
IV. Shape Transitions in the Interacting Boson Model	2177	References	2207
A. Finite-size precursors of quantum phase transitions	2177		
B. Description of structural evolution in the symmetry triangle	2180		
1. Signatures of first-order phase transitions	2180		
2. Comparison with second-order phase transition	2182		

## I. INTRODUCTION

The study of the evolution of structure in atomic nuclei with changing numbers of their proton and neutron constituents dates back to the early days of the field. It was fundamental, for example, to the development of the shell model with the recognition of magic numbers and inert closed shells. The appearance of certain characteristic excitation spectra in other nuclei led to the

development of early paradigms of collective structure—simple models for spherical nuclei that can vibrate and ellipsoidally shaped nuclei that can both vibrate and rotate—and encouraged study of manifestations of structure intermediate between these idealizations.

Yet the last years have seen major developments in the experimental study of structural evolution with proton, neutron, and mass numbers ( $Z$ ,  $N$ , and  $A$ ), in understanding this phenomenology with simple models, and in seeking its microscopic foundations in nucleonic motion and interactions. Many of these advances are due to, or inspired by, important technological developments in the production and exploitation of exotic nuclei, in the development of more powerful instruments (such as those for the selection of nuclei produced in heavy ion reactions and for their spectroscopy or of trapping devices and storage rings for mass measurements), and in the capacity of modern computers both to handle such data and to facilitate the often increasingly complex theoretical descriptions.

Among the most dramatic developments in recent years are those related to the expansion of our knowledge of these new nuclei, on the one hand, and, on the other hand, the study of regions of rapid structural (shape) change—often drastic changes within a span of a change of only two nucleons—and their description in terms of quantum phase transitions (QPTs). The latter area is the prime focus of this review. The concept of a QPT (sometimes also called zero temperature or ground-state phase transitions) refers to a sudden transformation in the structure of the ground or equilibrium state as a function of some variable.<sup>1</sup> QPTs in atomic nuclei are reflected by rapid structural changes with varying  $N$  or  $Z$ . In general, QPTs are related to (but different from) the more familiar thermodynamic phase changes seen in many macroscopic systems. A key issue that we address is the implications for nuclear QPTs arising from the fact that nuclei are finite systems whereas the idea of phase transitions is traditionally reserved for infinite systems.

This review has the following structure: We start in Sec. II with an empirical overview of nuclear structure and its evolution in terms of simple nuclear models and the most useful observables. This is followed by an outline of the microscopic underpinnings of the development of collectivity and deformation. Section III introduces basic quantitative approaches to treat shape transitions in nuclei: the geometric model, the interacting boson model, and some microscopically oriented

techniques. Attention is then mostly focused on the first two models. Section IV discusses the evolution of collective behavior within the interacting boson model and Sec. V deals with the geometric model. While the attention in Sec. IV is focused on finite-size precursors of nuclear shape-phase transitions and on the definition of phases in terms of symmetries, in Sec. V we look more closely at the critical point itself, introducing specific approximate critical-point solutions of the geometric Hamiltonian, particularly the models known as X(5) and E(5) for first- and second-order spherical-deformed phase transitions, respectively (Iachello, 2000, 2001). In all cases, predictions of the models are compared with available experimental data. Section VI extends the discussions to more exotic types of transitions and more sophisticated models. This section also contains discussions of common aspects of nuclear phase transitions which may be relevant in general many-body systems. The last section provides a summary.

It needs to be stressed that in this review we aim mostly at *macroscopic* models of nuclear collective dynamics. Microscopic approaches to shape transitions represent a principal subject of nuclear-structure physics, addressed in a large number of studies (some of them cited below), but are not of our primary concern here. With few exceptions, nearly all the discussions will deal with even-even nuclei. Similar ideas apply to odd- $A$  species but have been much less studied experimentally and much less worked out theoretically.

Our focus here is on the conceptual underpinnings of QPTs and structural evolution in nuclei rather than attempting a complete cataloging of all experimental and theoretical results. In this regard note that there have been several other recent reviews by Casten (2006, 2009), Casten and McCutchan (2007), and Cejnar and Jolie (2009) to which we refer the interested reader for a detailed discussion of such results.

## II. EVOLUTION OF NUCLEAR STRUCTURE

An important challenge of nuclear structure physics is to map out the evolution of structure with nucleon number and to understand this phenomenology both microscopically and macroscopically. Microscopically, one deals with nucleon degrees of freedom and their interactions. Current microscopic nuclear theory is in the midst of a renaissance due to the advent of immensely growing computing power. There is a roadmap for future progress, centered around such concepts as effective field theory (Epelbaum *et al.*, 2009) and the use of density functional theory (Bender *et al.*, 2003; Stoitsov *et al.*, 2003, 2007). Yet, a detailed understanding of nuclear structure as a function of  $N$ ,  $Z$ , and  $A$  is still well in the future. Even if such a goal is achieved, collective model approaches, which express structure directly in terms of the many-body degrees of freedom, symmetries, and their associated quantum numbers, provide an invaluable and complementary perspective.

It is our task in this section to give an overview of how the structure of even-even nuclei evolves. To set the

<sup>1</sup>The term quantum phase transition originates from condensed-matter physics, where it was introduced for transitions between specific ordered and disordered phases (like ferromagnetic and paramagnetic states of a spin-lattice system) driven by a varying interaction strength at zero temperature (Hertz, 1976). Because of vanishing thermal fluctuations, the only motions responsible for the onset of disorder are the quantum fluctuations. Reviews of QPTs in condensed matter physics were given by Sachdev (1999) and Vojta (2003).

stage for the theoretical descriptions that follow we start in Sec. II.A with some remarks on the theoretical modeling of atomic nuclei. This is followed by an extensive look at actual data on structural evolution (Sec. II.B). Of course, the greatest interest will naturally focus on regions of rapid structural change where there is often a competition between various degrees of freedom and where the interplay of microscopic (shell structure) drivers and macroscopic (collective) behavior is often the most crucial. In Sec. II.C we also discuss the microscopic background of structural evolution in a qualitative way.

### A. Theoretical underpinning

Theoretical descriptions of nuclei invariably proceed by a number of simplifications in order to make the task tractable and, often, more physically intuitive. In principle, one would want to derive the structure of nuclei from the interactions of quarks and gluons. In practice, this is a very long term goal. A first approximation is to utilize the concept of nucleons and their interactions. Electron scattering experiments at Jefferson Laboratory (Cardman, 2006) and related calculations have shown that the approximation of treating nuclei in terms of nucleons works well down to surprisingly small distance scales ( $\approx 0.5$  fm) and that the quark-gluon based description is more appropriate at the level of  $\approx 0.1$  fm. The description at the nucleon level is an approximation that nearly all nuclear models adopt and we will also.

So-called *ab initio* models attempt to derive nuclear properties in terms of the free interactions of their constituent nucleons (Pieper *et al.*, 2002; Navrátil *et al.*, 2009). Even so, the many-body problem rapidly becomes intractable with increasing  $A$ , and such approaches are limited to very light nuclei. For heavier nuclei, the full many-body problem can be grossly simplified by assuming a one-body mean field potential, that is, it is assumed in first approximation that all the nucleons conspire to create a single potential in which they orbit independently (of course, for protons, one needs to add the Coulomb force).

Over many years, various refined prescriptions have been adopted to obtain this mean field potential but, basically, it closely resembles a Wood-Saxon shape, that is, a rounded square well that asymptotically goes to zero at a distance of a few femtometers (Heyde, 2004). Such a potential, supplemented by a spin-orbit interaction, naturally gives a clustering of levels of different oscillator and angular momentum quantum numbers. When combined with the Pauli principle, which limits the number of identical nucleons that can fill a given orbit of angular momentum  $j$  to  $2j+1$ , the famous magic numbers are obtained. These correspond to closed shells analogous to the inert gases of atomic structure.

The principal magic numbers coincide with nucleon numbers 2, 8, 20, 28, 50, 82, and 126, with 40 and 64 sometimes serving that role. However, we immediately stress that these traditional benchmarks of structure were originally motivated by the data on nuclei near stability and that an important aspect of the study of

nuclei far from stability in the last years has been the recognition that the magic numbers themselves can and do change as a function of  $N$  and  $Z$  (Janssens, 2005).

While the nuclear independent particle model (IPM) does usually give the correct ground-state spins for odd- $A$  nuclei with a single particle outside closed shells and often also those of low-lying excited states, it faces immediate difficulties when extended to nuclei with more than one “valence” nucleon. Hence follows the well-known need to introduce residual interactions beyond the mean-field potential. That is, we can think in terms of a Hamiltonian of the general form

$$H = H_{\text{IPM}} + H_{\text{resid}}. \quad (2.1)$$

The IPM supplemented by residual interactions is the shell model (Haxel *et al.*, 1950; Mayer, 1950; de-Shalit and Talmi, 1963), which has remained for half a century as the conceptual underpinning of microscopic approaches to nuclear structure. Many choices of  $H_{\text{resid}}$  appear in the literature. Normally they are restricted to two-body interactions, depending on the distance and spin coordinates of the two particles. An essential feature of the residual interactions is a short-range and mostly attractive character.<sup>2</sup> For some purposes, a  $\delta$  function gives a good guide and matches experimental results for nuclei with, say, two valence nucleons of one type. This type of interaction gives rise to fundamental pairing correlations in nuclei. The remaining part of the residual interactions (that of long range) creates correlations of individual nucleons at large distances across the nucleus. It is a consequence of these interactions that collective features emerge in nuclei with an increasing number of nucleons outside a closed shell (Åberg *et al.*, 1990; Nazarewicz, 1992).

When extended to nuclei with large numbers of valence nucleons, each allowed to occupy any of several IPM orbits, the number of configurations for each total angular momentum grows combinatorially, and, consequently, the shell model entails the solution of a Hamiltonian matrix of larger and larger dimensions, rapidly becoming intractable. Today, one can deal with up to about  $10^9$  basis states (multinucleon configurations) using various approximation or Monte Carlo schemes and computational algorithms (Caurier *et al.*, 2005). However, even a nucleus such as  $^{154}\text{Sm}$ , which is far from midshell, has approximately  $3 \times 10^{14}$  states with angular momentum and parity  $L^\pi = 2^+$  if one considers only single active proton and neutron major shells. Such a Hilbert space is totally intractable. Moreover, even if matrices of this size could be diagonalized, it would be extremely difficult to develop a conceptual understanding of the resultant structure since the degrees of freedom would remain those of the nucleons rather than of the many-body ensemble itself.

<sup>2</sup>Note that even an overall attractive force can have repulsive components for some angles between the orbital planes of the two interacting nucleons. This is discussed by Heyde (1989) and Casten (2000).

The emergence of collective observables in complex systems is a crucial problem of many-body physics and of quantum mechanics in general (Omnès, 1992). The shape of a nucleus can be extracted from such observables. Vast empirical evidence shows that the shape plays a major role in the classification of nuclei and their basic excitations. However, it is not obvious how the shape observables can be incorporated into the microscopic theory. This has given rise to generations of macroscopic models based on a purely geometric description of shapes or on some more refined types of symmetry in the nucleus. Free parameters contained in these models are adjusted in applications to specific nuclei, which opens the way to describing shape evolution across the nuclear chart by means of varying properties of the ground state and low-lying excited states with the model parameters. This is how the idea of the quantum phase transition enters the field. Much of our discussion in later sections will be couched in terms of these approaches.

## B. Empirical observables

Before entering into a detailed discussion of phase-transitional behavior, it is important to develop a feeling for the data that needs to be understood and we therefore turn to an overview of nuclear structural evolution from an empirical standpoint, cast in terms of very simple models (Casten, 2000). We first discuss a few key observables that will appear many times in what follows. Unless otherwise indicated, the data are taken from the Nuclear Data Sheets.

### 1. Energies of $2_1^+$ and $4_1^+$ states

In even-even nuclei the ground state always has total angular momentum (traditionally called the “spin” in nuclear physics) and parity  $L^\pi=0^+$ . Although the origins of this have been much discussed in recent years [see, for example, Johnson *et al.* (1998)], such a feature is a natural consequence of a short-range attractive interaction and the Pauli principle which favors the coupling of two identical nucleons in the same orbit to angular momentum zero and, in the many-body system, leads to a condensate of such pairs. (In nuclei with many valence nucleons, this picture is highly oversimplified but such a pairing mechanism, reminiscent of Cooper pairs in electronic systems, still plays a pivotal role.)

Above the ground state are excited levels with a variety of spins, and the spectra can be quite complex. However, almost always, the first excited state is a  $2^+$  level, and very often the next is a  $4^+$  state. It is quite revealing to inspect the relative energies of these  $2^+$  and  $4^+$  states as a function of nucleon number, as well as their ratio  $R_{4/2}=E(4_1^+)/E(2_1^+)$ , where the subscripts denote the first state of each spin.

Although nuclei are complex strongly interacting many-body systems with up to hundreds of nucleons in close proximity orbiting  $\sim 10^{21}$  times per second, they often display remarkable simplicities and regularities. In

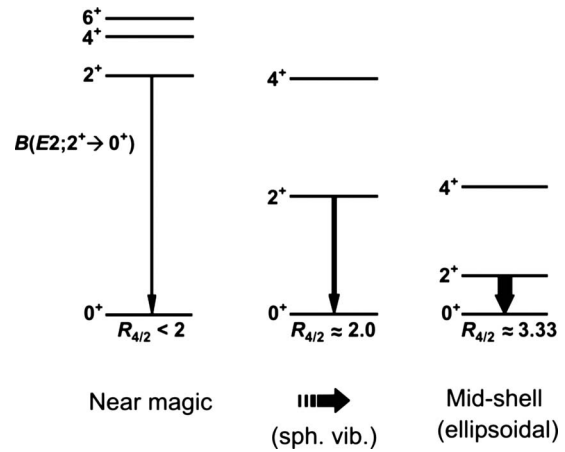


FIG. 1. Stages of structural evolution from near magic to mid-shell. The thicknesses of the transition arrows roughly indicate the strength of the  $B(E2)$  values.

much of this section overviewing the essential data relevant to the equilibrium structure of nuclei, we see abundant evidence for these regularities.

We start by considering the simplest case of nuclei with just two like particles above a doubly magic core (examples would be  $^{134}\text{Sn}$  with  $Z=50$  and  $N=84$  or  $^{210}\text{Pb}$  with  $Z=82$  and  $N=128$ ). In such a case, the low-lying levels can be described by IPM configurations of the type  $|j^2, L\rangle$  with both particles in a state characterized by the angular momentum  $j$ . A short range, predominantly attractive, residual interaction gives a spectrum with a large jump in energy from the  $0^+$  ground state to a close-lying set of states with spins  $L=2, 4, \dots, (2j-1)$ .<sup>3</sup> Such a typical spectrum is seen on the left in Fig. 1. Hence,  $R_{4/2} < 2$ .

As valence nucleons are added, configuration mixing is generated by the residual interactions, and collective behavior emerges. Typically, as we discuss below, this situation leads to  $R_{4/2} \geq 2.0$ . To illustrate how the  $2_1^+$  and  $4_1^+$  levels behave for such nuclei, Fig. 2 shows the energy  $E(4_1^+)$  plotted against  $E(2_1^+)$  for all collective nuclei with  $Z$  between 38 and 82 (a large swath of the nuclear chart). A remarkably simple phenomenology appears. Nearly all the data points are aligned along two linear segments, with slopes 2.00 and 3.33 and with a sharp change between these slopes at  $E(2_1^+) \approx 120$  keV. The line with slope 2.00 has a finite intercept: these data points therefore approximately satisfy  $E(4_1^+) = 2E(2_1^+) + \varepsilon_4$ . We will see shortly that this corresponds to a model of a nucleus that can undergo small amplitude quadrupole (angular momentum 2) oscillations about a spherical equilibrium shape. The line with  $R_{4/2} = 3.33$  will be seen to correspond to nonspherical (deformed) nuclei that rotate according to the eigenvalue expression for a quantum mechanical symmetric top.

<sup>3</sup>Odd- $L$  states are forbidden for two identical fermions (as well as for two identical bosons) as a consequence of the antisymmetrization (symmetrization) procedure.

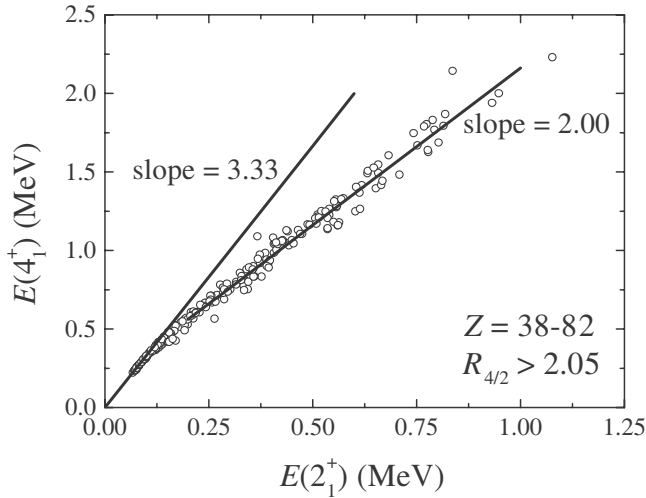


FIG. 2. A correlation plot for energies of the  $4_1^+$  and  $2_1^+$  states in even-even nuclei with  $Z=38-82$  and  $E(4_1^+)/E(2_1^+) > 2.05$ . The two straight lines demarcate two distinct types of nuclear structure. Adapted from [Casten \*et al.\*, 1993](#).

We now turn to a somewhat more detailed discussion of vibrational and rotational states in nuclei and to the simple models that describe them. Near singly closed shells, i.e., for nuclei with either  $N$  or  $Z$  just above a magic value, the number of nucleons outside of a deformable core is small and the zero-point energy of the lowest oscillations is greater than the energy of deformation. Therefore, the shape of the core is not stabilized. These vibrational nuclei have a spherical ground-state shape and exhibit surface vibrations around the equilibrium form when they are excited. While the microscopic description of such motions in terms of fermionic degrees of freedom can be rather complex, a macroscopic perspective in terms of quantized surface oscillations (phonons with angular momentum  $\lambda$ ) is very simple.

Without knowing the underlying microscopic structure, one can introduce creation and annihilation operators of phonons,  $Q_{\lambda\mu}^\dagger$  and  $Q_{\lambda\mu}$  (where  $\mu$  is for the angular momentum projection), to relate different vibrational states of the nucleus. These operators fulfill the standard boson commutation rules,  $[Q_{\lambda\mu}, Q_{\lambda'\mu'}^\dagger] = \delta_{\lambda\lambda'} \delta_{\mu\mu'}$ , all other commutators being zero. The operator counting the number of  $\lambda$  phonons is given by  $N_\lambda = \sum_\mu Q_{\lambda\mu}^\dagger Q_{\lambda\mu}$  and the simplest vibrational Hamiltonian becomes the one of the harmonic oscillator,

$$H_{\text{vib}} = \sum_\lambda \hbar\omega_\lambda (N_\lambda + \lambda + \frac{1}{2}), \quad (2.2)$$

where  $\omega_\lambda$  is the oscillator frequency associated with the selected mode. The eigenvalues of this Hamiltonian are obtained by substituting  $N_\lambda = 0, 1, 2, \dots$

As noted above, almost all even-even nuclei have as the first excited state a  $2^+$  state corresponding to dominant  $\lambda=2$  (quadrupole) phonons. At a higher energy, there is evidence for a  $3^-$  excitation, which can be described by an octupole phonon with  $\lambda=3$ . A single-phonon state with  $\lambda=2$  has angular momentum  $L=2$  and

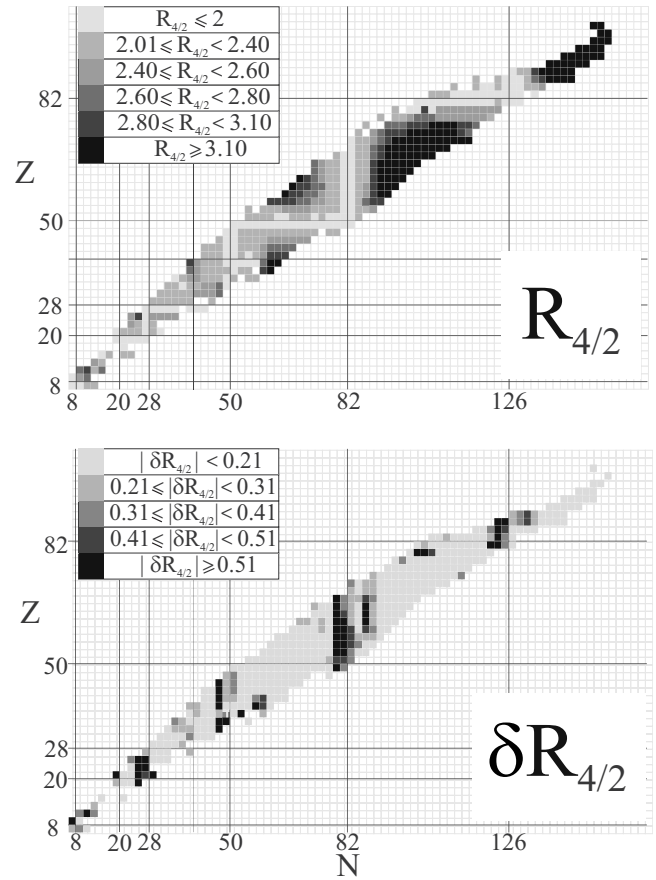


FIG. 3. Values of  $R_{4/2} = E(4_1^+)/E(2_1^+)$  (upper panel) and  $\delta R_{4/2} = |R_{4/2}(Z, N) - R_{4/2}(Z, N+2)|$  (lower panel) across the nuclear chart. From [Cakirli \*et al.\*, 2009](#).

excitation energy  $E_{\text{ex}} = \hbar\omega_2$ . Using angular-momentum coupling and symmetrization, the two-phonon states turn out to have  $L=0, 2, 4$  and  $E_{\text{ex}} = 2\hbar\omega_2$  which gives the ratio  $R_{4/2} = 2$ .

A few states of such a spectrum are indicated in the middle panel of Fig. 1. Many nuclei are observed with spectra approximating such patterns. However, harmonic vibrations following Eq. (2.2) require that phonons do not interact with each other. As demonstrated in Fig. 2, real nuclei often exhibit anharmonic effects (indicated by the intercept  $\varepsilon_4$  characterizing the sequence of vibrational nuclei), which can be described by introducing appropriate residual interactions of phonons. Then one often sees spectra with  $R_{4/2}$  values between  $\approx 2.2$  and  $\approx 2.4$  (see also Figs. 3 and 4, discussed further below). Examples of these are found in the  $A \approx 80$  region, in Cd isotopes, and elsewhere.

If the number of nucleons outside the deformable core is such that the zero-point energy of the oscillations is much less than the energy of deformation, the system can develop a stable deformed shape. In this case, surface vibrations still represent existing collective modes, but the lowest-energy collective motion becomes the rotational one. This leads to typical rotational spectra of deformed nuclei with both  $N$  and  $Z$  well away from magic numbers.

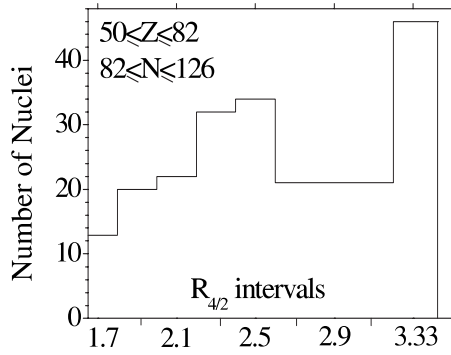


FIG. 4. The distribution of  $R_{4/2}$  values in the  $Z=50-82$ ,  $N=82-126$  major shell. Figure courtesy of R. B. Cakirli.

From classical considerations, we know that if the system has a permanent nonspherical shape, there exists a body-fixed system (1,2,3) in which the inertial tensor is diagonal. It is related to the laboratory-fixed system ( $x, y, z$ ) by an Euler transformation. The inertial tensor then has components  $(\mathcal{I}_1, \mathcal{I}_2, \mathcal{I}_3)$ , so that the rotational Hamiltonian is just

$$H_{\text{rot}} = \frac{L_1^2}{2\mathcal{I}_1} + \frac{L_2^2}{2\mathcal{I}_2} + \frac{L_3^2}{2\mathcal{I}_3}, \quad (2.3)$$

with  $L_i$  the body-fixed components of angular momentum. The simplest rotational system is an axially symmetric quadrupole<sup>4</sup> rotor (with the symmetry axis 3), for which the moments of inertia  $\mathcal{I}_1 = \mathcal{I}_2 \equiv \mathcal{I}$  and the rotation around the symmetry axis does not contribute to energy. Then the energies are directly found to be  $E_{L,K} = \hbar^2[L(L+1) - K^2]/2\mathcal{I}$ , where  $L$  is the total angular momentum quantum number and  $K$  is a projection of the angular momentum to the symmetry axis.

If the lowest state is  $0^+$  (hence  $K=0$ ), the symmetry with respect to the reflection of the third axis ensures that only states with even  $L$  and positive parity appear in the rotational band. The band above the ground state of an even-even nucleus therefore follows the sequence  $0^+, 2^+, 4^+, \dots$ . Applying the last formula we find  $R_{4/2} = 3.33$  (see the rightmost panel in Fig. 1). As we know from Fig. 2, this ratio is actually observed in many rotational nuclei (although the sequence of points with the slope 3.33 in Fig. 2 is relatively short, it contains a large number of nuclei; see also Figs. 3 and 4). These rotational nuclei mostly show prolate (cigarlike) or, less commonly, oblate (pancakelike) quadrupole equilibrium shapes.

Taken as a whole, Fig. 1 shows schematically the sequence of spectra often seen as a function of successively larger numbers of valence nucleons. Associated

with these spectra are the corresponding shapes. Once midshell is reached, one thinks in terms of the numbers of missing nucleons (holes) to the next closed shell and the structure, along with the systematics of these observables, roughly reverses the pattern in Fig. 1.<sup>5</sup>

Figure 3 (upper panel) shows  $R_{4/2}$  values across the nuclear chart. The patterns reflect the above comments:  $R_{4/2}$  is less than 2 near magic numbers and then increases toward  $\approx 3.33$  in the center of each box bounded by pairs of magic numbers. How large the region of deformation depends largely on shell size: a certain minimum number of valence nucleon interactions is needed. Key to this is the competition between the spherical-driving pairing interaction and the configuration-inducing deformation-driving valence proton-neutron ( $p$ - $n$ ) interaction. We codify this competition in Sec. II.C. Note that the extent of the deformed regions is highly mass dependent. In light nuclei, the shells are smaller and hence a much smaller range of nucleon numbers is available for the development of deformed shapes. In heavy nuclei, in contrast, perhaps half are situated in deformed regions. This, in fact, is one reason that much of the study of QPTs concerns the structure of medium and heavy nuclei. We will see more focused views of the behavior of  $R_{4/2}$  later.

While  $R_{4/2}$  values are interesting, if one wants to discuss changes in structure, even more revealing are differences of  $R_{4/2}$  for even-even nuclei with proton numbers  $Z$  and  $Z+2$  or neutron numbers  $N$  and  $N+2$ . The differences with respect to  $N$  are shown in the lower panel of Fig. 3. Here one sees the rapid changes in structure that occur in narrow regions of the chart, specifically in nuclei that are a few protons and neutrons removed from doubly magic nuclei. The most studied of these regions, and the one in which QPTs were first discussed, is that near  $N=90$ , around  $Z \approx 62$ . Here  $\delta R_{4/2}$  values reach magnitudes above 0.5 for adjacent even-even nuclei. The  $A \approx 100$  region is another well-known region of extremely rapid structural change. The rate at which this evolution occurs depends on many factors, including the underlying shell structure, the strength of residual interactions, the number of nucleons spanned by each major shell, and the possible changes in underlying shell or subshell structure. Some of this will be discussed below.

The relevance of the simple models (anharmonic vibrator and symmetric rotor) to real nuclei was shown in Fig. 2. Figure 4 shows the same data in a different way in terms of a frequency occurrence histogram of  $R_{4/2}$  values. A wide range of values appears but we note the peaks at  $R_{4/2} \approx 2.3$  and 3.33. The former corresponds to slightly anharmonic spherical vibrators and the latter, of

<sup>4</sup>Higher-order distortions, such as octupole or hexadecapole shapes, can also occur but they are typically at higher energy. This is plausible since they involve changes in shape that occur more rapidly with angular position on the nuclear surface and hence have shorter wavelengths and higher energies. The Rayleigh criterion for a liquid drop gives such a result.

<sup>5</sup>We note that this is not strictly true because the single-particle angular momenta for a major oscillator shell in typical mean-field potentials are large at the beginning of a shell and small at the end. Therefore, both the effects of the Pauli principle and of residual interactions differ, and hence structural evolution is not fully symmetric about midshell.

course, to deformed nuclei with rotational spectra. We caution here (and will return to this point in Sec. III.B.3) that  $R_{4/2}$  alone does not uniquely determine the structure (except at extremes such as 2.0 or 3.33).

In new regions of nuclei far from stability, only sparse data will be available and it is useful to have indicators that are even simpler to measure. Since the development of collectivity entails extensive configuration mixing, which lowers the energy of the collective state, it is not surprising that the first  $2^+$  state energy rapidly decreases going into deformed regions of nuclei. This was sketched in Fig. 1 and demonstrated by real data in Fig. 2. Absolute values of  $E(2_1^+)$  are not as immediately useful as  $R_{4/2}$  values because they exhibit mass-dependent variations due to changes in the inertial parameter, which scales as  $A^{-5/3}$ . However, within a mass region, they can be revealing. Since  $E(2_1^+)$  decreases as deformation develops, while  $R_{4/2}$  increases, it is, in fact, more useful to plot  $1/E(2_1^+)$ . An example will be shown later.

## 2. $E2$ transition strengths

Since deformation and collectivity go hand in hand, another observable that acts as a sensitive signature of structure is the strength of the electric quadrupole ( $E2$ ) transition between the  $2_1^+$  and  $0_1^+$  states,  $B(E2:2_1^+ \rightarrow 0_1^+)$ , which can be expressed in  $e^2 \text{fm}^2 = 10^{-2} e^2 \text{b}^2$  or in Weisskopf units (W.u.) (Bohr and Mottelson, 1975). As collectivity grows, so do these  $B(E2)$  values (see the simple toy model in Sec. II.C). The data for the  $Z=50-82$ ,  $N=82-126$  major shells are shown in Fig. 5. The growth from negligible values near magic numbers, to a peaking near midshell, and a parallel decrease toward the next doubly magic region is clear. The  $B(E2)$  value (in  $e^2 \text{fm}^2$ ) can be related to the intrinsic quadrupole moment  $Q$  (in e fm) and the Bohr deformation parameter  $\beta$  (see Sec. III.A.1) through

$$|Q| = \sqrt{16\pi B(E2:2_1^+ \rightarrow 0_1^+)} = \frac{3Ze}{\sqrt{5\pi}} R_0^2 (\beta + 0.16\beta^2), \quad (2.4)$$

where  $R_0$  (in fm) parametrizes the nuclear radius. This formula, based on a rotor model, is not reliable in spherical nuclei but gives an overall perspective on the shape evolution through the connection to the quadrupole deformation  $\beta$ .

Some other  $B(E2)$  values, as well, turn out to be important indicators of shape. For instance, the  $E2$  strength of the  $4_1^+ \rightarrow 2_1^+$  transition also increases in the spherical-to-deformed transition, but the ratio  $B_{4/2} = B(E2:4_1^+ \rightarrow 2_1^+)/B(E2:2_1^+ \rightarrow 0_1^+)$  decreases. Both transitions in this case connect states within the ground-state band.

The transitions between different bands are also sensitive to shape changes. As an example, consider the  $2_2^+ \rightarrow 2_1^+$  transition. In an axially symmetric deformed nucleus this transition connects the so-called  $\beta$  or  $\gamma$  vibrational band with the ground-state band and is there-

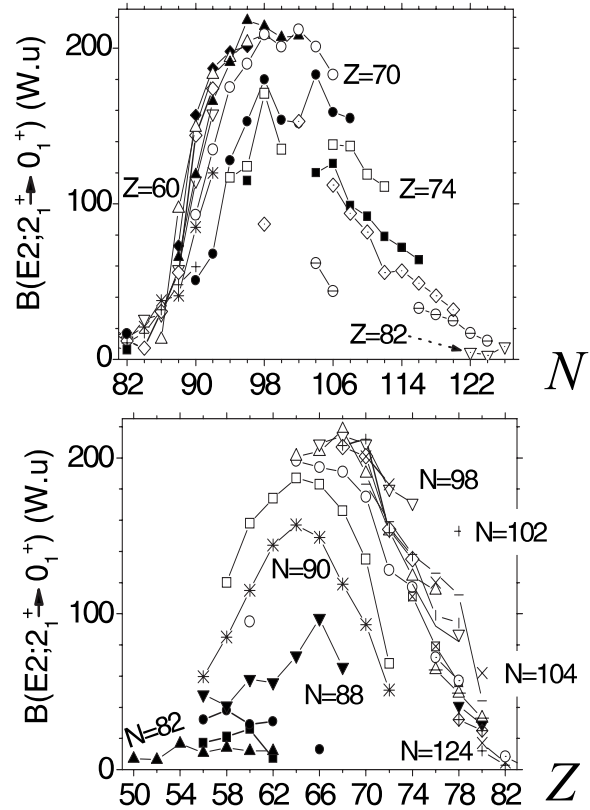


FIG. 5.  $B(E2:2_1^+ \rightarrow 0_1^+)$  values in Weisskopf units for the  $Z=50-82$ ,  $N=82-126$  major shells. Figure courtesy of R. B. Cakirli.

fore relatively weak. In deformed nuclei which are unstable against the onset of triaxiality, the strength of this transition rises considerably, while a moderate increase is observed also in vibrational nuclei. Note that some interband  $E2$  transitions were considered as signatures of coexisting vibrational and rotational spectral structures in nuclei at the critical point between spherical and deformed shapes (Zamfir *et al.*, 1999). Other transitions, such as  $2_2^+ \rightarrow 0_1^+$ , vanish in the deformed, axially unstable, and vibrator limits but peak in transition regions for which they therefore serve as useful indicators.

## 3. Two-neutron separation energies

Thus far, we have discussed observables based on excitation spectra. However, the structure of nuclei is also seen in their masses and binding energies which reflect the sum of all binding effects, both single particle and residual interactions. As these binding energies (roughly 8 MeV per nucleon) can reach values well above 1 GeV in heavy nuclei, it is more convenient to deal with various differences of binding energies. Here we consider separation energies. In particular, to avoid oscillations between odd and even nuclei due to pairing, we look at the two-neutron separation energies  $S_{2n}$ . This is shown for two mass regions in Fig. 6. The most obvious feature is the large decrease in  $S_{2n}$  just after closed shells which occurs because the valence nucleons now enter significantly less bound orbits in a new shell. Such data, in fact,

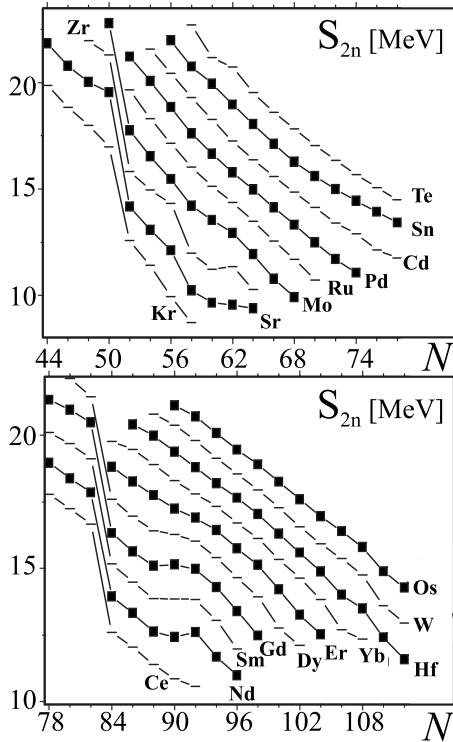


FIG. 6. Two-neutron separation energies vs neutron number for two mass regions with quantum phase transitions. Data from the 2003 AME (Audi *et al.*, 2003). Figure courtesy of R. B. Cakirli.

were among the early indicators of the magic numbers.

Besides these dramatic drops, there are other characteristic features of the  $S_{2n}$  systematics. Often, they are typified by long, nearly linear, segments for each isotopic or isotonic chain. This feature emerges naturally (Fossion *et al.*, 2002) from global properties [see, for example, the Bethe-Weizsäcker mass formula (Heyde, 2004)]. The primary contribution to the linear behavior is the asymmetry term which gives rise to changes in binding as successive independent particle model orbits are filled.

Superposed on this are contributions from collective effects. Collectivity in nuclei corresponds to mixing of various shell model configurations or, in the interacting boson approximation (IBA) approach (Iachello and Arima, 1987), of bosonic degrees of freedom, which are related to pairing properties of shell model configurations. Such collective effects contribute both to the linearity of  $S_{2n}$  and to nonlinearities. The most visible of these (see the bottom panel of Fig. 6) appears near  $N=90$  where a local increase in  $S_{2n}$  values (a flattening) relative to the linear decrease occurs. This happens at neutron numbers where deformation rapidly sets in and reflects the extra binding associated with the deformed equilibrium shape. As noted above, this is, in fact, the region where first-order QPT behavior was initially recognized, and these nuclei will be a focus of our attention below. In the corresponding plot of  $S_{2n}$  vs  $Z$ , the successive isotonic sequences bunch together in this same mass region. Besides these highly visible deviations from lin-

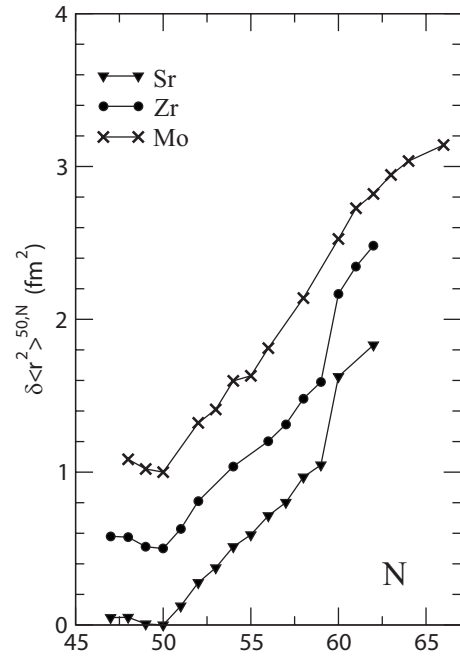


FIG. 7. Relative isotope shifts in the Sr, Zr, and Mo isotopic chains showing the jumps at  $N=60$  when deformation sets in (each curve adjusted to an arbitrary value at  $N=50$ ). Based on Buchinger *et al.*, 1990, Lievens *et al.*, 1991, and Charlwood *et al.*, 2009.

earity at phase-transitional points, one sees more subtle curvatures in Fig. 6 as well, such as for the isotopes of Dy-Hf. These too arise from and can be highly sensitive to collective correlations (García-Ramos *et al.*, 2001; Fossion *et al.*, 2002; Cakirli *et al.*, 2009).

#### 4. Other observables

Other observables also reflect structural evolution. Three will be discussed below:  $E0$  transitions, isotope shifts, and two-nucleon transfer cross sections.

Electric monopole ( $E0$ ) transitions, especially between the excited collective  $0^+$  states and the ground state, have long been associated with shape changes (Wood *et al.*, 1999). It was shown by von Brentano *et al.* (2004), in the context of the IBA, that the strength  $\rho^2(E0:0_2^+ \rightarrow 0_1^+)$  should be small in spherical nuclei, increase rapidly in regions of shape change, and remain large in deformed nuclei. We return to the discussion of  $E0$  transitions in Sec. IV.B.1.

Isotope shifts, that is, differences  $\delta \langle r^2 \rangle$  of average squared nuclear radii  $\langle r^2 \rangle$  between the different isotopes of the same element as a function of  $N$ , also reflect changes in structure (Wilets *et al.*, 1953). They exhibit an odd-even staggering indicating pairing effects and, naturally, large jumps at shell closures, but, more relevant for this review, they show kinks or discontinuities at spherical-deformed shape phase transition regions. Figure 7 shows this for  $Z=38-42$  isotopes.

Finally, two (identical) nucleon transfer reactions, e.g., the  $(p,t)$  and  $(t,p)$  ones, can also signal rapid shape change. Normally, cross sections to  $0^+$  states are domi-

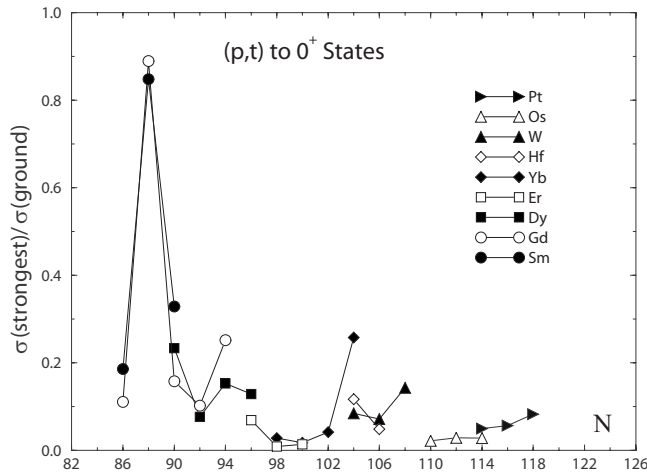


FIG. 8. Cross sections for excited  $0^+$  states in the  $(p,t)$  reaction at forward angles for rare earth nuclei. Shown is the ratio of the cross sections for the strongest transition to an excited  $0^+$  state relative to the ground-state cross section. Figure courtesy of R. M. Clark.

nated by the ground state, with excited-state cross sections representing less than 20% (most often, only a few percent) of the ground-state cross sections. However, when  $R_{4/2}$  changes rapidly, the cross section is shared between ground and excited states (Hinds *et al.*, 1965; Bjerregaard *et al.*, 1966; Maxwell *et al.*, 1966; Fleming *et al.*, 1971; Oothoudt and Hintz, 1973). The data for the  $(p,t)$  reaction in the rare earth region are shown in Fig. 8 and display exactly this behavior near  $N=90$ .

### C. Microscopic considerations

There is an intimate relation between correlations on the nucleonic level and collectivity and shape on the macroscopic level (Åberg *et al.*, 1990; Nazarewicz, 1992). Indeed, these two viewpoints provide complementary perspectives with which to view nuclear structure and its evolution. In this section, we explore some simple aspects of this relation and, in the process, discuss a simple indicator of collective structure founded in the interactions of valence nucleons.

Collectivity and the development of nonspherical shapes demand mixing of shell model configurations. The specific mechanism responsible for the onset of deformation in nuclei seems to be very closely related to the process of spontaneous symmetry breaking described for the first time by Jahn and Teller (1937). The concept was initially applied in molecular physics, where it was shown that a molecule can develop a symmetry-breaking ground-state form due to the interaction between degenerate electronic excitations and collective modes of the molecule. In a similar way, the interaction of degenerate nucleonic states with collective vibrations of the nucleus mediates a strong coupling between single-particle states, which may break the spherical symmetry of the ground state (Reinhard and Otten, 1984; Nazarewicz, 1994). In the context of this review, an

essential feature of the Jahn-Teller effect (which is nowadays relevant in many different branches of physics) is its critical character.

The rise of collectivity with mixing can be seen with the following simple toy model. Imagine a set of  $n$  shell model configurations  $|\phi_i\rangle$  for  $2^+$  states. Assume they are all degenerate. Further assume that all have identical reduced  $E2$  matrix elements for decay to the  $0^+$  ground state, that is,  $\langle 0_1^+ || T^{E2} || \phi_i \rangle = W$  for all  $i=1, \dots, n$ . This corresponds to a  $B(E2: 2^+ \rightarrow 0_1^+) = W^2/5$ . Now assume that each of these  $2^+$  basis states mixes due to some residual interaction, with every other one and with equal matrix elements,  $\langle \phi_i | H_{\text{resid}} | \phi_j \rangle = -|V|$ . Solving this toy model is trivial and well known:  $n-1$  levels move up by an energy  $\Delta E = +|V|$ , and one comes down by  $\Delta E = -(n-1)|V|$ . Moreover, the wave function of the lowest state is a linear combination  $|\Psi_{\text{lowest}}\rangle = n^{-1/2} \sum_i |\phi_i\rangle$  with equal amplitudes for all the basis states. This result, for the lowest state, can be visualized as arising from successive mixing with each of the other  $n-1$  degenerate ( $i>1$ ) basis states, each of which pushes the  $i=1$  state lower by an amount  $V$  and contributes an equal mixing amplitude.

Now calculate the  $B(E2)$  from the lowest  $2^+$  state to the ground state. It is given by

$$B(E2: 2_1^+ \rightarrow 0_1^+) = \frac{1}{5} \langle 0_1^+ || T^{E2} || 2_1^+ \rangle^2 = n \frac{W^2}{5}, \quad (2.5)$$

which is  $n$  times each of the unperturbed values. Thus, not only is one state (the collective state) lowered significantly in energy, but it collects all the  $E2$  strength.

In practice, of course, shell model configurations, even within a pair of major shells, are not at all degenerate nor, involving different orbits and seniorities, would they have equal matrix elements to the  $0^+$  ground state, nor equal mixing with each other, and, moreover, the ground state itself is a coherent mixture. Therefore the estimate in Eq. (2.5) is many orders of magnitude too large. Nevertheless, the basic physics is correct. In fact, it gives further insight into the ingredients needed for collectivity. Not only is mixing of configurations essential but the collectivity will grow with the number  $n$  of mixing configurations. Therefore, in general, collective effects in nuclei require a certain minimum number of valence nucleons and grow rapidly as that number is increased. This is exactly the pattern seen in Figs. 3 and 5. Below we exploit this further. We end this discussion by noting that in typical deformed heavy nuclei the enhancement factor of  $B(E2: 2_1^+ \rightarrow 0_1^+)$  values easily reaches a couple of hundreds, as again seen in Fig. 5.

Residual interactions lend another ingredient to the evolution of structure (Heyde *et al.*, 1985). One can expand the angular part of a residual interaction in multipoles—Legendre polynomials in the angle between the orbital planes of the interacting nucleons. The angles at which each multipole is largest are the angles at which they have the most effect. If the semiclassical angle between the orbital planes of two interacting particles in a total  $L$  state of a configuration  $|j_1 j_2 L\rangle$  is close to the angle where a given multipole of the residual interaction

is large, that part of the residual interaction will be important in determining the energy of that two-particle configuration. Of course, these angles and therefore the affected  $L$  values will depend on the interaction: a  $\delta$  force or quadrupole interaction would have quite different effects in configurations of high  $j$  orbits. However, the monopole part is unique in this regard as it is given by just a constant, independent of angle. Its role is therefore to lower the energy of each level equally, that is, to lower the energy of the entire multiplet. This is equivalent to a change in single particle energies. As a consequence, residual interactions can also affect shell structure. Thus, in studying the development of collectivity and correlations, both configuration mixing and changes in shell structure due to the residual interactions need to be considered.<sup>6</sup>

It is widely recognized that the emergence of collective phenomena in nuclei is intimately connected to a competition between the spherical-driving  $L=0$  coupled pairing interaction and the deformation-driving valence  $p$ - $n$  (proton-neutron) interaction (de-Shalit and Goldhaber, 1953; Talmi, 1962; Federman and Pittel, 1977; Federman *et al.*, 1979; Dobaczewski *et al.*, 1988; Nazarewicz, 1992; Werner *et al.*, 1994). The importance of the  $p$ - $n$  interaction in contrast to  $p$ - $p$  and  $n$ - $n$  interactions comes as a result of Pauli blocking, which reduces the number of nonvanishing interaction matrix elements in the like-particle cases. One can develop a simple guide to this mechanism. The pairing interaction scales as the number of valence protons and neutrons,  $N_p + N_n$ , since each nucleon pairs with only one other in the time reversed state of the same orbit. In contrast, the valence  $p$ - $n$  interaction acts between all valence nucleons. These interactions are not all equal—they are highly orbit dependent but let us assume they are all the same strength for a moment. Then the total  $p$ - $n$  strength scales as  $N_p N_n$ . Hence a useful indicator of the pairing versus  $p$ - $n$  competition is (Casten *et al.*, 1987)

$$P = \frac{N_p N_n}{N_p + N_n}. \quad (2.6)$$

Since the pairing interaction in heavy nuclei is roughly 1.5 MeV and the  $p$ - $n$  interaction is roughly 300 keV, it takes roughly five  $p$ - $n$  interactions to begin to overcome the pairing interaction. Thus  $P \approx 5$  should (and, remarkably, does) mark a boundary between spherical and axially deformed ( $R_{4/2} \geq 3.0$ ) regions. Since  $P$  is always less than the lower of  $N_p$  and  $N_n$ , it is clear that  $P \approx 5$  requires a fair number of both valence protons and neutrons. If a given pair of proton and neutron major shells

<sup>6</sup>There is another effect by which, in nuclei far from stability, shell model energies can be altered, namely, if the mean-field potential itself changes due, for example, to the presence of weakly bound nucleons that contribute differently to the potential than well-bound core nucleons. Indeed, an active research area of late lies in studying changes in shell structure, and disentangling which of these effects—residual interactions or the mean-field itself—is at work.

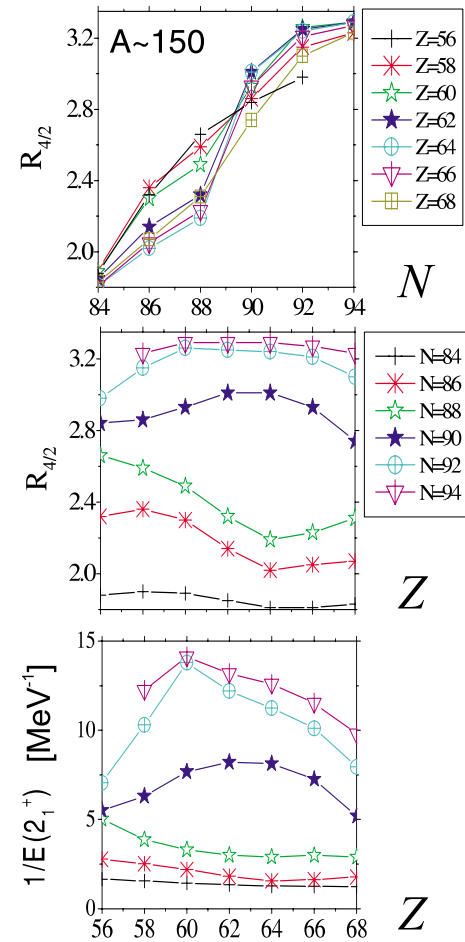


FIG. 9. (Color online)  $R_{4/2}$  vs  $N$  (top) and  $Z$  (middle) and  $1/E(2_1^+)$  vs  $Z$  (bottom) for the rare-earth region. Adapted from Cakirli and Casten, 2008.

is large enough, then there will always be a region of nuclei within the shell where deformation and associated collective behavior occurs, at least near midshell. In medium mass and heavy nuclei, Fig. 3 shows that there are large regions of deformed nuclei and careful inspection shows that the locus of large changes in  $R_{4/2}$  (see Fig. 3) lies close to the locus of  $P \approx 5$ .

With this background, it is useful to inspect a particular mass region to see how these ideas play out. The upper and middle panels of Fig. 9 focus on  $R_{4/2}$  values for the rare earth region plotted against  $N$  (top) and  $Z$  (middle). The upper plot shows a rapid rise of  $R_{4/2}$  near  $N=90$  from values typical of vibrational nuclei to those corresponding to well deformed rotors signaling the onset of deformation. Rapid changes of  $R_{4/2}$  (seen also in Fig. 3) were one of the original motivations for treating this mass region in terms of phase-transitional behavior. Not much more is easily gleaned from the upper panel except one notices an intriguing pattern in which the  $R_{4/2}$  values for Nd-Dy cross from below to above those of Ba and Ce.

The plot in the middle panel of Fig. 9 shows the same data and reveals the same physics but much more as well. Of course, it shows a rapid rise in  $R_{4/2}$  to values

near 3.33, but the sudden, phase-transitional, behavior is even more evident in going from the  $N=88$  curve to that at  $N=90$  or  $92$ . Recalling that  $R_{4/2}$  is a minimum near closed shells (see Fig. 3) and a maximum near midshell, we see that  $Z=64$  acts as a semiclosed shell for  $N \leq 88$ , while, for  $N \geq 90$ , the value  $Z=64$  behaves as a nearly midshell number (64 is nearly midway between 50 and 82). The change from a minimum to a maximum at  $Z=64$  leads to a kind of “bubble” pattern (Cakirli and Casten, 2008).

We recall that while protons in these nuclei are in the midoccupancy of the shell with orbitals  $2d_{5/2}, 1g_{7/2}, 1h_{11/2}, 2d_{3/2}, 3s_{1/2}$ , neutrons start filling the orbitals  $2f_{7/2}, 1h_{9/2}, 2f_{5/2}, \dots$  of the next shell. The middle panel of Fig. 9 can be interpreted as a breakdown in subshell structure at  $N=90$ . Microscopically, this has been explained (Casten *et al.*, 1981) in terms of the Federman-Pittel mechanism (Federman and Pittel, 1977, 1979; Federman *et al.*, 1979) as a consequence of the lowering of the proton  $1h_{11/2}$  orbit so that the gap after the  $1g_{7/2}$  and  $2d_{5/2}$  proton orbits at  $Z=64$  is obliterated. This occurs as a function of neutron number due to the strong monopole  $p$ - $n$  interaction (Heyde *et al.*, 1985) between these highly overlapping orbits as the neutron  $1h_{9/2}$  orbit begins to fill.

The consequences of this are easy to see. Excitation of protons into the  $1h_{11/2}$  orbit expands the configuration space and therefore produces a more deformed state. Initially, the state is at relatively high energy, and the two sets of proton orbits ( $1g_{7/2}$  and  $2d_{5/2}$ , and  $1h_{11/2}$ ) are still somewhat separated, creating a situation in which one has a spherical ground state and a more collective or slightly deformed excited  $0^+$  state. As the neutron number increases and the proton  $1h_{11/2}$  orbit drops in energy, the energy of the deformed state decreases and mixing of the two spaces increases. At  $N \approx 90$  the rather sudden disappearance of the gap at  $Z=64$  is tantamount to a sudden increase in the effective number of valence protons and in the size of the valence space and to the rapid onset of deformation. Thus the middle panel of Fig. 9 not only shows phase-transitional behavior, as does the upper one, but also shows that it results from a change in the underlying shell structure and is driven largely by the valence  $p$ - $n$  interaction. Indeed, it has been shown that empirical measures of  $p$ - $n$  interaction strengths are directly correlated with  $R_{4/2}$  (Cakirli and Casten, 2006).

It turns out that pairs of crossing and bubble patterns appear frequently in medium mass and heavy nuclei. Their appearance is a signature of phase-transitional behavior that is mediated by a change in underlying subshell structure, and the nucleon type which experiences the subshell change is that in terms of which one sees a bubble pattern. The bottom panel of Fig. 9 shows an additional example of the bubble pattern in the  $Z$  dependence of  $1/E(2_1^+)$ , which will often be far more readily available experimentally in exotic nuclei. These findings highlight the fact that looking at the same data from different perspectives can often reveal physics that is more hidden otherwise.

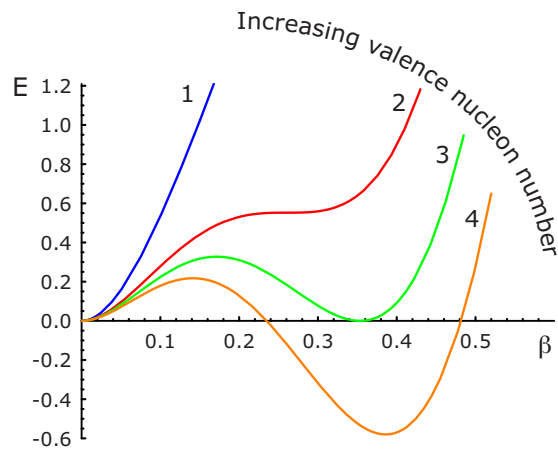


FIG. 10. (Color online) Illustration of potential-energy curves (vertical axis in arbitrary units) vs quadrupole deformation parameter  $\beta$  for a region of first-order phase transition. The curves were calculated by the coherent-state formalism of the interacting boson model (see Sec. III.B.2). Curve 3 corresponds to the critical point of the spherical-to-deformed transition. Figure courtesy of R. Casperson.

It is interesting and relevant to our later discussion of phase transitions and critical-point solutions to think of the process just described in terms of energy surfaces. The concept of potential energy surface (PES), i.e., the dependence of the nuclear binding energy on shape parameters, will be often used in the forthcoming parts. Figure 10 shows, in a schematic way, possible evolution of the PES dependence on the Bohr deformation parameter  $\beta$  (Bohr and Mottelson, 1975) introduced in Sec. III.A.1. For just a few valence nucleons the energy surface has a single minimum at deformation parameter  $\beta = 0$  (spherical shape). As the number of valence nucleons increases, a second highly excited minimum appears at  $\beta > 0$  (deformed shape). This minimum decreases in energy with more valence nucleons added and, at some point, it becomes degenerate with the spherical minimum. This is the critical point of the phase transition (we are describing a first-order phase transition for which phase coexistence occurs). For still more valence nucleons, the deformed minimum becomes the ground state. We will see in Sec. V that such a picture provides the conceptual backdrop for the critical-point solutions.

Note several important features of this scenario. First, the change in equilibrium deformation is discontinuous—a signature of a first-order phase transition according to the Ehrenfest criterion (Ehrenfest, 1933). Second, again associated with a first-order phase transition, there is phase coexistence (two minima appear for some nucleon numbers, or for a certain range of the control parameter as we will see later). Third, recalling the obvious fact that nuclei contain integer numbers of nucleons and therefore their properties change discretely, it is clear that there is no mandate that any given nucleus happens to land at exactly the critical point. This may happen and, fortunately, seems to be the case, at least in the region near  $A \approx 150$ , and this happenstance was one of the factors influencing the development of

the critical-point descriptions that we will discuss later. In other regions, phase-transitional behavior may well occur but may not happen to produce a specific nucleus at the critical point.

### III. MODELS FOR SHAPE TRANSITIONS

In the previous section, we discussed basic experimental data on shape transitions in nuclei and outlined some fundamental theoretical concepts for their interpretation. This section will introduce concrete approaches designed to quantitatively describe the evolution of nuclear shapes. The focus is set mainly on two phenomenological models, the geometric collective model (Sec. III.A) and the interacting boson model (Sec. III.B), while fermionic models (which are not of our main interest here) are mentioned in Sec. III.C.

#### A. Geometric collective model

The geometric or collective model of atomic nuclei was introduced by Bohr (1952) and has been extensively elaborated in the 1960s. A generalized geometric approach, referred to as the geometric collective model (GCM), was presented by Gneuss *et al.* (1969). In the following, we use the acronym GCM for the whole family of geometric models, including a recent revival of this type of description.

The model sees the nucleus as a droplet described by a set of collective coordinates  $\alpha$ . The clearest interpretation of these coordinates is through an expansion of the nuclear radius into spherical harmonics  $R = R_0(1 + \sum_{\lambda\mu} \alpha_{\mu}^{(\lambda)*} Y_{\mu}^{(\lambda)})$ , with  $\alpha^*$  standing for the coefficients at each multipolarity. Since the dominant type of nuclear deformation is the quadrupole one (see footnote 4), the above sum can be, with a good degree of approximation, restricted just to the terms with  $\lambda=2$  (hence  $\mu=-2, \dots, +2$ ).

It should be stressed that the basic form of the geometric model, as presented in Sec. III.A.1, has some drawbacks in confrontation with data. In particular, its oversimplified expression for the collective kinetic energy generates unrealistic moments of inertia [see, e.g., Caprio (2009)]. This problem can in principle be treated by the inclusion of more refined kinetic terms into the GCM Hamiltonian (Gneuss *et al.*, 1969), which, however, extends the number of unknown parameters or by switching to the related interacting boson model, which naturally contains more sophisticated kinetic terms controlled by a moderate number of parameters. The latter model will be introduced in Sec. III.B.

#### 1. Bohr Hamiltonian and its phase structure

We begin with some formal remarks on the GCM Hamiltonian and then turn to an analysis of the collective potentials describing a range of nuclear shapes and transition regions. The assumption of  $\lambda=2$  in the nuclear-radius expansion implies that coordinates  $\alpha$  describing common nuclear deformations form a second-

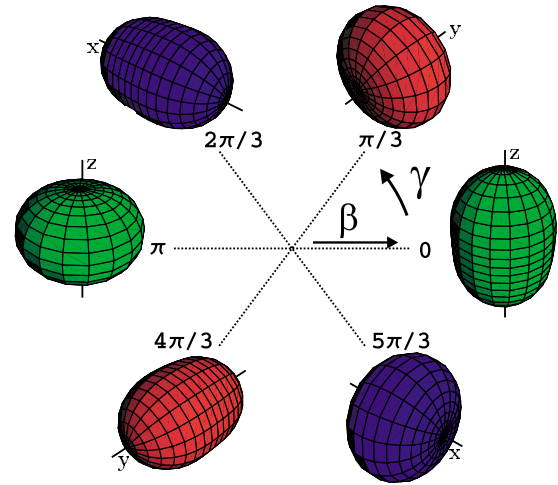


FIG. 11. (Color online) Bohr variables  $\beta$  and  $\gamma$  schematically associated with the corresponding axially symmetric quadrupole shapes. Nonaxial shapes appear between the indicated values of  $\gamma$ . Adapted from Fortunato, 2005.

rank spherical tensor. We know that the Hamiltonian must be a scalar. For the quadrupole tensor  $\alpha$ , there are only two independent scalar combinations (Noack, 1968), namely,

$$[\alpha \times \alpha]^{(0)} \propto \beta^2, \quad [[\alpha \times \alpha]^{(2)} \times \alpha]^{(0)} \propto \beta^3 \cos 3\gamma. \quad (3.1)$$

Note that we use the symbol  $[A \times B]^{(\lambda)}$  for the coupling of arbitrary tensors  $A$  and  $B$  (with ranks  $\lambda_1$  and  $\lambda_2$ , respectively) to angular momentum  $\lambda$ ; therefore  $[A \times B]_{\mu}^{(\lambda)} = \sum_{\mu_1, \mu_2} (\lambda_1 \mu_1 \lambda_2 \mu_2 | \lambda \mu) A_{\mu_1}^{(\lambda_1)} B_{\mu_2}^{(\lambda_2)}$ . We usually skip the projection index  $\mu$  in the tensor notation.

In Eq. (3.1), the parametrization (up to proportionality constants) in terms of Bohr shape variables  $\beta$  and  $\gamma$  is given. These parameters capture the shape of the nucleus in the intrinsic (body-fixed) frame, while any dependence on the Euler angles  $\Theta \equiv (\theta_1, \theta_2, \theta_3)$ , describing the orientation of the nucleus in an arbitrary laboratory frame, is eliminated. Note that the usual way of introducing the shape variables is through the transformation  $\alpha \rightarrow \bar{\alpha}$  of the deformation tensor into the frame connected with the principal axes of the quadrupole deformation. There one gets  $\bar{\alpha}_{\pm 1}^{(2)} = 0$ , while the remaining components are parametrized as  $\bar{\alpha}_0^{(2)} \equiv x = \beta \cos \gamma$  and  $\sqrt{2} \bar{\alpha}_{\pm 2}^{(2)} \equiv y = \beta \sin \gamma$ .

The parameters  $\beta$  and  $\gamma$  can be seen as polar coordinates in the plane  $x \times y$  (see Fig. 11). The radius  $\beta$  quantifies the degree of deformation:  $\beta=0$  corresponds to spherical nuclei and growing values of  $\beta$  generate increasingly deformed shapes. The angular variable  $\gamma$  specifies the type and orientation of the deformed shape: values of  $\gamma$  equal to multiples of  $\pi/3$  correspond to axially symmetric prolate or oblate shapes with different symmetry axes (as shown in Fig. 11), while intermediate values of  $\gamma$  are associated with triaxial shapes, i.e., deformed shapes with no axial symmetry. As various spatial orientations of the deformed drop are mutually

equivalent, it is sufficient to consider just a third of the whole  $2\pi$  domain, e.g., the interval  $\gamma \in (-\pi/3, \pi/3]$  or (due to the additional  $\gamma \leftrightarrow -\gamma$  symmetry) just the sextant  $[0, \pi/3]$ .<sup>7</sup>

Exploiting relations (3.1), we can write the most general expression for the potential energy of the nuclear droplet as  $V = V(\beta^2, \beta^3 \cos 3\gamma)$ . If the deformation is assumed to be small, it is well justified to consider only a truncated Taylor expansion in parameter  $\beta$ . The simplest reasonable formula of this type is

$$\begin{aligned} V &= A\beta^2 + B\beta^3 \cos 3\gamma + C\beta^4 \\ &= \sqrt{5}A[\alpha \times \alpha]^{(0)} - \sqrt{\frac{35}{5}}B[[\alpha \times \alpha]^{(2)} \times \alpha]^{(0)} \\ &\quad + 5C([\alpha \times \alpha]^{(0)})^2, \end{aligned} \quad (3.2)$$

where  $A$ ,  $B$ , and  $C$  stand for arbitrary coefficients. The constraint  $C > 0$  is imposed to stabilize a finite deformation. Note that the square-root factors in the second of Eq. (3.2) reflect some particular values of Clebsch-Gordan coefficients and, in fact, define the proportionality constants that we skipped in Eq. (3.1).

The most general expression for the kinetic energy depends on scalar combinations containing momenta  $p$  associated with coordinates  $\alpha$ . There are many combinations of this type, namely,  $[p \times p]^{(0)}$ ,  $[[p \times \alpha]^{(2)} \times p]^{(0)}$ ,  $[[p \times p]^{(2)} \times \alpha]^{(0)}$ ,  $[[p \times p]^{(2)} \times p]^{(0)}$ , etc. In most applications, only the first term is considered,

$$T = \frac{\sqrt{5}}{2\mathcal{M}}[p \times p]^{(0)} = T_{\text{rot}} + T_{\text{vib}}, \quad (3.3)$$

where  $\mathcal{M}$  is a generalized mass parameter. The terms on the right-hand side of Eq. (3.3) represent the rotational and vibrational kinetic energies (Bohr, 1952),

$$\begin{aligned} T_{\text{vib}} &= -\frac{\hbar^2}{2\mathcal{M}} \left( \frac{1}{\beta^4} \frac{\partial}{\partial \beta} \beta^4 \frac{\partial}{\partial \beta} + \frac{1}{\beta^2 \sin 3\gamma} \frac{\partial}{\partial \gamma} \sin 3\gamma \frac{\partial}{\partial \gamma} \right), \\ T_{\text{rot}} &= \frac{1}{2\mathcal{M}} \sum_{k=1}^3 \frac{L_k^2}{4\beta^2 \sin^2 \left( \gamma - \frac{2\pi}{3}k \right)}. \end{aligned} \quad (3.4)$$

To compare predictions of the geometric model with data, one also needs operators for the electromagnetic transitions. The simplest and most important one is the  $E2$  operator, which in the general case represents a  $\lambda = 2$  tensor and can be expanded as

$$\mathcal{T}^{E2} = A\alpha^* + B[\alpha^* \times \alpha^*]^{(2)} + \dots, \quad (3.5)$$

where  $A, B, \dots$  are arbitrary coefficients. Usually only one or two terms in Eq. (3.5) are taken into account, the coefficients being derived from a model with charge uni-

formly distributed within the nuclear radius [cf. Eq. (2.4)].

As we see in Eq. (3.4), the operator corresponding to the vibrational energy is composed of derivatives with respect to  $\beta$  and  $\gamma$  and of expressions containing these variables. This is natural since vibrations are connected solely with the shape of the nucleus. The rotational energy includes operators  $L_k$  of the angular momentum components in the intrinsic frame. These operators are expressed through the Euler angles and derivatives with respect to them. The rotational energy in Eq. (3.4) still depends on shape variables  $\beta$  and  $\gamma$  through the moments of inertia  $\mathcal{I}_k(\beta, \gamma)$  present in the denominator. Therefore, the rotational and vibrational degrees of freedom are coupled together in the geometric Hamiltonian.

The complicated form of the kinetic energy makes the solution of the five-dimensional (two shape variables and three Euler angles) Schrödinger equation  $H\Psi = E\Psi$  with

$$H = T_{\text{rot}} + T_{\text{vib}} + V \quad (3.6)$$

a difficult task in general. Here we will not discuss the methods of solution and their properties, at least not in their full complexity. This is not necessary since in the macroscopic limit of the model the potential alone is capable to describe basic features of the GCM critical properties. The macroscopic limit is obtained either as  $\mathcal{M} \rightarrow \infty$  (i.e., the GCM effective mass going to infinity) or as  $\hbar \rightarrow 0$  (vanishing Planck constant implies that we are settling down into the domain of classical physics). Both possibilities are fully equivalent here because the GCM Hamiltonian contains only the combination  $\hbar^2/\mathcal{M}$  of both parameters. In this limit, the zero-point motion vanishes and the absolute minimum of the potential in one of the three angular sectors determines the shape of the ground state.

We therefore analyze the form of potential (3.2) with the aim to derive the basic GCM phase diagram shown in Fig. 12. For  $A < 0$  ( $C > 0$ ), the potential has only one minimum at  $\beta > 0$  and  $\gamma = 0$  or  $\pi/3$ , depending on the sign of parameter  $B$ . This corresponds to a deformed axially symmetric shape, either prolate or oblate. As  $A$  increases, one eventually reaches the point  $A_1 = 0$  (the vertical line in Fig. 12), where a secondary minimum of the potential appears at  $\beta = 0$ . Using the terminology of phase transformations in condensed-matter physics, this point is sometimes called spinodal. The minimum is small at first but it deepens as  $A$  increases. At the critical value  $A_c = \frac{1}{4}B^2/C$  (the thick parabola in Fig. 12), both minima, the old one at  $\beta > 0$  and the new one at  $\beta = 0$ , swap. Increasing  $A$  further, the minimum at  $\beta > 0$  flattens quickly until it disappears at the antispinodal point  $A_2 = \frac{9}{32}B^2/C$  (the thin parabola in Fig. 12). For  $A > A_2$ , there is again a single global minimum, the one at  $\beta = 0$ , which determines the spherical shape. Here is a list of the spinodal, critical, and antispinodal values,

<sup>7</sup>If considering only axially symmetric shapes, some prefer to set  $\gamma = 0$  and allow for both positive and negative values of  $\beta$ . This case is equivalent to  $\beta > 0$  and  $\gamma = 0$  or  $\pi$ , corresponding therefore to both prolate and oblate shapes having  $z$  as the symmetry axis.

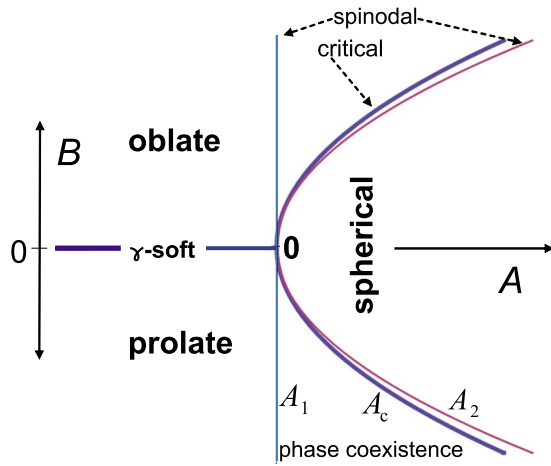


FIG. 12. (Color online) The phase diagram associated with potential (3.2) of the geometric model. The scale on both axes is determined by the chosen value of the parameter  $C > 0$  and is not shown here. The spherical-prolate, spherical-oblate, and prolate-oblate phase transitions are of the first order, except at the “triple point”  $(A, B) = (0, 0) \equiv 0$  where the transitions are of the second order.

$$A_1 = 0, \quad A_c = \frac{1}{4} \frac{B^2}{C}, \quad A_2 = \frac{9}{32} \frac{B^2}{C}. \quad (3.7)$$

Having passed the trajectory between  $A < A_1$  and  $A' > A_2$ , one has completed the deformed-to-spherical or spherical-to-deformed transformation of the nucleus. The crucial observation is that this change of shape has a critical or phase-transitional character. Indeed, as the spherical and deformed minima swap at  $A_c$  for  $B \neq 0$ , the slope (i.e., the derivative with respect to the running parameter  $A$ ) of the potential minimum energy  $E_0$  (which in the macroscopic limit coincides with the ground-state energy) changes suddenly. Such a behavior constitutes a *first-order* ground-state phase transition in terms of the Ehrenfest classification.<sup>8</sup> The curve  $A_c$ , where both potential minima are equally deep, represents the critical curve of the transition. The other curves  $A_1$  and  $A_2$  define a region of phase coexistence (spinodal region), where spherical and deformed shapes are simultaneously “present” in the spectrum of the system.

As we know, the deformed phase exists in two basic forms: with the minimum either at  $\gamma = 0$  (for  $B < 0$ ) or at  $\gamma = \pi/3$  (for  $B > 0$ ). These cases correspond to deformed prolate and deformed oblate shapes of the nucleus, respectively. Both forms transform to each other at  $B = 0$ ,

where the potential does not depend on  $\gamma$  (hence is  $\gamma$  soft). The line  $B = 0$  for  $A < 0$  constitutes a transition between the prolate and oblate shapes. Again, this transition has a critical character, defining another first-order transition. This can be verified by evaluating the first derivative of  $E_0$  with respect to  $B$ .

The phase diagram of the geometric model with the basic potential (3.2), as shown in Fig. 12, has phase transitions located along the critical parabola  $A = A_c$  and along the  $\gamma$ -soft halfline  $B = 0$  for  $A < 0$ . We found earlier that these transitions are of the first order in the sense of the Ehrenfest classification. However, there exists one exception from the first-order type of behavior: it is the point  $A = B = 0$ . When following the deformed-to-spherical transition along the  $B = 0$  line, the sombrero-shaped potential valid for  $A < 0$  changes into the quartic oscillator potential valid for  $A > 0$ . The minimum is at

$$\beta_0 = \begin{cases} \sqrt{-\frac{A}{2C}} & \text{for } A < 0 \\ 0 & \text{for } A \geq 0, \end{cases} \quad (3.8)$$

and the minimum energy  $E_0$  changes with a discontinuous second derivative  $d^2 E_0 / dA^2$  at  $A = 0$ . This defines a *second-order* ground-state phase transition with the critical exponent<sup>9</sup> equal to  $\frac{1}{2}$ . Interestingly, the intersection of the first-order transitional lines in the second-order transition constitutes a triple point of the phase diagram.

The actual realization of the simple phase diagram from Fig. 12 in atomic nuclei was disclosed with the aid of the interacting boson model (Dieperink *et al.*, 1980; Feng *et al.*, 1981; Jolie *et al.*, 2001), which will be addressed in Sec. III.B. It should be stressed that the phase structure of the above-described type was first discussed by Landau (1937) within his classical theory of phase transitions. Since an application of the Landau theory in the interacting boson model (Jolie *et al.*, 2002) requires a sophisticated formalism of coherent states (Gilmore and Feng, 1978; Gilmore, 1979) (see Sec. III.B.2), the geometric model, which yields an equivalent phase structure, was given priority here for pedagogical reasons. Note that the phase diagram from Fig. 12 can be equivalently described also in the framework of catastrophe theory (López-Moreno and Castaños, 1996) in terms of the so-called cusp catastrophe (Gilmore, 1981; Stewart, 1982). The same phase diagram will appear in the somewhat different guise of a symmetry triangle in our discussion of the IBA.

## 2. Separable and quasiseparable potentials

The shape types contained in the above-described version of the geometric collective model (with  $\lambda = 2$  and the potential up to the  $\beta^4$  term) capture the main structural

<sup>8</sup>The Ehrenfest classification (Ehrenfest, 1933) was originally elaborated in connection with thermal phase transition. It asserts that the transition is of the  $k$ th order if the  $k$ th derivative of the free energy with respect to temperature changes discontinuously at the transitional point. It turned out that such a statement is not always applicable since the derivatives may be singular. The use of the Ehrenfest classification for structural transitions of the ground state relies on the analogy between the free energy (as a function of temperature) and the ground-state energy (as a function of an external control parameter).

<sup>9</sup>Critical exponents determine the behavior of some quantities in a vicinity of the critical point in terms of power-law dependences. Here we extract the critical exponent associated with the equilibrium deformation parameter  $\beta_0$ .

paradigms of nuclear physics, namely, (i) vibrational nuclei with a spherical equilibrium shape, (ii) rotational nuclei with  $\gamma$ -rigid (axially symmetric) deformed shapes (either prolate or oblate), and (iii) rotational nuclei with  $\gamma$ -soft (axially unstable) deformed shapes (Zhang *et al.*, 1997). Possible nonaxially deformed and even more exotic shapes will be discussed in Sec. VI.A. The shape types (i)–(iii) can be obtained by a convenient (but not unique) choice of the control parameters  $A, B, C$  in the basic potential (3.2). As we saw, variation of these parameters enables one to move along various paths between the shape types. Applications of the basic geometric Hamiltonian from Eqs. (3.2) and (3.3) to nuclei in the phase-transitional regions can be found in Zhang *et al.* (1999) and Caprio (2003).

In order to improve the agreement with data while keeping the problem mathematically tractable (in an optimal case on the analytic or approximate analytic level), a plethora of other potentials has been considered in the past as well as in recent years. Although these potentials go beyond the simple form (3.2) and its extensions to higher-order terms, they mostly keep within the basic typology (i)–(iii). Two major results achieved in the last couple of years are a semianalytic description of spectra at the critical points of shape-phase transitions (Iachello, 2000, 2001) and new algebraic methods for a more efficient numerical solution (Rowe, 2004b; Turner, 2005; De Baerdemacker *et al.*, 2007; Rowe *et al.*, 2009). The critical-point geometric potentials will be discussed in Sec. V.A. Some special families of parameter-dependent potentials interpolating between different shape types will be mentioned in Sec. V.B. Here we introduce the problem of separability, which applies in a general case.

Geometric potentials proposed for analytic treatment can be sorted into two groups: either (a) they do not include a dependence on the variable  $\gamma$  or (b) they do. In the majority of cases belonging to group (b), the separation of potentials for  $\beta$  and  $\gamma$  is invoked, assuming either (Iachello, 2001)

$$V(\beta, \gamma) = V_1(\beta) + V_2(\gamma) \quad (3.9)$$

or (Wilets and Jean, 1956; Bonatsos, Lenis, McCutchan, *et al.*, 2007)

$$V(\beta, \gamma) = V_1(\beta) + V_2(\gamma)/\beta^2. \quad (3.10)$$

As discussed below, in case (3.9) the separation of variables  $\beta$  and  $\gamma$  can be done only approximately, while in case (3.10) it is exact. The dependence on  $\gamma$  is most commonly approximated by a harmonic potential  $V_2 = c\gamma^2$ , where  $c > 0$ , implying a prolate equilibrium deformation. These assumptions are not exactly consistent with the required dependence of  $V$  on the shape variable combinations from Eq. (3.1), but they can be taken as a reasonable approximation of the dynamics in the vicinity of the potential minimum.

Equipped with the above simplifications, one can find exact or approximate solutions of the GCM eigenvalue problem. In case (a) and also in case (b) with the potential of the form (3.10), the solution  $\Psi(\beta, \gamma, \Theta)$  of the five-

dimensional Schrödinger equation can be factorized to a part  $\xi(\beta)$ , depending solely on  $\beta$ , and a part  $\psi(\gamma, \Theta)$ , depending on  $\gamma$  and the Euler angles  $\Theta$  (Wilets and Jean, 1956). The second part, constrained by

$$\left[ -\frac{1}{\sin 3\gamma} \frac{\partial}{\partial \gamma} \sin 3\gamma \frac{\partial}{\partial \gamma} + \sum_{k=1}^3 \frac{(L_k/\hbar)^2}{4 \sin^2(\gamma - 2\pi k/3)} + \frac{2\mathcal{M}}{\hbar^2} V_2(\gamma) \right] \psi(\gamma, \Theta) = \Gamma \psi(\gamma, \Theta), \quad (3.11)$$

is inserted into the Schrödinger equation  $H\Psi = E\Psi$ , yielding an equation for the  $\beta$  degree of freedom

$$\left[ -\frac{1}{\beta^4} \frac{\partial}{\partial \beta} \beta^4 \frac{\partial}{\partial \beta} + \frac{\Gamma}{\beta^2} + \frac{2\mathcal{M}}{\hbar^2} V_1(\beta) \right] \xi(\beta) = \frac{2\mathcal{M}E}{\hbar^2} \xi(\beta). \quad (3.12)$$

Here  $\Gamma$  is a separation constant. The application of the above  $\beta$ – $\gamma$  separation technique is hindered by the fact that analytic solutions  $\psi(\gamma, \Theta)$  and  $\Gamma$  of Eq. (3.11) are generally not known, except for the fully  $\gamma$ -independent case (a) with  $V_2(\gamma) = 0$  (Wilets and Jean, 1956). Note that  $\psi(\gamma, \Theta)$  is sometimes further factorized as  $\eta(\gamma) D_{M,K}^{(L)}(\Theta)$ , where  $D_{M,K}^{(L)}$  stands for a Wigner function carrying angular-momentum indices. The  $\gamma$ – $\Theta$  separation cannot be done in general, but the resulting wave functions can be used as a basis for exact diagonalization. In case (b) with the potential of the form (3.9), the  $\beta$ – $\gamma$  separation is approximate already on the level of the defining differential equations. This case will be discussed more in Sec. V.A.1.

We return to the geometric description in Sec. V, where we also present some comparisons of model predictions with the data on critical-point nuclei.

## B. Interacting boson model

In previous paragraphs, collective nuclear excitations (vibrations and rotations) have been treated without referring to the underlying shell structure. As indicated in Sec. II, the origin of collective phenomena in even-even nuclei lies in the microscopic degrees of freedom, which, in spite of the progress in recent years, cannot be treated in their full complexity yet. We deal with the newest microscopic approaches to nuclear shape transitions in Sec. III.C. Here we focus on a treatment which can be placed between the phenomenological geometric model and the microscopic shell model. In the so-called interacting boson approximation (IBA), proposed by Arima and Iachello (1976, 1978, 1979), collective excitations of nuclei are described in terms of bosons, which can be associated with pairs of valence fermions.

The IBA benefits from its proximity to the phenomenological geometric approach—it allows for exact (sometimes analytic) solutions—but at the same time it keeps links to the microscopic foundations. The mapping of the IBA to the fermionic space has been extensively investigated. Early work by Otsuka *et al.* (1978) was followed by a number of related approaches [see,

e.g., Geyer and Lee (1982); Kim and Vincent (1987); Klein and Marshalek (1991)]. Also the mapping to the quadrupole phonon model, a bosonized version of the geometric model, has been analyzed (Janssen *et al.*, 1974; Blaizot and Marshalek, 1978; Klein *et al.*, 1982; Marshalek, 2006). Additional arguments supporting the IBA assumptions were given by Dukelsky and Pittel, (2001). The discussion of these microscopic aspects is beyond the scope of the present review. Below we introduce the main elements of the model and analyze its phase structure.

### 1. Dynamical symmetries and forms of the Hamiltonian

An essential ingredient of the IBA is the use of two types of bosons: an  $s$  boson, with angular momentum and parity  $\lambda^\pi=0^+$ , and a  $d$  boson, with  $\lambda^\pi=2^+$  (Arima and Iachello, 1975). The connection to the shell model is provided by the realization that these bosons can represent valence nucleon pairs (Arima *et al.*, 1977). However, they at the same time turn out to be suitable building blocks for the description of collective excitations in nuclei. One can further refine the model by including a  $g$  boson with  $\lambda^\pi=4^+$ , as well as  $p$  and  $f$  bosons with  $\lambda^\pi=1^-$  and  $3^-$ , respectively, to treat negative parity states. One can also introduce bosons that distinguish between proton pairs and neutron pairs (or in light or exotic nuclei also proton-neutron pairs). An overview of the different versions of the interacting boson model can be found in Iachello and Arima (1987), Bonatsos (1988), Casten and Warner (1988), and Frank and Van Isacker (1994). Here we mostly restrict ourselves to the simplest version of the model: a single-component  $s+d$  interacting boson model abbreviated as IBM-1.

The interpretation of  $s$  and  $d$  bosons as fermion pairs has far reaching consequences. First, the total number of bosons  $N_B$  is fixed to half of the valence nucleon number or half the number of valence holes or a combination of both. So all collective states in a given nucleus involve the same number of bosons, which is in contrast to the phonon interpretation given in Sec. II.B, where the phonon number increases with the excitation (zero for the ground state, one for the  $2_1^+$  state, etc.). In a vibrational nucleus, the ground state will be made out of  $N_B$  bosons of type  $s$ , the first excited state contains  $N_B-1$  bosons of type  $s$  and a single boson of type  $d$ , and so on for higher excitations.

Second, while the electromagnetic transitions between excited states in the collective model are insensitive to the shell structure, in the IBA they are naturally described by an appropriate combination of creation and annihilation operators of the  $s$  and  $d$  bosons. This leads to  $N_B$ -dependent transition matrix elements which reflect the effects of a finite valence space.

Third, the use of  $s$  bosons, absent from the phonon approach, has major consequences for a group theoretical treatment of the nuclear many-body problem. We have seen in Secs. II.B and III.A that vibrational as well as rotational spectra find a natural explanation in terms of very simple models, which can be incorporated in a

unified framework in the geometric collective model. The same is possible, in an elegant algebraic way, also within the IBM-1.

Symmetry considerations have played an important role in the development of the IBA (Iachello and Arima, 1987). In order to be able to implement a good angular momentum, we redefine a general boson annihilation operator  $b_{\lambda\mu}$  (where  $\lambda$  and  $\mu$  are angular momentum and magnetic quantum numbers, respectively) such that it behaves as a spherical tensor  $\tilde{b}_{\lambda\mu} = (-1)^{\lambda+\mu} b_{\lambda(-\mu)}$ , and proceed to good angular momentum ( $\Lambda$ ) generators  $[b_\lambda^\dagger \times \tilde{b}_{\lambda'}]^{(\Lambda)}$ . The  $d$  bosons, in analogy to quadrupole phonons, can be coupled to 25 combinations of the form  $[d^\dagger \times \tilde{d}]^{(\Lambda)}$  with  $\Lambda=0,1,2,3,4$ , which are generators of the algebra  $U(5)$ . The introduction of the  $s$ -boson adds 11 generators of the form  $[s^\dagger \times s]^{(0)}$ ,  $[d^\dagger \times s]^{(2)}$ , and  $[s^\dagger \times \tilde{d}]^{(2)}$ , which together with the previous ones yield 36 generators of the algebra  $U(6)$ .

We first use the fact that  $U(5)$  is a subalgebra of  $U(6)$  and that Hamiltonians made out of generators of this subalgebra describe quadrupole vibrations. Moreover, within the generators of  $U(5)$  those with  $\Lambda=1$  are proportional to the angular momentum operators, which are generators of the  $O(3)$  rotational algebra.<sup>10</sup> The latter subalgebra must be contained in all allowed decompositions of  $U(5)$  as it ensures the rotational symmetry of the system. It turns out that in between  $U(5)$  and  $O(3)$  another nested subalgebra occurs,  $O(5)$ , made by the generators with  $\Lambda=1$  and 3.

Besides the  $U(5) \supset O(5)$  chain, the  $U(6)$  algebra turns out to have two more decompositions ending with  $O(3)$ . The first one contains  $SU(3)$  and describes an axially symmetric rotor. The other chain of algebras includes  $O(6) \supset O(5)$ , which turns out to describe axially unstable ( $\gamma$ -soft) rotors. The model thus contains three basic structural limits describing (i) vibrational nuclei, (ii) axially symmetric rotors, and (iii)  $\gamma$ -soft rotors. These limits are essentially the same as in the geometric model, but in the IBM-1 they are determined by the above-described algebraic reductions.

Associated to the algebras are the groups describing the corresponding transformations. These define basis states which transform as irreducible representations (irreps) of the groups and provide relevant quantum numbers of the problem. For the IBM-1, they can be summarized as follows:

$$\begin{array}{cccccc}
 U(6) & \supset & U(5) & \supset & O(5) & \supset & O(3) & \supset & O(2) \\
 \downarrow & & \downarrow & & \downarrow & & \downarrow & & \downarrow \\
 [N_B] & & n_d & & \tau & & \nu_\Delta L & & M \\
 \\
 U(6) & \supset & SU(3) & \supset & O(3) & \supset & O(2) & & \\
 \downarrow & & \downarrow & & \downarrow & & \downarrow & & \\
 [N_B] & & (\lambda, \mu) & & K_L L & & M & & 
 \end{array} \quad (3.13)$$

<sup>10</sup>Although we consider here the special transformations with determinant +1, the notation is usually  $O(n)$  instead of  $SO(n)$ .

$$\begin{array}{ccccccccc}
\text{U}(6) & \supset & \text{O}(6) & \supset & \text{O}(5) & \supset & \text{O}(3) & \supset & \text{O}(2) \\
\downarrow & & \downarrow & & \downarrow & & \downarrow & & \downarrow \\
[N_B] & & \sigma & & \tau & & \nu_\Delta L & & M
\end{array}$$

Here  $\nu_\Delta$  and  $K_L$  stand for the so-called missing labels following from the ambiguity of the O(3) embedding. Selection rules for the quantum numbers contained in these formulas can be found in [Iachello and Arima \(1987\)](#).

The subalgebras U(5), SU(3), O(6), O(5), and O(3) yield one linear and five quadratic Casimir operators. Denoting by  $C_n[G]$  the  $n$ th-order Casimir operator of the group G, the general Hamiltonian with up to two-body interactions,

$$\begin{aligned}
H_{\text{IBM1}} = E_0 + \epsilon_d n_d + \sum_{\lambda_1 \lambda_2 \lambda'_1 \lambda'_2 \Lambda} v_{\lambda_1 \lambda_2 \lambda'_1 \lambda'_2}^{(\Lambda)} & [[b_{\lambda_1}^\dagger \times b_{\lambda_2}^\dagger]^{(\Lambda)} \\
& \times [\tilde{b}_{\lambda'_1} \times \tilde{b}_{\lambda'_2}]^{(\Lambda)}]^{(0)}, \quad (3.14)
\end{aligned}$$

can be rewritten in the following way:

$$\begin{aligned}
H_{\text{IBM1}} = E'_0 + aC_1[\text{U}(5)] + bC_2[\text{U}(5)] + cC_2[\text{O}(5)] \\
+ dC_2[\text{O}(3)] + eC_2[\text{SU}(3)] + fC_2[\text{O}(6)]. \quad (3.15)
\end{aligned}$$

In these expressions,  $\{v_{\lambda_1 \lambda_2 \lambda'_1 \lambda'_2}^{(\Lambda)}\}$  and  $\{a, \dots, f\}$  represent alternative (equivalent) sets of external control parameters, while  $E_0$  and  $E'_0$  are constants.

The chains of subalgebras in Eq. (3.13) define three standard dynamical symmetries<sup>11</sup> of the IBM-1, which are denoted as U(5), SU(3), and O(6). Additional symmetries  $\overline{\text{SU}(3)}$  and  $\overline{\text{O}(6)}$  can be obtained from phase transformations of  $s$ - and  $d$ -boson operators (see below). In each of the dynamical-symmetry limits, the Hamiltonian (3.15) is expressed solely as a sum of commuting Casimir operators belonging to the respective group chain. As a consequence, analytical formulas for the eigenvalues can be written in terms of the conserved quantum numbers associated with the chains ([Iachello and Arima, 1987](#)). The dynamical symmetries correspond to integrable Hamiltonians and their associated spectra provide the benchmarks for shapes. General Hamiltonians are not analytically soluble but can be

<sup>11</sup>The concept of dynamical symmetry ([Iachello, 1979, 2006; Bohm et al., 1988](#)) is a generalization of the invariant symmetry. A system possessing an invariant symmetry under transformations of group  $G_{\text{inv}}$  has a Hamiltonian, which can be written as a function of the Casimir operator of  $G_{\text{inv}}$  and therefore commutes with all its generators. On the other hand, a system possessing a dynamical symmetry given by a chain  $G_1 \supset G_2 \supset \dots \supset G_{\text{inv}}$  has a Hamiltonian expressed as a function of Casimir invariants of all the groups involved. The Casimir operators commute with each other and hence also with the Hamiltonian, but not with generators of all groups. Only the last group  $G_{\text{inv}}$  represents the invariant-symmetry group since its generators commute with all the Casimir operators.

solved numerically in a basis provided by any of the three limits. These Hamiltonians describe transitions between the shapes.

Another general parametrization of the IBM-1 Hamiltonian is given by the following multipole form ([Iachello and Arima, 1987](#)):

$$\begin{aligned}
H_{\text{IBM1}} = E'_0 + \epsilon_d n_d + c_1(L \cdot L) + \kappa(Q_\chi \cdot Q_\chi) \\
+ \kappa_3(T^{(3)} \cdot T^{(3)}) + \kappa_4(T^{(4)} \cdot T^{(4)}), \quad (3.16)
\end{aligned}$$

where the center dot represents a scalar product  $(A \cdot B) \equiv (-1)^\lambda \sqrt{2\lambda+1} [A^{(\lambda)} \times B^{(\lambda)}]^{(0)}$  and

$$L = \sqrt{10} [d^\dagger \times \tilde{d}]^{(1)}, \quad (3.17)$$

$$Q_\chi = s^\dagger \tilde{d} + d^\dagger s + \chi [d^\dagger \times \tilde{d}]^{(2)}, \quad (3.18)$$

$$T^{(\lambda)} = [d^\dagger \times \tilde{d}]^{(\lambda)} \quad (3.19)$$

the angular momentum vector, the quadrupole deformation tensor, and an auxiliary set of tensors of order  $\lambda$ , respectively. The parameter  $\chi$  in the quadrupole tensor (3.18) is usually restricted to  $0 \leq |\chi| \leq \sqrt{7}/2$ . Within the so-called consistent- $Q$  formalism, the same value of  $\chi$  is used to define both the quadrupole interaction and the quadrupole transition operators ([Warner and Casten, 1982; Lipas et al., 1985](#)),

$$\mathcal{T}^{E2} = qQ_\chi, \quad (3.20)$$

where  $q$  is an effective boson charge adjusting absolute units for the transition rates. The sign of  $\chi$  is connected with the deformation type. The value  $\chi = -\sqrt{7}/2$  is used in the SU(3) limit, which describes prolate rotors,  $\chi = +\sqrt{7}/2$  is used in the  $\overline{\text{SU}(3)}$  limit, which describes oblate rotors, and  $\chi = 0$  is used in the O(6) limit, which describes  $\gamma$ -unstable rotors.

From the structural viewpoint, the terms  $\propto n_d$  and  $\propto (Q_\chi \cdot Q_\chi)$  in the multipole expansion (3.16) are the most important ones. In Sec. IV, the Hamiltonian will be further simplified to either

$$H_\chi(\eta) = a \left[ \eta n_d - \frac{1-\eta}{N_B} (Q_\chi \cdot Q_\chi) \right] \quad (3.21)$$

or alternatively

$$H_\chi(\zeta) = c \left[ (1-\zeta) n_d - \frac{\zeta}{4N_B} (Q_\chi \cdot Q_\chi) \right], \quad (3.22)$$

where  $N_B$  in the denominators ensures the appropriate (for  $N_B \gg 1$ ) relative scaling of one- and two-body terms. These parametrizations are related by a transformation

$$\eta = \frac{4-4\zeta}{4-3\zeta}, \quad a = c \left( 1 - \frac{3}{4}\zeta \right) \quad (3.23)$$

and will be used interchangeably, as they are in the literature.

The simple Hamiltonians (3.21) and (3.22) are of the same type as the Hamiltonian of the well-known Ising model ([Ising, 1925](#)). They have two incompatible parts. Here the first part leads to spherical (vibrational) solu-

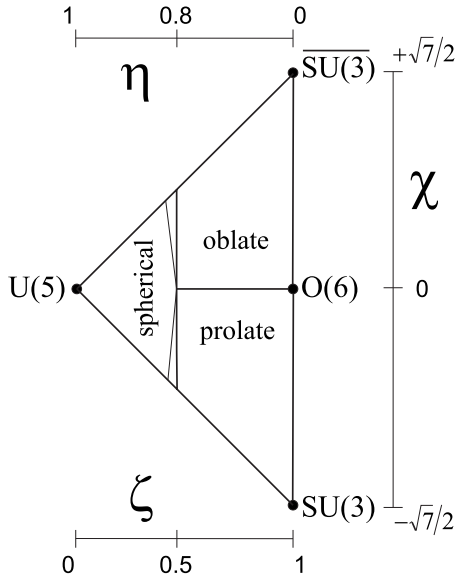


FIG. 13. An extended structural triangle of the interacting boson model. Parametrizations from Eqs. (3.21) and (3.22) are schematically shown (the  $\eta$  and  $\zeta$  axes are not in scale). The dots represent dynamical symmetries. Relevant shape phases and transitions between them are shown, the converging lines at  $\zeta \approx 0.5$  schematically indicating the regions of spherical-deformed (prolate or oblate) shape coexistence.

tions while the second part drives the system into a deformed (rotational) solutions. The parameter  $\eta$  or  $\zeta$  controls the transition between these types of dynamics. As mentioned, the parameter  $\chi$  selects the form of the deformed solution, going from prolate over  $\gamma$  soft to oblate shapes. The parameters  $a$  or  $c$  provide just an appropriate energy scale and as such they are irrelevant for the shape. So the above simplified parametrizations have just two essential control parameters.

A convenient representation of the Hamiltonians (3.21) and (3.22) is in the form of a triangle, in which the three corners correspond to the  $U(5)$ ,  $SU(3)$ , and  $\overline{SU(3)}$  dynamical symmetries, while  $O(6)$  is in the middle of the  $\eta=0$  ( $\zeta=1$ ) side (Jolie *et al.*, 2001). It is shown in Fig. 13. This triangle doubles the traditional IBM-1 triangle with vertices corresponding just to the standard dynamical symmetries  $U(5)$ ,  $SU(3)$ , and  $O(6)$  [see Casten (1981)]. For simplicity, we use the traditional triangle in the following (as in Fig. 14) whenever the path of structural evolution does not cross the prolate-oblate transition.

The  $\overline{SU(3)}$  symmetry can be derived from  $SU(3)$  by a similarity transformation keeping the energy spectrum unchanged (Shirokov *et al.*, 1998). Indeed, the upper and lower halves of the extended triangle in Fig. 13 (Hamiltonians with  $\eta$  or  $\zeta$  fixed and  $\chi = \pm|\chi|$ ) differ just by a relative sign between the  $s^\dagger$  and  $d^\dagger$  operators. Note that an analogous similarity transformation (with a relative phase factor between  $s^\dagger$  and  $d^\dagger$  equal to  $\pm i$ ) is applicable only if the term  $C_2[SU(3)]$  is missing in the Hamiltonian (3.15) (Shirokov *et al.*, 1998; Cejnar and Geyer, 2001). The corresponding isospectral partners are not included in the forms (3.21) and (3.22). In a more general param-

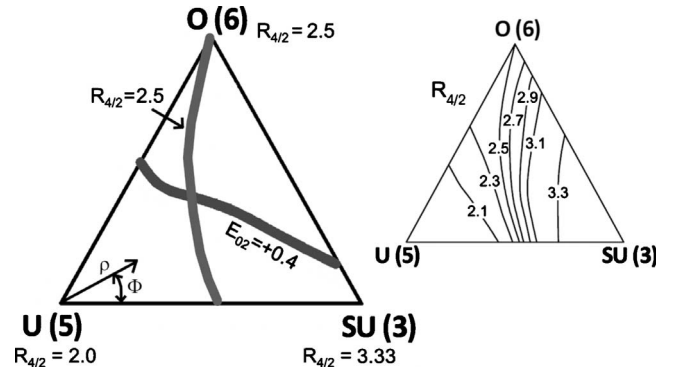


FIG. 14. The IBM-1 symmetry triangle. Left: Quantities  $\rho$  and  $\phi$  (related to  $\zeta$  and  $\chi$ ) and the idea of orthogonal crossing contours. Right: Contours of constant  $R_{4/2}$  for  $N_B=10$ .

etrization, this transformation leads to the presence of an additional dynamical symmetry  $\overline{O(6)}$  (Van Isacker *et al.*, 1985). Some consequences of the additional symmetries were discussed by Kusnezov (1997) and Cejnar and Jolie (1998a).

## 2. Coherent state formalism and phase transitions

The interacting boson model and its solutions are formulated in terms of algebras. The shape of the nucleus, on the other hand, is based on geometry. We therefore need to extract geometry from the IBA algebra. An efficient way how this can be achieved was proposed by Gilmore (1979) and subsequently applied by Dieperink and Scholten (1980), Dieperink *et al.* (1980), and Feng *et al.* (1981). The method, which relies on the so-called coset spaces and makes use of algebraic coherent states (Zhang *et al.*, 1990), applies not only to the interacting boson model in the form presented in Sec. III.B.1 but also to its various clones with the  $d$  boson replaced by bosons of other types (Cejnar and Iachello, 2007); examples include the well-known one-dimensional Lipkin model [see, e.g., Vidal *et al.* (2006)], as well as two- and three-dimensional vibron models of molecular physics [see, e.g., Dusuel *et al.* (2005b) and Pérez-Bernal and Iachello (2008)]. The use of algebraic coherent states in these models leads to a clear and physically transparent result formulated by means of boson condensate states (Bohr and Mottelson, 1980; Ginocchio and Kirson, 1980a, 1980b).

A condensate must satisfy the requirement that all  $N_B$  bosons present in the system happen to be in the same single-particle state, which in the IBM-1 case is given by a specific superposition of the  $s$  and  $d$  bosons. This means

$$|N_B, a\rangle = \frac{1}{\sqrt{N_B!}} \left[ \underbrace{\frac{1}{\|a\|} \left( a_s s^\dagger + \sum_{\mu=-2}^{+2} a_\mu d_\mu^\dagger \right)}_{\Gamma_0^\dagger} \right]^{N_B} |0\rangle. \quad (3.24)$$

Here,  $|0\rangle$  is the boson vacuum and  $a_s$ ,  $a_\mu$  (with  $\mu$

$= -2, \dots, +2$ ) stand for a “vector” of complex coefficients having a norm  $\|a\|^2 = |a_s|^2 + \sum_\mu |a_\mu|^2$ .

It has been shown (Ginocchio and Kirson, 1980b) that for a growing boson number  $N_B$  condensate states are increasingly good correlates of the IBM-1 ground-state wave function, and in the infinite-size limit they capture all its key properties. Clearly, the state (3.24) in general combines constituents with different angular momenta while the actual ground state must have a good angular-momentum quantum number  $L$ . The agreement of the results based on this technique with those of exact diagonalization is imperfect in the finite- $N_B$  cases, which can be improved by projecting the condensate state onto  $L=0$  before the variation of coefficients (Dobeš, 1985, 1990). However, the projected and unprojected results converge for  $N_B \rightarrow \infty$ , as follows from calculations using the  $1/N_B$  expansion technique (Kuyucak and Morrison, 1988), and in this limit the condensate-state approximation becomes exact.

Condensate states provide an intuitive distinction of phases of the bosonic system. If the  $N_B \rightarrow \infty$  ground state is represented by a pure condensate of  $s$  bosons, it is clear that the spherical symmetry of the system in its intrinsic frame is preserved. This corresponds to a spherical equilibrium shape. If, on the other hand, the system in its ground state condenses in a mixture of  $s$  and  $d$  bosons, then the spherical symmetry in the intrinsic frame is spontaneously broken. In this case we are dealing with a deformed equilibrium shape.

These considerations can be elaborated more quantitatively. Exploiting the freedom of choosing the overall phase factor in Eq. (3.24), we may assume  $a_s$  real. This coefficient may be then absorbed in the normalization factor,  $a_s=1$ , while the remaining coefficients can be parametrized as follows:  $a_\mu = \alpha_\mu^* + ip_\mu$ . It turns out that the components  $\alpha$  and  $p$  in this decomposition (their real or imaginary parts) are directly associated with coordinates and momenta, respectively, in the classical limit of the IBM-1 Hamiltonian (Hatch and Levit, 1982). The new components satisfy the usual relations  $\alpha_\mu^* = (-)^\mu \alpha_{-\mu}$  and the same for  $p$ , which are required for the quadrupole tensors of coordinates and momenta in the geometric collective model.

The above findings are important since they enable one to bridge the gap between the geometric collective model and the interacting boson model. This can be done by evaluating the expectation value  $\langle N_B, a | H | N_B, a \rangle \equiv F$  of a general Hamiltonian in the coherent state (3.24). The asymptotic expression  $\mathcal{H}_c(p, \alpha) = \lim_{N_B \rightarrow \infty} F(N_B, p, \alpha) / N_B$  can be associated with the classical version of the IBM-1 Hamiltonian written in terms of coordinates  $\alpha$  and momenta  $p$ .

To find the ground state in the  $N_B \rightarrow \infty$  limit (which in the IBA corresponds to the classical  $\hbar \rightarrow 0$  limit), we set the momenta  $p$  to zero (classically, the ground state corresponds just to absence of motion). For coordinates  $\alpha$ , the same parametrization as that in Eq. (3.1) can be used, yielding the IBM-1 counterparts of deformation parameters  $\beta$  and  $\gamma$ . These parameters may be directly

read out from Eq. (3.24) with the condensate boson

$$\Gamma_0^\dagger = \frac{1}{\sqrt{1 + \beta^2}} \left[ s^\dagger + \beta \cos \gamma d_0^\dagger + \beta \sin \gamma \frac{d_{+2}^\dagger + d_{-2}^\dagger}{\sqrt{2}} \right]. \quad (3.25)$$

The IBM-1 and GCM values of the deformation parameters  $\beta, \gamma$  are related by a simple proportionality relation  $\beta^{\text{IBM}} = c \beta^{\text{GCM}}$  (while  $\gamma^{\text{IBM}} = \gamma^{\text{GCM}}$ ), where  $c > 0$  is a constant.

The above-described procedure yields the following potential energy surface  $V \equiv F|_{p=0}$ :

$$V = \mathcal{E}_0 + \frac{A\beta^2 + B\beta^3 \cos 3\gamma + C\beta^4}{(1 + \beta^2)^2}. \quad (3.26)$$

Here the parameters  $\mathcal{E}_0, A, B$ , and  $C$  depend on the specific form of the IBM-1 Hamiltonian. For the Hamiltonian (3.21) with  $a=1$ , for instance, one gets  $\mathcal{E}_0 = -5(1 - \eta)$  and

$$\begin{aligned} A &= N_B \eta - (1 - \eta)(4N_B + \chi^2 - 8), \\ B &= 4\sqrt{\frac{2}{7}} N_B (1 - \eta) \chi, \\ C &= N_B \eta - (1 - \eta) \left[ \left( \frac{2}{7} N_B + \frac{5}{7} \right) \chi^2 - 4 \right], \end{aligned} \quad (3.27)$$

where we assumed  $N_B \gg 1$ .

The similarity of Eq. (3.26) with the corresponding geometric potential (3.2) is obvious. The only difference, i.e., the denominator, results from the normalization of coherent states and reflects the finiteness of the IBM-1 spectrum. Indeed, the potential (3.26) has a finite asymptotic value for  $\beta \rightarrow \infty$ , which means that the spectrum of bound states terminates at a certain maximal energy (which may differ from the asymptotic value).

The ground state can be obtained through the minimization of the potential (3.26) in  $\beta$  and  $\gamma$ . This procedure yields essentially the same phase structure as already described for the geometric model (Sec. III.A.1). We therefore do not need to repeat all the steps here and may just refer to Fig. 12. Note that the location of the spinodal curve on the right is slightly different for Eq. (3.26) than for Eq. (3.2), but this is not so important here. Otherwise, all structures remain at the same places.

Figure 12 with the bosonic content receives a qualitatively new interpretation. The spherical and deformed ground states (on the right- and left-hand sides of the critical parabola) have the following forms:

$$|\Psi_0\rangle \propto (s^\dagger)^{N_B} |0\rangle, \quad |\Psi_0\rangle \propto (s^\dagger \pm \beta_0 d_0^\dagger)^{N_B} |0\rangle, \quad (3.28)$$

respectively, where  $\beta_0$  is the value of the deformation parameter that minimizes the potential. We employed the fact that the minimum is either at  $\gamma_0=0$  or at  $\gamma_0=\pi$  (cf. footnote 7), therefore satisfying the condition  $\sin \gamma_0 = 0$ . The sign in the second formula of Eq. (3.28) distinguishes the cases with  $B < 0$  and  $B > 0$ , respectively, yielding prolate (sign +) or oblate (sign -) shapes symmetric with respect to the axis  $z$ . If  $B=0$ , the condensate can be taken with  $\gamma$  either 0 or  $\pi$ , but due to the circular

degeneracy of the potential minimum consistent results are obtained using integration of the condensate state over  $\gamma$ ,

$$|\Psi_0\rangle \propto \int_0^{\pi/3} d\gamma \sin 3\gamma \Gamma_0^\dagger(\beta_0, \gamma)^{N_B} |0\rangle, \quad (3.29)$$

that is, a projection onto good O(5) quantum number  $\tau=0$  (Ginocchio and Kirson, 1980b; Dobeš, 1990).

In Fig. 13, the spherical, prolate, and oblate ground-state shapes, which represent the three shape phases of the standard IBM-1, are drawn within the extended symmetry triangle. Although that triangle was discussed in Sec. III.B.1 in connection with the specific Hamiltonians (3.21) and (3.22), we want to stress here that it captures the phase structure of a broad class of Hamiltonians. This follows from the fact that Eq. (3.26) represents the most general form of the condensate-state energy functional for the IBM-1 with two-body interactions. Extensions following from the use of more sophisticated versions of the model will be outlined in Sec. IV.A.

For the simplified Hamiltonian (3.21) or (3.22), the decomposition (3.26) together with coefficients (3.27) enables one to calculate the critical values of control parameters  $\eta$  or  $\zeta$  and  $\chi$ . In particular, the locus of critical points for the spherical-prolate and spherical-oblate transitions is determined by

$$\eta_c \approx \frac{4 + 2\chi^2/7}{5 + 2\chi^2/7}, \quad \zeta_c \approx \frac{1}{2 + \chi^2/14}, \quad (3.30)$$

with the accuracy of order  $\mathcal{O}(N_B^{-1})$ . The critical point for the prolate-oblate transition is given by

$$\chi_c = 0 \quad (\text{for } \eta < \frac{4}{5} \text{ and } \zeta > \frac{1}{2}), \quad (3.31)$$

independently of  $N_B$ .

### 3. Mapping nuclei onto the symmetry triangle

The basic IBM-1 Hamiltonians (3.21) and (3.22) provide equivalent spectroscopic predictions for nuclei whose structure is linked to arbitrary internal points of the symmetry triangle. Here we use the Hamiltonian (3.22) since most mapping of nuclei onto the triangle has been done with this form. The dynamical symmetries correspond to the vanishing of one or the other term, along with specific choices of  $\chi=0$  or  $\pm\sqrt{7}/2$ . Interior points represent cases where both terms play a role and it is the competition between them that determines the structure.

We have often discussed structural evolution in terms of  $R_{4/2}$ . However, clearly this is not sufficient. Solutions of the basic geometric model depend on the relative values of coefficients in the potential energy (3.2), most commonly the coefficients of the terms (3.1) (cf. Fig. 12). Likewise, the simple IBM-1 Hamiltonian spans a two-dimensional triangle wherein the specification of a given point requires two coordinates. A given  $R_{4/2}$  value therefore only defines a contour in the triangle. Another observable is needed to specify a given point.

The parameter  $\zeta$  of Hamiltonian (3.22) is related to the ratio  $\epsilon_d/\kappa$  of the coefficients of the  $n_d$  and  $(Q_\chi \cdot Q_\chi)$  terms in the general form (3.16) by

$$\zeta = \frac{4N_B}{4N_B + \epsilon_d/\kappa}. \quad (3.32)$$

When the  $n_d$  term dominates, corresponding to  $\zeta \rightarrow 0$ , spherical nuclei with vibrational structure are obtained. When the  $(Q_\chi \cdot Q_\chi)$  term dominates, corresponding to  $\zeta \rightarrow 1$ , deformed nuclei result. The parameter  $\chi$  determines the  $\gamma$  softness, ranging from axially symmetric (minimum of  $V$  at  $\gamma=0$ ) for  $\chi=-\sqrt{7}/2$  (prolate case) to  $\gamma$  flat for  $\chi=0$ . Thus one can specify a position in the triangle by two quantities, one a radius vector of length  $\rho$  from U(5) to a given point and the other an angle  $\Phi$  of this vector off the U(5)-SU(3) axis. This vector is shown in Fig. 14 (left). The values of  $\rho$  and  $\Phi$  can be directly expressed in terms of  $\zeta$  and  $\chi$ .

Now consider a given value of  $R_{4/2}$ , say  $R_{4/2}=2.5$ . This is the characteristic value for O(6) arising from the  $\tau(\tau+3)$  term in the eigenvalue expression for this symmetry (Iachello and Arima, 1987). Thus, one point in the triangle corresponding to  $R_{4/2}=2.5$  is the O(6) vertex, as seen in Fig. 14 (left). However,  $R_{4/2}$  may take on a value of 2.5 elsewhere in the triangle as well. To illustrate this, note that, along the bottom axis of the triangle,  $R_{4/2}$  varies from 2.0 to 3.33 and therefore must pass through 2.5 at some point. The same argument applies inside the triangle and one can draw a contour such as that shown in Fig. 14 (left). Other values of  $R_{4/2}$  produce other contours, running more or less vertically in the triangle. Note that these contours are  $N_B$  dependent.

If we now can identify an observable whose contours run more or less perpendicularly to  $R_{4/2}$ , it should be straightforward to use empirical values of these observables to pinpoint the approximate location of a nucleus. Then, diagonalization of the IBM-1 Hamiltonian with the corresponding parameters  $\zeta$  and  $\chi$  produces a full set of energy and transition rate predictions (Harder and Tang, 1996; Chou *et al.*, 1997, 2001; McCutchan, Zamfir, and Casten, 2004; McCutchan, Casten, and Zamfir, 2005; McCutchan and Zamfir, 2005). Unfortunately, the contours of most easily measurable observables tend to run roughly parallel to the  $R_{4/2}$  contours. However, there is a class of observables that does work, constructed from energy differences of intrinsic states (cf. Sec. IV.C). The easiest to measure is

$$E_{02} = \frac{E(0_2^+) - E(2_2^+)}{E(2_1^+)}. \quad (3.33)$$

$E_{02}$  ranges from negative values along the bottom U(5)-SU(3) axis (that is, the  $0_2^+$  mode is lower than the quasi- $\gamma$  mode), through the zero value located along the arc of

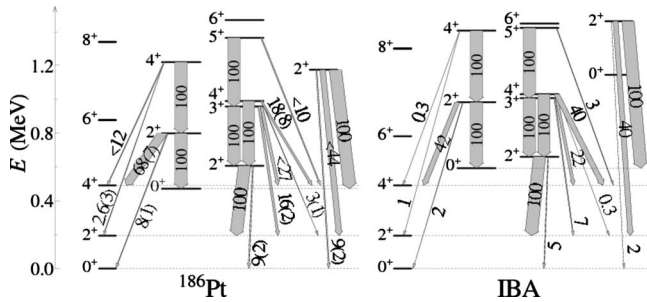


FIG. 15. Illustration of IBM-1 calculations with parameters obtained with a method closely allied to the technique of orthogonal crossing contours (McCutchan and Zamfir, 2005). The arrows represent relative  $B(E2)$  strengths.

regularity cutting through the triangle,<sup>12</sup> to positive values on the  $U(5)$ - $O(6)$  side above the arc. We illustrate the case of  $E_{02}=+0.4$  in Fig. 14. Thus, if we had a nucleus with 20 valence nucleons ( $N_B=10$ ) with empirical values  $R_{4/2}=2.5$  and  $E_{02}=+0.4$ , the crossing of these contours gives an excellent starting point for IBM-1 calculations.

This method (McCutchan and Casten, 2006) is often called the technique of orthogonal crossing contours. Generally, since Eq. (3.33) involves a difference of intrinsic excitation energies rather than a ratio, some tuning of parameters is often needed when adjusting the scale of the Hamiltonian to reproduce the scale of experimental excitation energies. If needed, additional terms such as one in  $L^2$  can be added to the Hamiltonian of Eqs. (3.21) and (3.22) although such a term is usually not needed or is quite small. In any case, it does not affect the wave functions or transition rates. As an example of this approach, Fig. 15 shows the comparison of calculated and experimental level schemes for  $^{186}\text{Pt}$ . Clearly, excellent levels of agreement can be obtained. We return to this approach in Sec. IV.B.

We note for the later discussion that calculations with the simplified IBM-1 Hamiltonians (3.21) or (3.22) near the critical points for realistic boson numbers ( $N_B \approx 10$ ) do not give spectra typical of actual transitional nuclei (e.g., they give  $R_{4/2} \approx 2.4$ ). The locus of  $R_{4/2} \approx 3$  is quite far off the phase-transitional line for such  $N_B$  but approaches it as  $N_B \rightarrow \infty$ .

### C. Fermionic approaches

The theoretical framework for the description of quantum phase transitions in nuclear shapes is not limited to the models discussed in previous sections. These transitions also appear in some fermion models of nuclear structure. In fact, the use of the term “phase

transition” in connection with nuclear shapes goes back to Thouless (1960, 1961), who worked in the context of the Hartree-Fock theory and the random phase approximation for vibrational states. Here (our prime concern being in the macroscopic models) we outline some results obtained in more microscopically oriented approaches. The interested reader is referred to the original literature for a more detailed description of these approaches.

#### 1. Phenomenological fermion models

One of the oldest fermionic many-body models in which the quantum phase transition has been much studied is the Lipkin model (Lipkin *et al.*, 1965). The model describes a system of  $N_F$  interacting fermions occupying a pair of single-particle levels, both having the same degree of degeneracy  $\Omega \geq N_F$ . Fermions on different levels interact through a pairing type of interaction. If the interaction strength is lower than a certain value, the ground state of the system has the form of a single-particle state in which all fermions are placed on the lower level (phase A). If, however, the interaction exceeds that value, the ground state becomes a superposition of single-particle configurations on both levels (phase B). We stress that the transition becomes truly critical only in the infinite-size limit ( $N_F, \Omega \rightarrow \infty$ ). This phenomenon was studied by Gilmore and Feng (1978) within the catastrophe theory for zero as well as nonzero temperatures.

There is a tight connection of the Lipkin model with the IBA. Indeed, the Lipkin model can be formulated in terms of the pseudospin  $SU(2)$  algebra of fermionic operators, which can be alternatively expressed (using the Schwinger mapping) in a bosonic way. The resulting form of the model is similar to the IBM-1 except that the  $d$  boson is replaced by a pseudoscalar  $t$  boson (Van Roosmalen, 1982; Vidal *et al.*, 2006). Using the bosonic coherent-state formalism (see Sec. III.B.2) one arrives at an equivalent description of the phase transition, with the phases A and B represented by condensates in the  $s$ -boson state and in an appropriate  $s+t$  superposition, respectively. Note that the Lipkin model became a useful toy for testing various approximations of nuclear physics as well as for investigating basic features of quantum phase transitions in many-body systems [see, e.g., Heiss (1988), Dusuel *et al.* (2005b), Leyvraz and Heiss (2005), and Arias *et al.* (2007)]. More sophisticated but still related models have been studied in connection with the pairing (superconducting) phase transition in nuclei [see, e.g., Davis and Heiss (1986), Chen *et al.* (1990), and Bahri *et al.* (1998)].

Another example of a fermionic model in which quantum phase transitions can be described exactly is the so-called fermion dynamical symmetry model (FDSM) (Ginocchio, 1980; Wu *et al.*, 1986). Designed as a fermionic counterpart of the IBA, the FDSM works with nucleon pairs of angular momentum  $\lambda=0$  (an  $S$  pair) and  $\lambda=2$  (a  $D$  pair). This is achieved by splitting the total single-nucleon angular momentum to pseudo-orbital

<sup>12</sup>The arc of increased regularity disclosed by Alhassid and Whelan (1991) and Whelan and Alhassid (1993) approximately coincides—on the deformed side of the triangle—with the degeneracy curve for the  $\beta$ - and  $\gamma$ -bandheads (Jolie, Casten, *et al.*, 2004; Macek *et al.*, 2007). A similar effect exists also in the geometric model (Stránský *et al.*, 2009a, 2009b).

and pseudospin components and assuming that only one of these components is active if two nucleons are coupled to a pair (the passive components are coupled to zero). The model is formulated in an algebraic language and possesses several dynamical symmetries, which are different from those present in the IBA. The infinite-size limit can be studied with the aid of algebraic coherent states, allowing for a similar geometric interpretation as the bosonic condensates studied above. A detailed analysis presented by [Zhang, Feng, and Ginocchio \(1988\)](#) and [Zhang, Wu, et al. \(1988\)](#) disclosed quantum (structural) phase transitions between spherical and deformed equilibrium shapes of the ground state. Similarly as in the IBM-1 case, the transitions can be of both first and second orders, depending on whether one deals with the  $\gamma$ -rigid or  $\gamma$ -soft case. In contrast to the IBM-1, however, an additional transition from axial to triaxial shapes appears as a consequence of Pauli blocking effects ([Zhang, Wu, et al., 1988](#)).

## 2. Microscopic calculations

The above-mentioned models are of a great heuristic importance as they show that quantum phase transitions of a rather similar nature as those observed within the GCM and IBA can be present also in the fermionic framework. They also allow one to perform calculations in the infinite-size limit explicitly, with the aid of algebraic coherent states. On the other hand, none of these models is sufficiently equipped for a realistic description of complex nuclei. Finite-size signatures (precursors) of the ground-state shape-phase transitions are therefore sought in truly microscopic calculations using the shell model or related approaches. Some of the relevant results were mentioned in Sec. II.C. Here we do not attempt to give an exhaustive list of references to all relevant works on the microscopic treatment of nuclear shape transitions. Instead, we sample the field by pointing out some selected analyses, illustrating the tremendous progress achieved within the last decades.

In an early work by [Federman et al. \(1979\)](#) the shell model was applied to  $^{96,98}\text{Zr}$  nuclei, with two valence protons and zero or two valence neutrons restricted just to three orbitals above the inert core of  $^{94}\text{Sr}$ . The dimensions of the Hamiltonian matrices for  $0^+$ ,  $2^+$ , and  $4^+$  states in  $^{98}\text{Zr}$  were between 35 and 145. In spite of these severe limitations, the authors were able to identify the essential factor driving the Zr nuclei to a deformed ground-state configuration (which is manifest in  $^{100}\text{Zr}$ ), namely, the residual interaction between specific proton and neutron orbitals (see Sec. II.C).

The above simple calculation can be compared with a much more recent large-scale shell model analysis by [Shimizu et al. \(2001\)](#) of the shape transition in  $^{138-150}\text{Ba}$  isotopes. The entire major shells  $50 \leq Z \leq 82$  and  $82 \leq N \leq 126$  were taken into account for 6 valence protons and 0–12 valence neutrons. To bypass the generic problem of an intractable number of basis states, a sophisticated Monte Carlo technique was used, which allowed them to select important configurations out of the whole

Hilbert space and to efficiently approximate exact diagonalization of the full shell model Hamiltonian. Realistic two-body residual interactions were employed and pairing correlations were taken into account. The calculation nicely reproduced basic trends in the spectra of the ground-band energies as well as the mass dependence of the  $B(E2:2_1^+ \rightarrow 0_1^+)$  value, showing a transition from vibrational to rotational spectral attributes within the chain of Ba isotopes.

In some cases, more instructive than evaluating the spectrum and transition rates for a given nucleus is the determination of the potential energy surface in the plane of quadrupole deformation parameters [if the  $\gamma$  degree of freedom is omitted, we speak about a potential energy curve (PEC)]. Such surfaces (or curves) are calculated by a series of variational evaluations of the lowest energy of the many-body system under changing constraints on the average quadrupole moment of the spatial density distribution. This approach was chosen, for example, by [Fossion et al. \(2006\)](#), who used the self-consistent relativistic Hartree-Fock-Bogoliubov theory to calculate PECs for Pd, Xe, Ba, Nd, Sm, Gd, and Dy isotopic chains and for some other heavy nuclei. The resulting curves display transitions between spherical and deformed (or between prolate and oblate) configurations. A similar study of a large sample of isotopic chains in various transitional regions was presented by [Robledo et al. \(2008\)](#), who extended the calculations to explore also the  $\gamma$  degree of freedom.

For a quantitative description of transitional nuclei, however, the mean-field calculations involving the standard treatment of pairing correlations are not sufficient. One needs to consider effects such as fluctuations of the deformation parameters, the restoration of rotational symmetry, and particularly the projection on a fixed particle number. Recently [Nikišić et al. \(2007\)](#) employed the relativistic density-functional formalism extended to adequately treat these effects to reproduce the shape transition in  $^{142-152}\text{Nd}$  isotopes. The results not only show the crossover from vibrational to rotational PECs and spectral characteristics but also indicate that the PEC of the transitional isotope  $^{150}\text{Nd}$  exhibits a relatively flat potential well in the variable  $\beta$  (see Fig. 16). This conforms with the assumption of the critical-point solution called X(5) for a first-order phase transition, as discussed in Secs. V.A.1 and V.A.2.

To simplify computations based on complex microscopic approaches, the constraint of a strict axial symmetry is often imposed, including the last cited work. However, [Caprio \(2005\)](#) studied  $\beta$ - $\gamma$  coupling effects in the kinetic energy term of the Bohr Hamiltonian and, in particular, the effects of  $\gamma$  stiffness on the predicted energies and transition rates and found considerable sensitivity to triaxial shapes. The importance of the  $\gamma$  degree of freedom was also examined on the microscopic level for the Nd isotopic chain by [Rodríguez and Egido \(2008\)](#), who showed that it may play a substantial role in transitional nuclei, although it does not modify the interpretation of Fig. 16.

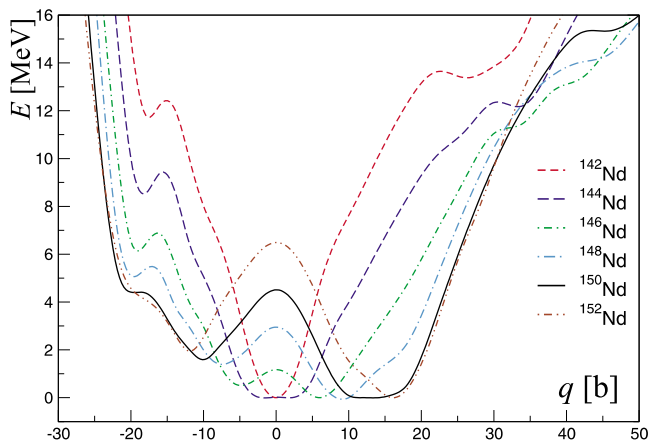


FIG. 16. (Color online) Potential-energy curves for axially deformed shapes ( $q$  is the mass quadrupole moment) calculated within the covariant density-functional formalism for a chain of Nd isotopes. From Nikšić *et al.*, 2007. Extended calculations (Rodríguez and Egidio, 2008; Li *et al.*, 2009) indicate that the oblate “minima” ( $q < 0$ ) are saddle points in the  $\beta$ - $\gamma$  plane.

The prospect of a systematic solution of this problem was outlined by Nikšić *et al.* (2009). They introduce a general geometric Hamiltonian and exploit the extended relativistic density-functional theory to determine all its unknown inputs (mass parameters, moments of inertia, and the collective potential) as functions of both quadrupole shape variables  $\beta$  and  $\gamma$ . The resulting geometric Hamiltonian is then solved numerically to obtain collective spectra and transition rates, results of these calculations being compared with experimental data in well-deformed Gd nuclei. Although these calculations were not performed in the shape-transitional region, this work opened the route for future studies and has been followed up by Li *et al.* (2009), who analyzed shape transitions in the Nd isotopes, including triaxial shapes. They confirmed the rapid structural changes at  $N=90$  and found that the phase transition is sharpest for  $^{150}\text{Nd}$  ( $^{152}\text{Sm}$  and  $^{154}\text{Gd}$ , in their calculations, are slightly past the critical point) where the resulting potential shows a rather flat bottom for a prolate shape, similar to X(5). Other recent microscopic calculations can be found in Meng *et al.* (2005), Sheng and Guo (2005), and Yu *et al.* (2006).

Finally, we note a new approach (Nomura *et al.*, 2008) which used a Skyrme Hartree-Fock plus BCS calculation on the microscopic side to guide the choice of parameters for a proton-neutron IBA Hamiltonian on the collective side. This offers preliminary indications that it might be possible to blend microscopic and macroscopic approaches to benefit from their complementarity in starting from nucleonic and many-body degrees of freedom, respectively.

To conclude this section, we note that fully microscopic calculations of the structure of heavy nuclei based on reliable nucleon interactions are still an ultimate task for future studies. Since progress in this field has accelerated dramatically in the past couple of years, one may also expect a rapid increase of knowledge on the nature

of nuclear shape transitions. We should stress that because the finite size of atomic nuclei is naturally built into the microscopic treatment, such calculations can never show really discontinuous shape transitions as those observed in the macroscopic models. Below, we focus on the description of shape-transitional nuclei by means of the IBA and GCM.

#### IV. SHAPE TRANSITIONS IN THE INTERACTING BOSON MODEL

In this section, the interacting boson model (introduced in Sec. III.B) will be applied in the description of atomic nuclei located in the shape-transitional regions of the structural triangle in Fig. 13. Section IV.A presents some introductory concepts and discusses the possibilities to detect the QPT behavior in finite nuclear systems. In Sec. IV.B, we focus on the specific signatures of various types of shape phase transitions in nuclei and their comparison with the IBM-1 predictions. Finally, Sec. IV.C presents a theoretical interpretation of these results in terms of quasidynamical symmetries. Application of the geometric model in transitional nuclei will be presented in Sec. V.

##### A. Finite-size precursors of quantum phase transitions

We use the simple IBM-1 Hamiltonian (3.21) to describe the spectra of nuclei going across spherical-deformed and prolate-oblate phase transitions. The interacting boson model deals in its actual application to nuclei with a limited number of bosons  $N_B$ , typically between 4 and 20. Therefore, strictly speaking, the signatures of quantum phase transitions that we may observe in nuclei are only precursors of real phase transitions, which would only occur for an infinite size of the nucleus (hence infinite number of bosons).<sup>13</sup> This property is common also to many other quantum systems, but in the case of nuclei we deal with a genuinely quantum object having at the same time numerous mesoscopic attributes.

Calculations allow a detailed study of phase-transitional behavior using a continuous variation of the control parameters and high boson numbers, making the precursors of the shape phase transitions more pronounced (Frank, 1989; Casten *et al.*, 1999; Cejnar and Jolie, 2000). As an example consider the Hamiltonian (3.21) with  $\eta=0$ . In this case the Hamiltonian contains one free parameter  $\chi$ , which we vary from the SU(3) value ( $\chi=-\sqrt{7}/2$ ) over the O(6) value ( $\chi=0$ ) to the SU(3) value ( $\chi=+\sqrt{7}/2$ ). In an inset of Fig. 17 the absolute energy of the ground state is shown. In the O(6) limit, i.e., at  $\chi=0$ , the energy of the ground state makes a kink whose sharpness increases with  $N_B$ . The first derivative

<sup>13</sup>A discontinuous change of the ground-state properties in a finite system is, in fact, possible if there exists a real crossing of the two lowest energy eigenstates [see, e.g., Arias, Dukelsky, and García-Ramos (2003)].

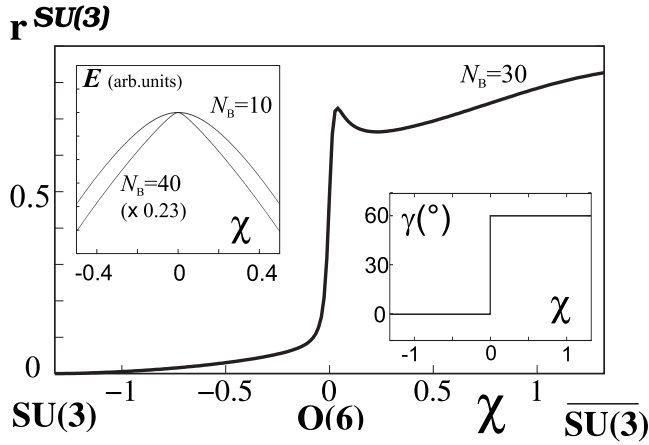


FIG. 17. The prolate-oblate transition for the Hamiltonian (3.21) with  $\eta=0$ . The main panel shows an exponential of the SU(3) wave function entropy (see text) for  $N_B=30$ . Insets: The ground-state absolute energy for  $N_B=10$  and 40, and the evolution of the shape parameter  $\gamma$ .

of the ground-state energy becomes discontinuous when  $N_B$  goes to infinity, indicating the first-order transition between prolate and oblate shapes. In the other inset of Fig. 17 the location of the potential energy minimum in  $\gamma$  (order parameter for the prolate-oblate transition) is drawn as a function of  $\chi$ , showing a flip from  $\gamma_0=0$  to  $\gamma_0=\pi/3$  [or, equivalently, to  $\gamma_0=\pi$  (see Fig. 11)] when  $\chi$  passes through zero.

A useful quantity to probe the critical character of a particular transition is the wave function entropy  $W = -\sum_i |a_i|^2 \ln |a_i|^2$ , which quantifies the fragmentation of a given eigenvector  $|\Psi\rangle = \sum_i a_i |\phi_i\rangle$  in a selected basis  $|\phi_i\rangle$  (Cejnar and Jolie, 1998a, 1998b). For the prolate-oblate phase transition, the SU(3) wave function entropy  $W_0^{\text{SU}(3)}$  measuring the spread of the ground state  $|\Psi_0\rangle$  in the SU(3) basis is most convenient. In the main panel of Fig. 17 we show the dependence of  $r_0^{\text{SU}(3)} \propto [\exp(W_0^{\text{SU}(3)}) - 1]$  on  $\chi$ . While  $r_0^{\text{SU}(3)}=0$  implies perfect localization of the ground state in the SU(3) basis, the normalization is chosen so that the case  $r_0^{\text{SU}(3)} \approx 1$  corresponds to a completely random overlap (obtained as an average for a randomly generated basis). We observe that the entropy exhibits a steplike increase around  $\chi=0$ , meaning that the wave function of the ground state gets spread significantly in the SU(3) basis just in a vicinity of the first-order critical point. The entropy in the  $\overline{\text{SU}(3)}$  basis would yield a complementary picture.

The control parameter for these changes is the value of  $\chi$  in the quadrupole operator. This brings in a subtle point. In a standard situation, the control parameter represents a linear weight factor between two competing parts of the Hamiltonian governing the phase transformation. Although linearity is not a necessary condition, it facilitates the analysis of the QPT effects [see, e.g., Cejnar and Jolie (2009) and Sec. VI.B]. This is fulfilled for the dependence on  $\eta$  but not for  $\chi$ , which enters the Hamiltonian (3.21) quadratically. Nevertheless, a linear

dependence is recovered in a local regime since near O(6) one obtains

$$H = -\frac{a}{N_B} [Q_0 \cdot Q_0 + \chi(Q_0 \cdot T^{(2)} + T^{(2)} \cdot Q_0) + \mathcal{O}(\chi^2)], \quad (4.1)$$

where  $Q_0$  (more clearly,  $Q_{\chi=0}$ ) and  $T^{(2)}$  are defined in Eqs. (3.18) and (3.19), respectively.<sup>14</sup>

Although the QPT behavior is seen in the evolution of the ground state, it is useful to see the dynamics of the whole spectrum in the transition through the critical point. Figure 18 shows absolute energies of all  $0^+$  eigenstates of the Hamiltonian (3.21) for  $N_B=30$  for three paths in the parameter plane: the one with  $\chi=-\sqrt{7}/2$  for the prolate-spherical transition (upper panel), the one with  $\eta=0$  for the prolate-oblate transition (middle panel), and the one with  $\chi=0$  for the  $\gamma$ -unstable-spherical transition (lower panel). Locations of the dynamical symmetries at the beginning and end of each trajectory are indicated.

One observes the phase transitions between spherical and deformed shapes around  $\eta=0.8$ , where the ground-state energy in the upper and lower panels suddenly becomes negative (on the deformed side). Also observable is the difference between first- and second-order phase transitions (upper and lower panels, respectively), whereby the latter exhibits a much smoother dependence. This is more clearly demonstrated in the upper and lower insets of Fig. 18 by the peaks of the second derivative of the ground-state energy. The quantity  $c_1 \propto -\eta d^2 E_0 / d\eta^2$ , displayed in the insets for  $N_B$  increasing from 10 to 80, is significant for the first- and second-order transitions. While the  $N_B \rightarrow \infty$  limit of  $c_1$  has a singularity of the  $\delta$ -function type in the first-order transition, it shows just a discontinuity in the second-order transition. For finite  $N_B$ , the observed dependence is always smooth and we see that the second derivative of  $E_0$  acts as a “magnifying glass” strongly emphasizing deviations from the infinite-size limit.

Since all states shown have the same angular momentum, there are some interesting effects connected to the symmetries present. At the four dynamical symmetry points some levels can cross without interaction as these points are characterized by good quantum numbers.<sup>15</sup> Especially at the U(5) dynamical symmetry large degeneracies are observed due to the absence of anharmonic

<sup>14</sup>Since  $\chi$  occurs in Eq. (4.1) in both linear and quadratic terms, the Hamiltonian is not a simple mirror reflection around  $\chi=0$ . On the other hand, the  $\chi<0$  and  $\chi>0$  halves of the dependence are connected by a unitary transformation  $(s^\dagger, d^\dagger) \mapsto (s^\dagger, -d^\dagger)$ , which ensures complete symmetry of the energy spectrum. This is a special case of the parameter symmetry discussed in Sec. III.B.1.

<sup>15</sup>Crossing of levels  $E_i$  and  $E_j$  requires that the difference of the respective diagonal elements of the Hamiltonian matrix vanishes simultaneously with the nondiagonal matrix element, which is unlikely except if the interaction of levels is zero due to symmetry constraints (von Neumann and Wigner, 1929).

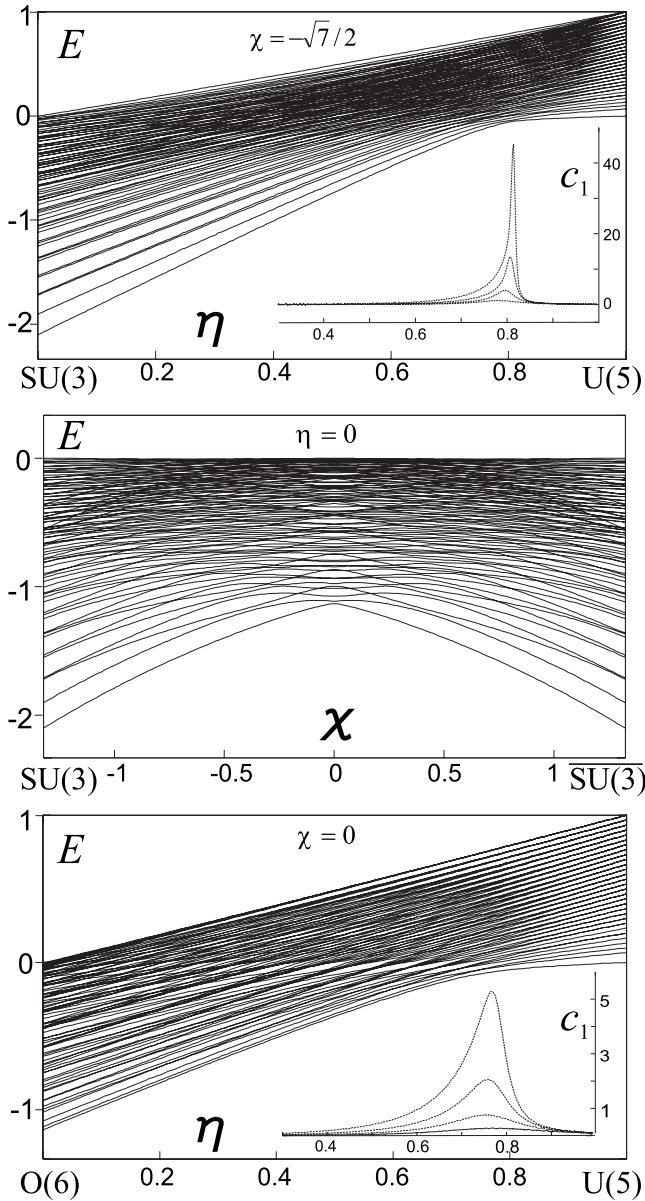


FIG. 18. Calculated absolute energies (arbitrary units) of all  $0^+$  states of the Hamiltonian (3.21) as a function of the respective control parameter for the prolate-spherical (top), prolate-oblate (middle), and  $\gamma$ -soft-spherical (bottom) transitions for  $N_B=30$ . The upper and lower insets show the quantity  $c_1$  (see text) in arbitrary units for  $N_B=10, 20, 40$ , and  $80$  increasing from lower to higher curves.

terms in the Hamiltonian. At O(6) in the middle panel, avoided level crossings occur when  $\chi$  differs from zero, but most levels are also nondegenerate at  $\chi=0$ . Around this point it is clear that the ground state and the first excited state interchange character and one can follow each state through its mixing with several states.

On the  $\eta < 0.8$  side of the second-order critical point of the O(6)-U(5) transition, in the lower panel of Fig. 18, one observes a bunching of levels with real crossings also present. The crossings are due to the fact that  $\tau$ , the O(5) quantum number called seniority, is preserved along the whole path between O(6) and U(5). The level

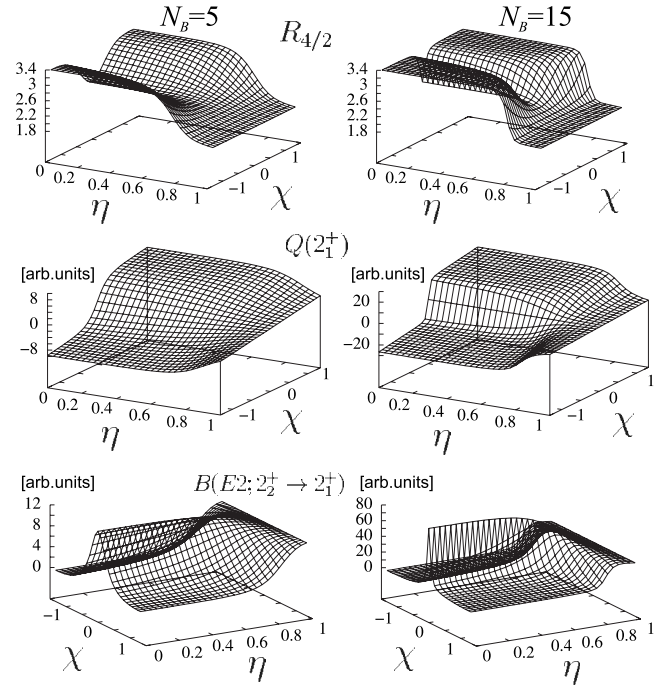


FIG. 19. Calculated values of  $R_{4/2}$ ,  $Q(2_1^+)$ , and  $B(E2; 2_2^+ \rightarrow 2_1^+)$  for the Hamiltonian (3.21) with  $N_B=5$  (left) and  $N_B=15$  (right).

dynamics for this transition can then be studied as a function of  $\tau$  (Heinze *et al.*, 2006). Such an analysis shows that levels with the same values of  $\tau$  exhibit a series of avoided crossings located in the bunching region. The sharpness of avoided crossings increases with decreasing  $\tau$ . As discussed in Sec. VI.C, these phenomena indicate nonanalytic evolutions of individual excited states in the limit  $N_B \rightarrow \infty$  (Cejnar *et al.*, 2006; Macek *et al.*, 2006). It can be shown that the bunching demarcates a border between the parts of the spectrum related to the limiting dynamical symmetries; while the U(5)-like part is located above the bunching, the O(6)-like part resides below it.

We now focus our attention to other observables that can be used to search for shape phase transitions in nuclei. Figure 19 shows some of observables discussed in Sec. II.B as functions of both  $\eta$  and  $\chi$  for  $N_B=5$  and  $15$ , namely, the energy ratio  $R_{4/2}$ , the quadrupole moment  $Q(2_1^+)$  of the first excited state, and a strength  $B(E2; 2_2^+ \rightarrow 2_1^+)$  of the  $E2$  transition between the first and second  $2^+$  states. The locations of the prolate-oblate and spherical-deformed transitions are clearly observed as the places of sudden changes of the observables. While  $R_{4/2}$  illustrates well the three different regions, it does not provide a unique signature for the determination of the deformation type. This can be achieved using  $Q(2_1^+)$  displayed in the middle panel of Fig. 19. The quadrupole moment of the first excited  $2^+$  state is directly proportional to the ground-state order parameter  $\beta_0$  when using the sign convention introduced in Sec. III.B.2. Therefore the middle panel shows the abrupt change in the order parameter, which flips from zero to positive or negative values at the spherical-deformed phase transi-

tion and from negative to positive at the prolate-oblate phase transition. The third observable, the  $B(E2:2_2^+ \rightarrow 2_1^+)$ , peaks sharply at the prolate-oblate phase transition. It shows almost exactly the opposite behavior as the  $R_{4/2}$  ratio. While for  $N_B=5$  the dependence of all observables at the phase transitions is rather smooth, already the use of 15 bosons makes the changes much sharper.

Several studies have used calculations with high boson numbers to analyze the QPT precursors in the interacting boson model [see, e.g., Cejnar and Jolie (2000), Arias, Alonso, *et al.* (2003), Arias, Dukelsky, and García-Ramos (2003), Cejnar *et al.* (2003, 2005, 2007), Rowe (2004a), García-Ramos, Dukelsky, and Arias (2005), Pan, Zhang, and Draayer (2005), Turner and Rowe (2005), Vidal *et al.* (2006), and Williams *et al.* (2008)]. These works are reviewed by Cejnar and Jolie (2009) and will be discussed in Sec. VI.B.

### B. Description of structural evolution in the symmetry triangle

So far we have mostly discussed the results at large values of  $N_B$ , for which the QPT signatures are most pronounced. In this section, the experimental evidence of shape phase transitions in real nuclei will be analyzed, hence calculations at low  $N_B$  become more relevant.

#### 1. Signatures of first-order phase transitions

Since the early days, the IBA was used not only to describe nuclei (such as  $^{110}\text{Cd}$ ,  $^{196}\text{Pt}$ , or  $^{156}\text{Gd}$ ) that constitute specific realizations of the dynamical symmetries (3.13) but also as a tool providing concrete predictions for nuclei located between the symmetry limits. The phase-transitional character of structural changes inside the symmetry triangle soon became an important issue (Dieperink and Scholten, 1980; Dieperink *et al.*, 1980). The first work on a systematic comparison of IBM-1 calculations with experimental data for the transitional region between U(5) and SU(3) dynamical symmetries was by Scholten *et al.* (1978). They studied in particular the samarium isotopes as examples of nuclei showing the spherical-deformed transition. It was found that  $^{152}\text{Sm}$  is located indeed close to the transitional region, some consequences being later discussed (already in the QPT context) by Casten *et al.* (1998), Iachello *et al.* (1998), and Jolie *et al.* (1999). Subsequent experimental studies, which will be described in Sec. V in connection with the X(5) critical-point solution, showed that this was the case for several  $N=90$  isotones (McCutchan, Zamfir, and Casten, 2005).

Detailed IBM-1 calculations of rare earth nuclei were done by García-Ramos *et al.* (2003). Chains of Nd, Sm, Gd, and Dy isotopes were fitted using the simple form (3.21) as well as a more general IBM-1 Hamiltonian. Good descriptions for the excitation energies and the  $B(E2)$  values were obtained together with the two-neutron separation energies  $S_{2n}$ . The latter are extracted from the calculated absolute energies  $E_0$  of the IBA

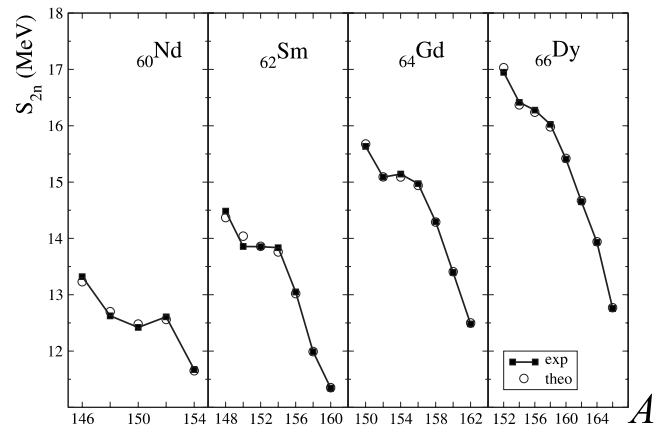


FIG. 20. Two-neutron separation energy for Nd, Sm, Gd, and Dy isotopes as a function of  $A$ . The IBM-1 predictions are drawn by solid lines. From García-Ramos *et al.*, 2003.

ground state for the two nuclei differing by two neutrons; therefore they can be considered as direct signatures of the QPT behavior (Dieperink *et al.*, 1980). If  $\xi$  and  $\xi'$  stand for the model control parameters (or sets of parameters) corresponding to both nuclei, while  $N_B$  and  $N_B+1$  are the associated boson numbers (for simplicity we assume nuclei below the midshell), the two-neutron separation energy is obtained using  $S_{2n}=E_0(\xi', N_B+1) - E_0(\xi, N_B) + \varepsilon$ , where  $\varepsilon$  is a constant shift adjusting the absolute energy. This yields

$$S_{2n} \approx \varepsilon + \frac{\partial E_0}{\partial N_B} + \frac{\partial E_0}{\partial \xi}(\xi' - \xi). \quad (4.2)$$

The calculated results (obtained by fitting the model parameters  $\xi$  with respect to specific low-energy observables in each nucleus) are shown in Fig. 20 along with experimental values. Since the dominant dependence of  $E_0$  on  $N_B$  is quadratic, the first two terms of Eq. (4.2) yield a smooth roughly linear decrease of  $S_{2n}$  with increasing neutron number  $N$  (or mass number  $A$ ). This is in agreement with the data. However, one expects an irregular dependence of  $S_{2n}$  at the first-order QPT points, where the last term of Eq. (4.2) is discontinuous in the infinite-size limit. Indeed, the experimental and theoretical plots show well distinguished “plateaux,” where the decrease of the separation energy with  $A$  is interrupted. As explained in Sec. II.B.3, these plateaux indicate the gain of energy due a rapid onset of deformation.

The behavior of other observables also gives information on the spherical-to-deformed shape evolution. Figure 21 shows  $E2$  strengths of the two lowest transitions in the ground-state bands of Sm and Gd. Experimental values are in a satisfactory agreement with the calculated ones, obtained by García-Ramos *et al.* (2003) using the same values of the IBM-1 parameters as in Fig. 20. As explained in Sec. II.B, the observed rise of  $B(E2)$  values for the ground-state band transitions indicates the onset of deformation for both nuclei localized in the critical region  $N \approx 90$ . Various  $B(E2)$  values and other

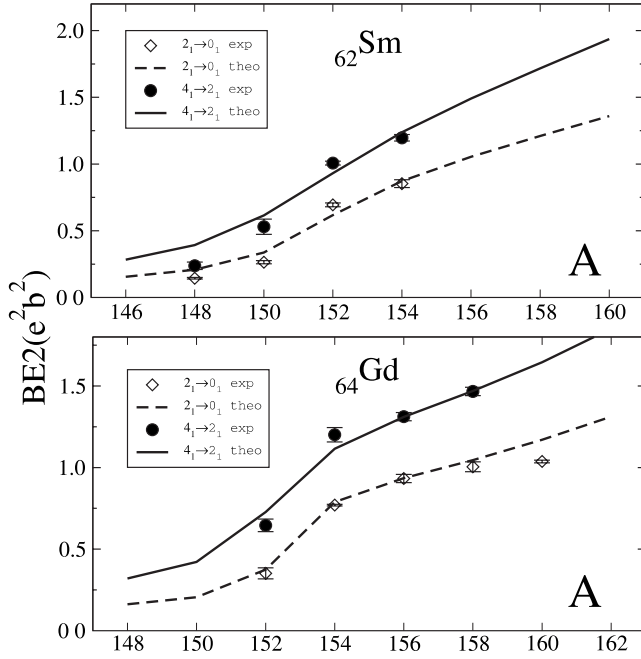


FIG. 21. Calculated and measured  $B(E2)$  values for the  $2_1^+ \rightarrow 0_1^+$  and  $4_1^+ \rightarrow 2_1^+$  transitions in Sm and Gd isotopes as a function of  $A$ . Adapted from [García-Ramos \*et al.\*, 2003](#).

observables were compared with the IBM-1 predictions for several chains of nuclei going across the first-order spherical-deformed phase transition by [Scholten \*et al.\* \(1978\)](#), [McCutchan, Zamfir, and Casten \(2004\)](#), and [García-Ramos, Heyde, \*et al.\* \(2005\)](#).

As discussed in Sec. II.B.4, another clear indicator of the transition to deformed shapes is a rapid increase in the rate of the  $E0$  transition between the ground state and  $0^+$  excited states on the deformed side of the transition. In the IBM-1, the  $E0$  transitional operator is given ([Iachello and Arima, 1987](#)) by

$$\mathcal{T}^{E0} = \mathcal{A}s^\dagger s + \mathcal{B}[d^\dagger \times \tilde{d}]^{(0)} = \mathcal{A}N_B + \left(\frac{\mathcal{B}}{\sqrt{5}} - \mathcal{A}\right)n_d, \quad (4.3)$$

with  $\mathcal{A}, \mathcal{B}$  adjustable coefficients, where only the second term in the last expression is relevant. The summed  $E0$  strength  $\sum_{i>0} |\langle 0_1^+ | \mathcal{T}^{E0} | 0_i^+ \rangle|^2$  for transitions to the ground state from all  $0^+$  states yields a value proportional to  $\delta \langle n_d^2 \rangle_{0_1^+} \equiv \langle 0_1^+ | n_d^2 | 0_1^+ \rangle - \langle 0_1^+ | n_d | 0_1^+ \rangle^2$ , which is the dispersion of the number of  $d$  bosons in the ground-state wave function. Clearly, for the spherical phase we get  $\delta \langle n_d^2 \rangle_{0_1^+} / N_B = 0$  in the limit  $N_B \rightarrow \infty$ , while in the deformed phase it is greater than zero. The calculation for the  $0_2^+ \rightarrow 0_1^+$  transition, performed by [von Brentano \*et al.\* \(2004\)](#), is in agreement with existing  $E0$  data for shape-transitional nuclei ([Wood \*et al.\*, 1999](#)) as well as with a recent measurement for  $^{154}\text{Sm}$  ([Wimmer \*et al.\*, 2009](#)). A comparison of experimental and theoretical  $\rho(E0)^2$  values is shown in Fig. 22.

The evolution of two identical particle transfer intensities (cf. Sec. II.B.4), as well, has been proposed as a

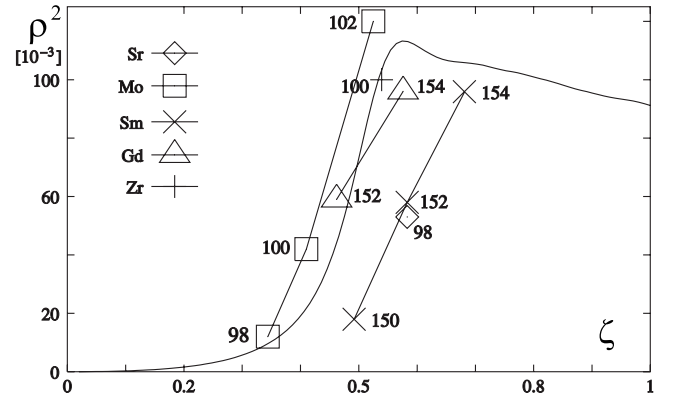


FIG. 22. Values of  $\rho^2(E0:0_2^+ \rightarrow 0_1^+)$  for Sr, Mo, Sm, Gd, and Zr isotopes close to the spherical-deformed phase transition ([von Brentano \*et al.\*, 2004](#)). Measured strengths are drawn vs the fitted value of  $\zeta$  from the parametrization (3.22) and compared with the IBM-1 prediction (full line). Figure courtesy of V. Werner.

specific indicator of shape phase transitions ([Fossion \*et al.\*, 2007](#)). Their evaluation in the IBM-1 framework is possible with a general form of the  $L=0$  pair transfer operator ([Iachello and Arima, 1987](#))

$$\begin{aligned} \mathcal{T}_{2n}^\dagger = & \mathcal{A}s^\dagger + \mathcal{B}[[d^\dagger \times d^\dagger]^{(2)} \times \tilde{d}]^{(0)} + \mathcal{C}[d^\dagger \times d^\dagger]^{(0)}s \\ & + \mathcal{D}s^\dagger[d^\dagger \times \tilde{d}]^{(0)} + \mathcal{E}s^\dagger s^\dagger s \end{aligned} \quad (4.4)$$

or with its various simplifications such as  $\mathcal{T}_{2n}^\dagger \propto s^\dagger$  employed by [Fossion \*et al.\* \(2007\)](#). For instance, the transfer intensity to the ground state can be obtained within the coherent-state formalism using  $I_{\text{gs} \rightarrow \text{gs}} \propto |\langle N_B + 1, \beta'_0 | \mathcal{T}_{2n}^\dagger | N_B, \beta_0 \rangle|^2$ , where  $\beta_0$  and  $\beta'_0$  are the ground-state deformation parameters associated with the initial and final nuclei characterized by boson numbers  $N_B$  and  $N_B + 1$ , respectively. Evaluation of the transfer amplitude shows that the ground and excited  $0^+$  state cross sections are strongly sensitive to changes in  $\beta$  ([Fossion \*et al.\*, 2007](#)). It has recently been shown ([Clark \*et al.\*, 2009](#)) that  $(p, t)$  and  $(t, p)$  cross sections depend on the magnitude of the change in structure (change in  $\zeta$  or  $\eta$ ) between initial and final nuclei. Large changes in  $R_{4/2}$ , for example, are expected to yield large cross sections to excited  $0^+$  states even in regions where there is no phase transition. However, first-order phase transitional regions (with large changes in  $R_{4/2}$ ) are the most obvious case where the two-nucleon transfer cross sections will be most shared between ground and excited  $0^+$  states, as indeed seen in Fig. 8.

Global properties of the spectrum of  $0^+$  excited states also carry important information on collectivity ([Chou \*et al.\*, 2001](#)). It turns out that at the spherical-deformed phase transition, the spectrum is considerably compressed in energy ([Cejnar and Jolie, 2000](#)). This can be understood in terms of a widening of the potential energy surface in the parameter region close to the critical point. Using the  $(p, t)$  reaction, an extended search for  $0^+$  states covering a large number of even-even rare-

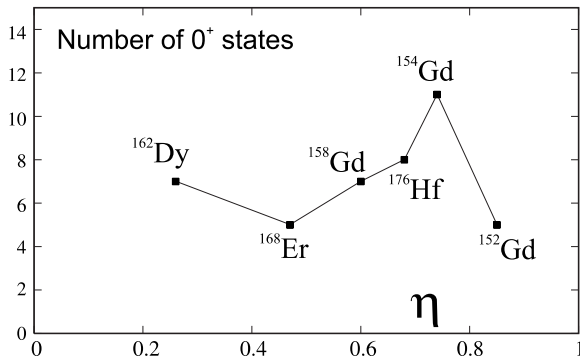


FIG. 23. Number of observed  $0^+$  states below 2.5 MeV as a function of  $\eta$  (see text). The lines just connect experimental points.

earth nuclei was performed at the Garching Q3D spectrometer (Meyer *et al.*, 2006). With this reaction and with the very high sensitivity and resolution of the spectrometer, it was possible to identify the  $0^+$  states up to relatively high energies. Figure 23 shows the observed numbers of  $0^+$  states below 2.5 MeV in a couple of nuclei as a function of parameter  $\eta$  [see Eq. (3.21)] determined by the technique of orthogonal crossing contours (see Sec. III.B.3). An increase of the  $0^+$  state density at low energy was observed for  $^{154}\text{Gd}$ , which is located close to the phase-transitional point  $\eta=0.8$ .

The technique of orthogonal crossing contours (McCutchan and Casten, 2006) has been extensively used to map the locations of many nuclei in the triangle. Using the simple Hamiltonian (3.22), McCutchan, Zamfir, and Casten (2004), McCutchan, Casten, Zamfir (2005), and McCutchan and Zamfir (2005) performed systematic fits of Gd-Pt isotopes, which allow the location of these isotopes in the triangle. This mapping and the trajectories of structural evolution it illustrates are shown in Fig. 24. It was found that the first-order phase transition is crossed in the interior of the triangle for

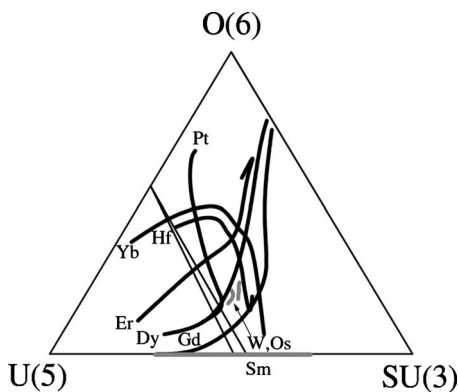


FIG. 24. Trajectories of structural evolution of nuclei in the rare earth region from calculations using an approach based on the method of orthogonal crossing contours (McCutchan, Zamfir, and Casten, 2004; McCutchan, Casten, and Zamfir, 2005; McCutchan and Zamfir, 2005). Two slant lines across the triangle demarcate the region of spherical-deformed phase coexistence.

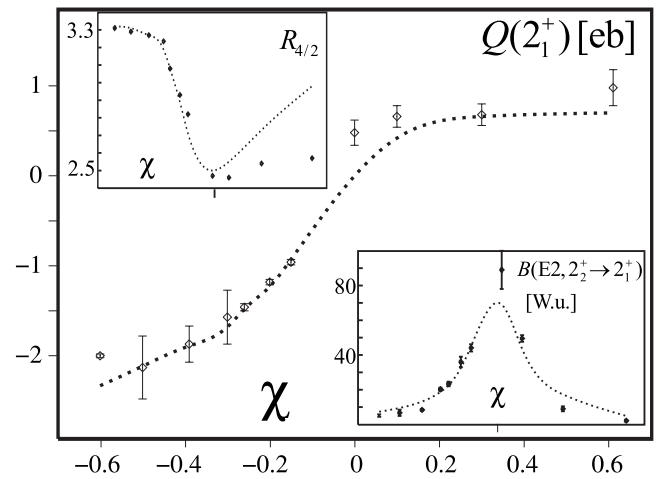


FIG. 25. Experimental values of  $Q(2_1^+)$  (the main panel),  $R_{4/2}$  (upper inset), and  $B(E2: 2_2^+ \rightarrow 2_1^+)$  (lower inset) for  $^{180}\text{Hf}$ ,  $^{182,184,186}\text{W}$ ,  $^{188,190,192}\text{Os}$ ,  $^{194,196}\text{Pt}$ , and  $^{198,200}\text{Hg}$  vs the fitted value of parameter  $\chi$  in the prolate-oblate transition (the  $\chi$  axes in insets have the same scale as the main plot). Adapted from Jolie and Linnemann, 2003.

$^{154}\text{Dy}$  and  $^{156}\text{Er}$ , while  $^{152}\text{Gd}$  lies on the U(5)-SU(3) leg before the phase transition and  $^{154}\text{Gd}$  lies close to it after the transition. As noted, Scholten *et al.* (1978) found the same behavior for  $^{152}\text{Sm}$ . The Yb and Hf isotopes do not cross the phase transition on the U(5)-SU(3) side, that is, all isotopes considered here are on the deformed side.

Finally we focus on the question whether there exist chains of nuclei showing the first-order transition between prolate and oblate shapes. Although nuclei with a well pronounced oblate deformation or those between the  $\gamma$ -soft and oblate forms are rather rare, they do occur in the Pt and Hg isotopes close to the well-known O(6) nucleus  $^{196}\text{Pt}$ . The three different observables from Fig. 19 were used by Jolie and Linnemann (2003) to identify the prolate-oblate transition in the neighboring nuclei. In an attempt to span a large part of the extended symmetry triangle we plot these quantities in Fig. 25 for nuclei ranging from the well-deformed prolate rotor  $^{180}\text{Hf}$  to  $^{200}\text{Hg}$ . A fit of the parameter  $\chi$  in the simple Hamiltonian (3.21) was performed in each nucleus associated with a specific  $N_B$ , the resulting value being shown on the abscissa of Fig. 25. Clearly, the quadrupole moments indicate the prolate-oblate phase transition and the other observables support this type of shape change.

## 2. Comparison with second-order phase transition

While there is ample evidence for the nuclei situated at or very close to the first-order phase transition between spherical- and prolate-deformed shapes, the situation is less clear for the second-order phase transition. This is so despite the fact that the U(5)-O(6) side of the IBM-1 symmetry triangle was thoroughly studied from the theoretical side. The second-order phase transition is

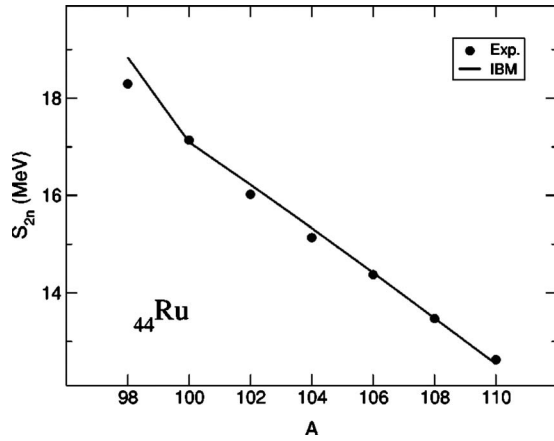


FIG. 26. Two-neutron separation energies in Ru nuclei with the IBM-1 predictions. From Frank *et al.*, 2001.

more difficult to observe in the data on nuclei since it generally yields smoother behavior of observable quantities than the first-order transition.

Early work indicated that the neutron-rich Ru and Pd isotopes are situated rather close to the second-order spherical-deformed phase transition (Stachel *et al.*, 1982). Later on, a chain of even-even Ru isotopes was reanalyzed by Frank *et al.* (2001) in order to locate the second-order critical nucleus. Using two-neutron separation energies, the systematics of level energies, and the  $E2$  transition rates, they concluded that the chain can be described in terms of the U(5)-O(6) transition, with the critical point situated at  $^{104}\text{Ru}$ .

Figure 26 shows the experimental and predicted two-neutron separation energy for Ru nuclei between  $A=98$  and 110, demonstrating the above-mentioned problem to verify the second-order phase-transitional behavior in nuclei. Indeed, while a first-order QPT leads to a discontinuity of the  $S_{2n}$  dependence, the second-order transition predicts just a sudden change of the slope. The latter effect is much more difficult to detect in finite quantum systems, as shown in Fig. 26, where both experimental and theoretical dependences have a smooth decrease. Note that the change of slope in theoretical values between  $A=98$  and 100 is not caused by the phase transition, which is located by a fit of the IBM-1 parameters close to  $A=104$ .

Recently, the Zn isotopes were also studied and  $^{64}\text{Zn}$  proposed to be near the critical point (Mihai *et al.*, 2007). Moreover, the search for nuclei showing the second-order critical-point solution E(5), which will be discussed in Sec. V.A.3, gives indications that  $^{134}\text{Ba}$  (Casten and Zamfir, 2000) and  $^{128}\text{Xe}$  (Clark *et al.*, 2004) are promising candidates.

In view of experimental ambiguities, it is rather important to find observables which would discriminate between the first- and second-order phase-transitional behavior in nuclei. Iachello and Zamfir (2004) proposed the quantity  $\nu_2 = (\langle 0_2^+ | n_d | 0_2^+ \rangle - \langle 0_1^+ | n_d | 0_1^+ \rangle) / N_B$ , which is proportional to the isomer shift  $\langle r^2 \rangle_{0_2^+} - \langle r^2 \rangle_{0_1^+}$  between

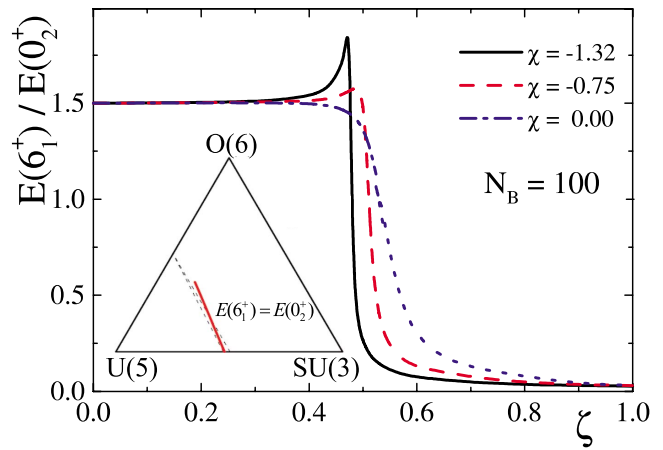


FIG. 27. (Color online) The ratio  $R_{6/0} = E(6_1^+) / E(0_2^+)$  calculated with the Hamiltonian (3.22),  $N_B=100$ , for first-order ( $\chi = -1.32$  and  $-0.75$ ) and second-order ( $\chi=0$ ) phase transitions. The locus of  $E(6_1^+) = E(0_2^+)$  in the symmetry triangle (for the same boson number) is shown in the inset. Adapted from Bonatsos, McCutchan, Casten, and Casperson, 2008.

the first two  $0^+$  states.<sup>16</sup> It is positive in the spherical phase and negative in the deformed phase. Since the first-order QPT can be locally interpreted as a sharp avoided crossing of the  $0_1^+$  and  $0_2^+$  states (Zamfir, von Brentano, *et al.*, 2002) while the second-order QPT is seen as a much softer bunching of a larger number of  $0^+$  states (Heinze *et al.*, 2006; Cejnar *et al.*, 2007), the observed dependence of  $\nu_2$  on the control parameter with a moderate value of  $N_B$  is different for the first- and second-order transitions. Unfortunately, experimental data on the isomer shifts are presently available only for a limited number of isotopes and not the shifts between  $0^+$  states but rather those between the  $2_1^+$  and  $0_1^+$  states (Laubacher *et al.*, 1983). Therefore, more measurements are needed to verify the above-outlined predictions.

An alternative observable capable to distinguish QPTs of both orders is the energy ratio  $R_{6/0} = E(6_1^+) / E(0_2^+)$  introduced by Bonatsos, McCutchan, Casten, and Casperson (2008). This quantity is much easier to measure (even in exotic nuclei) and, in fact, its analysis in the IBA framework was inspired by the X(5) critical-point solution of the geometric model, for which one obtains  $E(6_1^+) \approx E(0_2^+)$  and therefore  $R_{6/0} \approx 1$  (see Sec. V.A.1). Figure 27 shows  $R_{6/0}$  as a function of  $\zeta$  in the IBM-1 parametrization from Eq. (3.22) for three  $\chi$  values. Note that  $R_{6/0} = 1.5$  in the U(5) limit ( $\zeta=0$ ), as follows from the ratio between excitation energies of the three-phonon  $6^+$  and two-phonon  $0_2^+$  states. On the other hand, in the

<sup>16</sup>The isotope (or isotone) shifts, discussed in Sec. II.B.4, are connected to the differences between expectation values  $\langle 0_1^+ | n_d | 0_1^+ \rangle$  obtained for boson numbers  $N_B$  and  $N_B+1$  and for the control parameter values corresponding to the two respective nuclei. They are therefore straightforwardly related to the changes of the order parameter  $\beta$ . For a comparison of IBM-1 predicted isomer shifts with data see McCutchan, Zamfir, and Casten (2004).

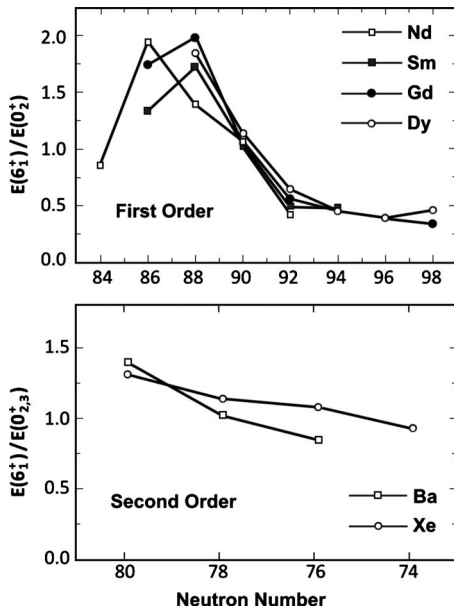


FIG. 28. Experimental  $R_{6/0}$  values for regions of (top) first- and (bottom) second-order phase transitions. Adapted from Bonatsos, McCutchan, Casten, and Caspersen, 2008.

deformed limit of  $\zeta=1$  the value of  $R_{6/0}$  drops to small values (tending to zero in the limit  $N_B \rightarrow \infty$ ).

There are two important predictions relevant to phase-transitional behavior in Fig. 27. First,  $R_{6/0}$  is unity at or near the critical point for a wide interval of  $\chi$  values and this is the unique locus of  $E(6_1^+) = E(0_2^+)$  in the triangle. The locus is shown in the inset of Fig. 27 up to the point of an avoided crossing of  $0_2^+$  and  $0_3^+$  levels, where the nature of the  $0_2^+$  state changes. Above that point, one can switch to the line  $E(6_1^+) = E(0_3^+)$  (not shown in the figure) which continues to the second-order transitional region. This means that a generalized ratio  $R_{6/0} = E(6_1^+)/E(0_{2,3}^+)$ , namely, the condition  $R_{6/0} \approx 1$ , is a rather simple and general signature characterizing the whole spherical-deformed phase-transitional region.

Second, as seen in the main panel of Fig. 27,  $R_{6/0}$  can actually distinguish first- and second-order phase-transitional behavior. In a first-order transition, it rises just before the phase transition (reaching a value above 1.5) before dropping through unity to smaller values. For a second-order case, the decrease is monotonic starting (slowly) from the U(5) limit. We note that this behavior is muted for finite  $N_B$  but the general features persist (for smaller  $N_B$ , the  $R_{6/0} \approx 1$  as well as  $R_{4/2} \approx 3$  lines lie to the right of their locations in the large  $N_B$  limit).

Figure 28 shows the experimental data on the  $E(6_1^+)/E(0_{2,3}^+)$  ratio for two known transition regions. The data nicely reflect the IBA predictions for the  $A \approx 150$  region, which exhibits first-order phase-transitional behavior. Here the  $R_{6/0}$  dependence peaks just before the critical value  $N=90$  (see the upper panel). In contrast, in the second-order,  $\gamma$ -soft, spherical-deformed region of the Ba and Xe nuclei below  $N=82$ ,

the behavior (shown in the lower panel) is softly and monotonically decreasing with increasing valence neutron number  $N_n$ . This again demonstrates the smoothening of the second-order QPT effects in finite nuclei (cf. Fig. 26).

Another proposed signature of the spherical-deformed transitions of both types, namely, the ratio of E2 strengths  $B_{4/2} = B(E2: 4_1^+ \rightarrow 2_1^+)/B(E2: 2_1^+ \rightarrow 0_1^+)$  was discussed by Rowe *et al.* (2004). Its behavior in the first- and second-order transitions is qualitatively similar to that of  $R_{6/0}$  or  $\nu_2$ , hence allowing in principle one to discriminate between the two cases. We also point out that the U(5)-SU(3) and U(5)-O(6) transitional paths were subject to comparative numerical studies focused on several specific observables by Pan *et al.* (2003), Pan, Zhang, and Draayer (2005) and Zhang *et al.* (2007) and particularly by Rowe (2004c) and Rosensteel and Rowe (2005). Related analyses were also performed by means of the so-called quadrupole shape invariants (Werner *et al.*, 2000, 2002, 2008).

We have seen that the IBM-1 Hamiltonian provides a simple means of describing a rich range of collective structures with extreme parameter efficiency. Indeed, except for scale, most collective nuclei can be reasonably well described, and the structural evolution with  $Z$  and  $N$  mapped, using only two parameters,  $\zeta$  or  $\eta$ , which describes the spherical-deformed character, and  $\chi$ , which quantifies the  $\gamma$  softness (distinguishing the first- and second-order transitions). In recent years, developments in geometrical models have opened a major new, complementary, avenue to explore the phenomenology of collectivity in nuclei. This will be discussed in Sec. V.

### C. Quasidynamical symmetries

Apart from the above-analyzed signatures of critical behavior in finite nuclei, a rather interesting aspect of structural transitions concerns the definition of phases. We know that the phases are associated with shape types and, in the IBA, the latter can be linked to particular dynamical symmetries which represent specific realizations of nuclei with given shapes. One may therefore wish to relate shape phases to the limiting dynamical symmetries. This seems possible in spite of the fact that exact symmetries are usually broken near the critical regions. The key concept for the symmetry-related definition of phases is the so-called quasidynamical symmetry.

Quasidynamical symmetries (QDSs) were first discussed by Rowe *et al.* (1988) and later invoked in the context of a transition between superconducting and rotational nuclear phases (Bahri *et al.*, 1998; Rowe *et al.*, 1998). The application to the IBM-1 phase transitions was presented by Rowe (2004a, 2004c), Rowe *et al.* (2004), and Rosensteel and Rowe (2005). The term QDS expresses the situation when some well-pronounced empirical signatures of a certain dynamical symmetry occur in a system in which the actual symmetry is badly broken. In other words, a system possessing a QDS exhibits some attributes of an exact symmetry irrespective of the

fact that this symmetry is not actually present. A formal description makes use of the term embedded representation of a group  $G$  (Rowe *et al.*, 1988), which is introduced as a representation formed by a coherent mixing of basis states associated with various irreducible representations of  $G$ . It turns out that such a coherent mixing of irreps stands behind the surprising persistence of numerous symmetry attributes in some systems far away from dynamical symmetry limits.

In practice, a quasidynamical symmetry (which is usually limited to a certain low-energy fraction of the spectrum) can be expressed through the approximate validity of a specific description based on or inspired by the corresponding exact symmetry. The QDS approach to quantum phase transitions then leads to a picture in which two distinct types of quasidynamical symmetry exist on either side of the transition (defining the two “phases”) while the width of the transitional region (with both symmetries broken) shrinks with increasing size of the system. The IBM-1 quasidynamical symmetries are connected with the following methods of description.

- (i) In the spherical phase, the low-energy spectrum is expressed in terms of the bosonic random phase approximation (RPA). It starts from an uncorrelated  $s$ -boson condensate  $|\Psi_0\rangle \propto (s^\dagger)^{N_B}|0\rangle$ , from which the excitations are created by applying operators

$$D_m^\dagger = \frac{1}{\sqrt{N_B}}(X d_m^\dagger s - Y s^\dagger d_m) \quad (4.5)$$

with coefficients satisfying  $|X|^2 - |Y|^2 = 1$ . This choice ensures that for  $n_d \ll N_B$  the operators are well approximated by  $D_m^\dagger \approx X d_m^\dagger - Y d_m$  with boson commutation relations  $[D_m, D_{m'}^\dagger] \approx \delta_{mm'}$ . While in the U(5) limit one gets  $(X, Y) = (1, 0)$ , away from the U(5) symmetry the coefficients are determined through the pair of RPA equations (Rowe, 2004a, 2004c).

A Hamiltonian close to U(5) is roughly given by  $H \approx \varepsilon \sum_m D_m^\dagger D_m$ , where the oscillator energy  $\varepsilon$  is determined from the RPA equations and depends on the control parameters. This means that operators (4.5) play a role of phonons: the correlated RPA ground state coincides with the  $D$ -phonon vacuum while excited states have  $n_D = 1, 2, \dots$ . The quality of this approximation increases with  $N_B$ , but it is strictly limited to the spherical phase since at the critical point the nature of the ground state changes and  $\varepsilon \rightarrow 0$  (tending to imaginary values on the deformed side). The range of applicability of the RPA description defines the domain of the U(5)-based QDS or in other words the U(5)-like phase of the system.

- (ii) In deformed prolate and oblate phases, the low-energy spectrum is described by the bosonic mean-field (BMF) basis with separated vibrational and rotational excitations (Leviatan, 1987). It is

derived from the boson condensate operator (3.25) supplemented by  $\beta$ - and  $\gamma$ -boson operators

$$\Gamma_\beta^\dagger = \frac{1}{\sqrt{1 + \beta_0^2}} \left[ -\beta_0 s^\dagger + \cos \gamma_0 d_0^\dagger + \sin \gamma_0 \frac{d_2^\dagger + d_{-2}^\dagger}{\sqrt{2}} \right], \quad (4.6)$$

$$\Gamma_\gamma^\dagger = -\sin \gamma_0 d_0^\dagger + \cos \gamma_0 \frac{d_2^\dagger + d_{-2}^\dagger}{\sqrt{2}},$$

with  $\beta_0, \gamma_0$  associated with the ground-state deformation parameters and by three additional operators (involving orthogonal superpositions of  $d_{\pm 1}^\dagger$  and  $d_{\pm 2}^\dagger$ ) related to angular momentum.

The ground state for  $N_B \rightarrow \infty$  is given by  $|\Psi_0\rangle \propto (\Gamma_0^\dagger)^{N_B}|0\rangle$ , while  $|\Psi_\beta\rangle \propto \Gamma_\beta^\dagger (\Gamma_0^\dagger)^{N_B-1}|0\rangle$  and  $|\Psi_\gamma\rangle \propto \Gamma_\gamma^\dagger (\Gamma_0^\dagger)^{N_B-1}|0\rangle$  represent  $\beta$  and  $\gamma$  vibrational excitations of a deformed nucleus, respectively. A combined application of operators from Eqs. (3.25) and (4.6) generates an appropriate basis of vibrational states with  $n_\beta$  and  $n_\gamma$  excitation quanta of both types, providing information on the bandheads of the rotational states built on these excitations (hence the term intrinsic states). To derive energies and wave functions of the individual members of these bands, one has to apply a suitable angular-momentum projection technique. In the SU(3) or  $\overline{\text{SU}}(3)$  limits we get  $\beta_0 = \sqrt{2}$  and  $\gamma_0 = 0$  or  $\pi$ , respectively. Away from these symmetries, the value of  $\beta_0$  must be redefined by the minimization of the potential energy surface (3.26), but the essence of the method remains valid until one gets very close to the prolate-oblate or deformed-spherical phase separatrix (Rowe *et al.*, 2004; Rosensteel and Rowe, 2005). Figure 29 shows the quality of the mean-field description of individual states in three basic low-energy bands. Theoretical BMF predictions of wave function components, shown by the leftmost column in each panel, are confronted with actual (numerical) components for states with spins  $L \leq 8$ . This figure shows the characteristic property of an SU(3)-based QDS description, namely, a coherent mixing of distinct SU(3) irreps, which are classified by labels  $(\lambda, \mu)$ , in the actual eigenstates.

It has been found (Jolie, Casten, *et al.*, 2004) that the  $\beta$  and  $\gamma$  bandheads are nearly degenerate along a unique trajectory in the interior of the triangle following the arc of regularity (see footnote 12). Recently Bonatsos *et al.* (2010) found that all of the SU(3) degeneracies persist along this arc, perhaps suggesting that an SU(3) QDS underlies the arc on the deformed side of the triangle. Bunching patterns of levels near the arc were studied by Macek *et al.* (2007). Nevertheless, the coherent behavior of wave functions (similar to that shown in Fig. 29) exists (Macek *et al.*, 2009) also away from the arc, covering a wide area of the triangle within the

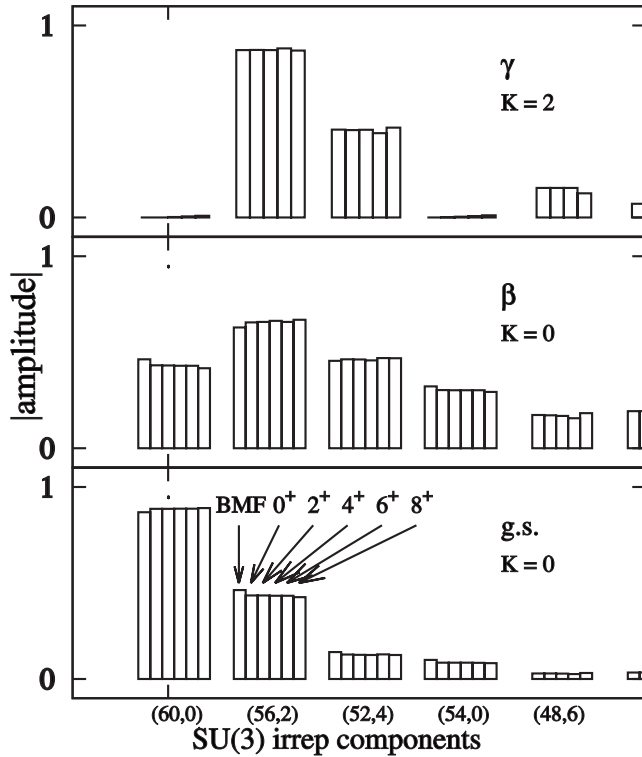


FIG. 29. Absolute components of numerical wave functions for the Hamiltonian (3.21) with  $(\eta, \chi) = (0.5, -1.3)$  and  $N_B = 30$  in a fraction of the  $SU(3)$  basis. Three panels show the components for  $0^+$ ,  $2^+$ ,  $4^+$ ,  $6^+$ , and  $8^+$  states in the ground-state band (bottom), the  $\beta$  band (middle), and the  $\gamma$  band (top). The “BMF” column in each panel shows the value obtained by applying the mean-field operators (3.25) and (4.6). For an extended picture see Macek *et al.* (2009).

domain of  $\gamma$ -rigid deformed shapes.

- (iii) The deformed  $\gamma$ -soft phase (that coincides with the prolate-oblate phase transition) can be characterized by a so-called shifted oscillator approximation (Rowe, 2004a, 2004c). This technique makes use of a substitution  $x = 2(n_d/N_B) - 1$ , which in the limit  $N_B \rightarrow \infty$  becomes a continuous variable entering wave functions  $\psi_i(x) \equiv \langle n_d | \psi_i \rangle$  of individual Hamiltonian eigenstates  $|\psi_i\rangle$ . The  $O(6)$ - $U(5)$  transitional Hamiltonian (in the energy-per-boson form) then transforms into a differential operator (Cejnar *et al.*, 2006)

$$\frac{H}{N_B} \approx -\frac{\mathcal{K}}{N_B^2} \frac{d}{dx} (1-x^2) \frac{d}{dx} + \mathcal{A}(x-x_0)^2 + E_0, \quad (4.7)$$

where the parameters  $\mathcal{K}$ ,  $\mathcal{A}$ ,  $x_0$ , and  $E_0$  depend on the control parameter, e.g., on  $\eta$  or  $\zeta$  in parametrizations (3.21) or (3.22). In the  $O(6)$  limit one gets  $x_0 = 0$ , but as proceeding toward the  $U(5)$  limit the centroid position  $x_0$  decreases to negative values. The value of  $E_0$  follows the evolution of the ground-state energy in the mean-field approximation.

In a general case, Eq. (4.7) can be identified with a

shifted oscillator having an  $x$ -dependent kinetic term. The applicability of such a description defines in the QDS language the  $O(6)$ -like phase of the system. Since the definition of  $x$  allows values  $-1 \leq x \leq +1$ , the shifted oscillator approximation fails for states whose domain  $\psi_i(x) \geq 0$  exceeds this interval. As a consequence, there exists an upper energy and a certain critical value of the control parameter where the quasi- $O(6)$  approximation loses its sense. The critical parameter value (the one for which  $x_0 = -1$ ) coincides with the point of the second-order QPT to the spherical phase.

We finally note that while the quasidynamical symmetries describe low-energy spectra on both sides of the QPT critical point, some other symmetry-inspired approaches have been developed which apply at the critical point itself. One of those approaches resorts to the so-called partial dynamical symmetries (Leviatan, 1996) and is relevant at the first-order phase transition (Leviatan, 2005, 2006, 2007). A semianalytic description of the second-order shape-phase transition can be found in Leviatan and Ginocchio (2003). A widely recognized approach based on the so-called critical-point symmetries (solutions) will be discussed in the next section in the framework of the geometric model.

## V. SHAPE TRANSITIONS IN THE GEOMETRIC MODELS

Despite the richness of the geometric model (see Sec. III.A), little work has been actually done until recently in terms of specific studies for a variety of potentials  $V(\beta, \gamma)$ . One approach, incorporating higher-order terms into the geometric Hamiltonian, is that of Gneuss *et al.* (1969). However, in its most general form it contains eight parameters and has been little used. A simplified version of the model was discussed by Zhang *et al.* (1997), who used the potential (3.2) and presented a GCM structural triangle similar to that of the IBM-1 (see Fig. 30).

Recently, an important development in geometrical models is in the treatment of QPT with the concept of critical-point solutions (CPSs) to describe nuclei at the quantum phase-transitional point. In Sec. V.A we introduce these ideas, compare them with the data, and discuss various alternate CPSs, while in Sec. V.B we sketch some recent geometrical models of structural evolution.

### A. Critical-point solutions

Nuclei at a shape-transitional point have always been the most challenging and difficult to treat theoretically [see, e.g., Kumar (1974)]. In the last decade, a new class of explicitly geometric models derived from critical-point solutions of the Bohr Hamiltonian has been proposed. These models are based on simple assumptions, involving approximate potentials simulating the phase-transitional point that allow simple (sometimes approxi-

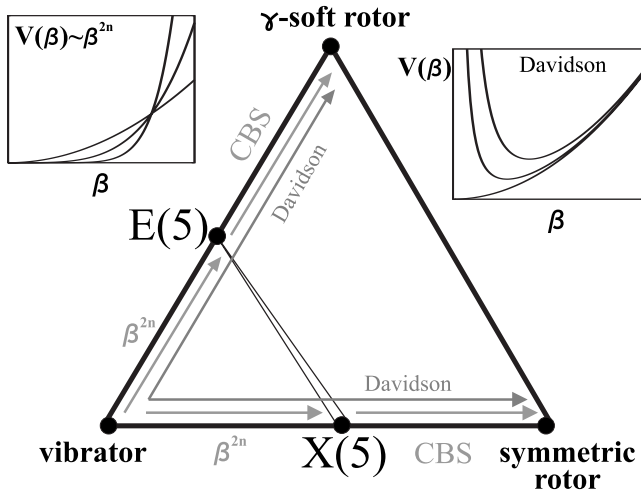


FIG. 30. Geometrical structural triangle analogous to the symmetry triangle for the IBM-1. The X(5) and E(5) critical-point solutions are identified along with the first-order transition trajectory linking them (the two lines indicate the region of phase coexistence). Potentials allowing semianalytic treatments of the structural evolution (see Sec. V.B) and the domains of their applicability are sketched.

mate) solutions of the Schrödinger equation.<sup>17</sup> Originally developed by Iachello (2000, 2001), the concept has now spawned a new generation of geometric treatments of a variety of structures and even of ranges of structure evolving in specific ways. Here we first discuss the X(5) critical-point solution for a first-order phase transition in detail and E(5) for a second-order case and compare their predictions with the available data. Some of the disagreements with the data will be valuable in pointing to shortcomings, modifications, and refinements of these CPS.

The starting point for the CPS *Ansatz* goes back to Fig. 10 and, in particular, to the thick curve (No. 3) where the spherical and deformed minima are degenerate, with a small barrier between them. The idea behind the CPS is to simplify this behavior so that it can be easily solved. This simplification consists of assuming that the barrier between the minima is weak and can be ignored and assuming that the rise in the potential at large  $\beta$  is very steep. Taken to the extreme this leads to an infinite square well model for nuclei at the critical point. One also needs to introduce the other quadrupole shape variable  $\gamma$  and three Euler angles, arriving therefore at a five-dimensional problem.

The difference between X(5) and E(5) lies in the  $\gamma$  dependence of their potentials. Reference to a geometrical structural triangle given in Fig. 30 shows that E(5) lies along the vibrator to  $\gamma$ -soft rotor leg where the potential is completely  $\gamma$  independent. On the other hand,

<sup>17</sup>The term critical-point symmetry is often used in the literature, which however is not rigorous since only in some CPS cases the actual dynamical symmetry of the Hamiltonian can be identified.

X(5) represents a shape transition from a spherical vibrator to an axial rotor (along the bottom leg of the triangle), which justifies a quadratic approximation of the  $\gamma$  dependence near the potential minimum.

We note that while these CPSs and the IBA can both test phase-transitional behavior, they are quite different approaches. As is evident from Eq. (3.26), the IBM-1 energy surface is not a square well in  $\beta$  and, for realistic boson numbers, gives predictions quite different than those we will see for X(5) and E(5).

### 1. The X(5) critical-point solution

We start our discussion of X(5) by inserting the approximate potential

$$V(\beta, \gamma) = V_{\text{well}}(\beta) + c(\gamma - \gamma_0)^2 \quad (5.1)$$

into the Bohr Hamiltonian of Eqs. (3.4) and (3.6). Here, as explained above,  $V_{\text{well}}(\beta)$  stands for a square-well potential,  $V_{\text{well}}=0$  for  $\beta \in [0, \beta_M]$  and  $V_{\text{well}}=\infty$  for  $\beta > \beta_M$ , while the second term represents a quadratic approximation ( $c > 0$ ) of the  $\gamma$  dependence in a vicinity of minimum  $\gamma_0$  (most commonly  $\gamma_0=0$ ).

The essential step in the X(5) solution is to make a separation of variables  $\beta$  and  $\gamma$ . As discussed in Sec. III.A.2 the separation is possible for a potential (3.10), which is of a slightly different form than that in Eqs. (3.9) and (5.1). The separation in X(5) is therefore only an approximation. Nevertheless, it is key to the analyticity and simplicity of X(5). As we will see, the X(5) *Ansatz* works extremely well, especially recognizing that for an essential part of the energy spectrum it is parameter-free except for scale.

However, having said that, the separability approximation can be quite severe. To achieve separability, in Eq. (3.4) one replaces  $\beta$  in the terms containing  $\gamma$  by an “average” value  $\beta_0$ . The impact of this approximation thus depends on the softness of the potential in  $\gamma$ , being worse for the  $\gamma$ -stiff case with  $\gamma_0=0$ , where the second term in  $T_{\text{vib}}$  is large. The effect of replacing  $\beta$  by  $\beta_0$  in this term reduces its significance since it removes any contributions from small  $\beta$  values. We return to this point later and show results from an exact diagonalization with no separability assumption.

For now, we follow Iachello (2001). We seek solutions of the Schrödinger equation  $H\Psi = E\Psi$  of the form

$$\Psi_{L,M,K}(\beta, \gamma, \Theta) = \varphi_{L,K}(\beta, \gamma) D_{M,K}^{(L)}(\Theta), \quad (5.2)$$

where  $\varphi_{L,K}$  is a function to be determined, while  $D_{M,K}^{(L)}$  stands for the Wigner function of Euler angles  $\Theta$  depending on angular momentum quantum numbers  $L$  (total angular momentum),  $M$  (projection to the  $z$  axis), and  $K$  (projection on the body-fixed symmetry axis). Carrying out the approximate separation of  $\beta$  and  $\gamma$ , one obtains  $E \approx E^{(\beta)} + E^{(\gamma)}$  and  $\varphi_{L,K}(\beta, \gamma) \approx \xi_{L,K}(\beta) \eta_K(\gamma)$ , where the  $\beta$  degree of freedom is determined by the following Bessel equation:

$$\frac{d^2 \tilde{\xi}_\nu}{dz^2} + \frac{1}{z} \frac{d \tilde{\xi}_\nu}{dz} + \left(1 - \frac{\nu^2}{z^2}\right) \tilde{\xi}_\nu = 0. \quad (5.3)$$

Here we introduced a reduced variable  $z = k_\beta \beta$  with  $k_\beta^2 = 2\mathcal{M}E^{(\beta)}/\hbar^2$ , a function  $\tilde{\xi}_\nu(z) = \beta^{3/2} \xi_{L,K}(\beta)$ , and

$$\nu = \sqrt{\frac{L(L+1) - K^2}{3} + \frac{9}{4}}. \quad (5.4)$$

Note that the last formula is due to Bijker *et al.* (2003), while the original treatment of Iachello (2001) is valid for  $K=0$ .

Solutions of Eq. (5.3) are Bessel functions  $\tilde{\xi}_\nu(z) \propto J_\nu(z)$  constrained by the boundary condition  $\tilde{\xi}_\nu(k_\beta \beta_M) = 0$  following from the square-well *Ansatz*. Denoting  $z_{s,\nu}$  the  $s$ th zero of the Bessel function  $J_\nu(z)$ , the spectrum of energies for the  $\beta$  degree of freedom is given by

$$E_{s,L,K}^{(\beta)} = \frac{\hbar^2}{2\mathcal{M}} \left( \frac{z_{s,\nu}}{\beta_M} \right)^2. \quad (5.5)$$

We stress that the order of the Bessel function solutions is an *irrational* number given by Eq. (5.4).

We now proceed to discuss the  $\gamma$  degree of freedom. Since X(5) corresponds to an axially symmetric structure we can take  $\gamma_0=0$  (prolate) or  $\gamma_0=\pi/3$  (oblate). For simplicity we consider the prolate case which is more frequently encountered. Then the equation for the  $\gamma$  degree of freedom is well approximated by the radial equation of an isotropic two-dimensional harmonic oscillator with angular momentum  $K/2$  and the frequency related to the parameter  $c$  in Eq. (5.1). Its solutions  $\eta_K(\gamma)$  are Laguerre polynomials, which contribute to the total energy by

$$E_{n_\gamma}^{(\gamma)} \approx \sqrt{\frac{2\hbar^2 c}{\mathcal{M}\beta_0^2}} (n_\gamma + 1), \quad (5.6)$$

where  $n_\gamma=0,1,2,\dots$  is the number of  $\gamma$  phonons. The allowed values of  $K=0,\pm 2,\pm 4,\dots$ , and  $n_\gamma$  are interrelated by a simple selection rule (Iachello, 2001).

Putting both formulas (5.5) and (5.6) together, we express the total energy in the following form:

$$E_{s,n_\gamma,L,K} = \mathcal{E}_0 + \mathcal{E}_1 z_{s,\nu}^2 + \mathcal{E}_2 n_\gamma, \quad (5.7)$$

where the coefficients  $\mathcal{E}_0$ ,  $\mathcal{E}_1$ , and  $\mathcal{E}_2$  depend on the parameters  $\mathcal{M}$ ,  $\beta_M$ , and  $c$  and on the average value  $\beta_0$ . We will see later that  $E2$  transition strengths introduce effectively two additional parameters. In all, X(5) gives parameter-free predictions for relative excitation energies and relative  $B(E2)$  values involving sequences of states based on successive  $0^+$  states, while to obtain absolute predictions, including states with  $K \neq 0$ , requires in total four parameters.

Figure 31 (left) presents an extensive level scheme for X(5) which includes the ground-state band and several excited bands based on  $0^+$  states. The levels are classified by the quantum number  $s$  (the ordinal number of the  $J_\nu$  zero for given  $L$ ) into different families: the choice

$s=1$  leads to yrast<sup>18</sup> levels which form a quasiground band (although with properties far from those of a rotor, see below). For  $s=2$ , one has a  $0_2^+$ -based sequence reminiscent of (but again, different from) a  $\beta$  band. The  $\gamma$  band in X(5) is separately parametrized and will be discussed below.

Since X(5) is a singular point in the structural pantheon, it brings with it a full set of correlated predictions that cannot be varied to fit particular nuclei. Indeed, as emphasized above, the model predictions in Fig. 31 are fixed except for scales. The  $E2$  rates can be calculated with the aid of the general first- and second-order quadrupole transition operators [Eq. (3.5)]. Neglecting the second-order terms we obtain

$$\mathcal{T}_\mu^{E2} = t\beta \left\{ D_{\mu,0}^{(2)}(\Theta) \cos \gamma + [D_{\mu,2}^{(2)}(\Theta) + D_{\mu,-2}^{(2)}(\Theta)] \frac{\sin \gamma}{\sqrt{2}} \right\}, \quad (5.8)$$

where  $t$  stands for an adjustable parameter, additional to  $\mathcal{E}_1$  and  $\mathcal{E}_2$  from Eq. (5.7). Since the  $E2$  matrix elements depend on the scale of wave functions, e.g., on the value of  $\beta_M$ , the treatment of absolute transition rates in its most general form adds in total two parameters to the two already discussed. Note that an analogous expression for the second-order term from Eq. (3.5), yielding an additional free parameter, can be found, e.g., in Caprio and Iachello (2007), but usually only the first-order term given in Eq. (5.8) is used.

It is easier to see the characteristic predictions if we focus on the low-lying levels and transitions of X(5) as shown on the left in Fig. 31. The most obvious prediction of X(5) involves just the lowest yrast quasirotational states, namely,  $R_{4/2}=2.91$ . A value in this range is, of course, reasonable for a potential intermediate between a spherical vibrator ( $R_{4/2}=2.0$ ) and a deformed axial rotor ( $R_{4/2}=3.33$ ). In fact, the entire yrast sequence of states in X(5) has energies intermediate between a vibrator and a rotor as we will see later. Reference to Figs. 3 and 4 shows that values near 2.9 are rare, as befits a value in a rapidly traversed transition region in a finite system. Inspection of the rare earth region shows that  $R_{4/2} \approx 2.9$  occurs in nuclei such as <sup>150</sup>Nd, <sup>152</sup>Sm, <sup>154</sup>Gd, <sup>162</sup>Yb, and <sup>178</sup>Os, which have  $P$  factors of 4.4–5.1, 5.4, and 4.6, all near the typical transition point of  $P \approx 5$ . However, it is essential to recognize that not all nuclei with  $R_{4/2} \approx 2.9$  are necessarily X(5)-like: as our treatment of the IBA in Sec. III.B.3 showed,  $R_{4/2}$  is only one indicator of structure and, indeed, any given  $R_{4/2}$  value actually refers to a range of structures.

Perhaps the most striking and characteristic prediction of X(5) is  $R_{0/2} \equiv E(0_2^+)/E(2_1^+) = 5.66$ . This directly links the yrast energies to those of the lowest intrinsic

<sup>18</sup>The name ‘‘yrast’’ is reserved for the state of a given spin  $L$  which has the lowest energy, while ‘‘yrare’’ is sometimes used to denote the next excited state with the same  $L$ .

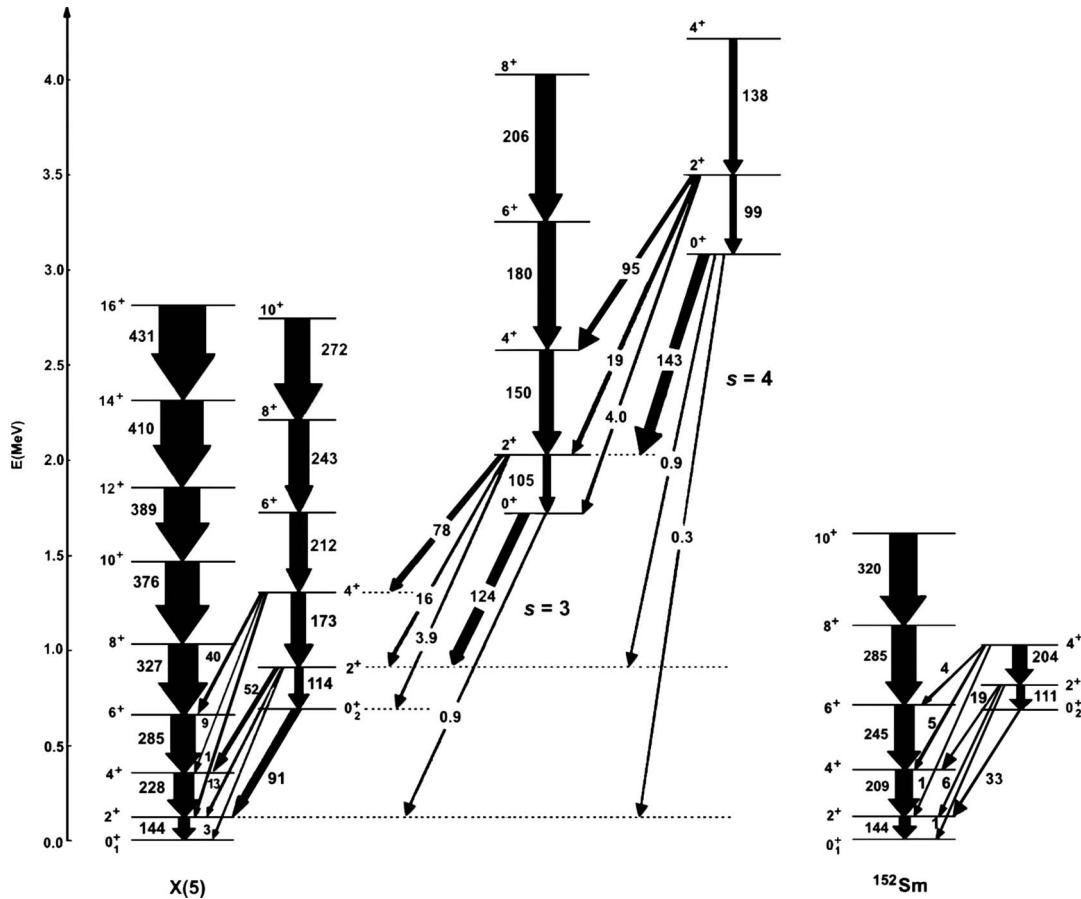


FIG. 31. Partial level scheme and some  $E2$  transition rates for the X(5) model (Iachello, 2001) compared with data on the yrast and yrare levels in  $^{152}\text{Sm}$  (Casten and Zamfir, 2001). Data from Zamfir *et al.* (1999, 2002a); Klug *et al.* (2000); Kulp *et al.* (2005).

state. Stemming from the relation between  $E(0_2^+)$  and  $E(2_1^+)$  and the energetics of the quasi-ground-state band, one has the complementary prediction that  $R_{6/0} \equiv E(6_1^+)/E(0_2^+) = 0.96$ . This particular near degeneracy has a rather deep meaning, and in fact, as discussed in Sec. IV.B.2, in the large  $N_B$  limit of the IBM-1,  $R_{6/0} = 1.0$  has a unique locus along the first-order phase-transitional line (Bonatsos, McCutchan, Casten, and Casperson, 2008).

Of course, there are many other characteristic X(5) predictions, especially concerning transition rates. We encounter them in more detail below when we compare X(5) with nuclei that have been suggested as manifesting a structure close to this CPS.

## 2. Empirical manifestations of X(5)

The first nucleus discussed to manifest an approximate X(5) description was  $^{152}\text{Sm}$  (Casten and Zamfir, 2001), which, along with  $^{150}\text{Nd}$  (Krücken *et al.*, 2002), remains the best studied empirical example. As we have seen (Secs. II.B and IV.B.1), there is abundant empirical evidence for a rapid spherical-deformed shape change in this region. The increase in quadrupole deformation  $\beta$  [see Eq. (2.4)] implied in Fig. 5 has been confirmed by a more rigorous treatment in terms of quadrupole invariants (Werner *et al.*, 2008). This gives ground band quad-

rupole invariants for  $^{152,154}\text{Gd}$  of  $1.77(17) e^2 b^2$  and  $3.89(2) e^2 b^2$ . Therefore this region is an ideal one in which to compare the predictions of X(5) with the data.

Figure 31 includes on the right a level scheme for  $^{152}\text{Sm}$  providing, along with a few additional figures below, a detailed comparison of the predictions of X(5). Given the extreme simplicity of X(5) it is noteworthy that it works at all. The  $R_{4/2}$  values of the lowest two quasibands in X(5) are 2.91 and 2.80. In  $^{152}\text{Sm}$  the empirical values are 3.01 and 2.69.  $R_{0/2}$  is 5.62 and  $R_{6/0}$  is 1.03, both close to the X(5) predictions. The next yrast energies also are close to X(5) as shown in Fig. 32 (left).

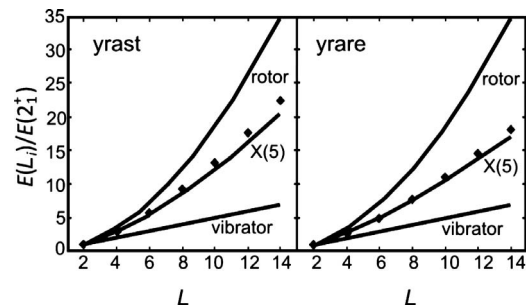


FIG. 32. Values of  $E(L)/E(2_1^+)$  for yrast and yrare levels in  $^{152}\text{Sm}$  compared to the harmonic vibrator, symmetric rotor, and X(5). Adapted from Casten and Zamfir, 2001.

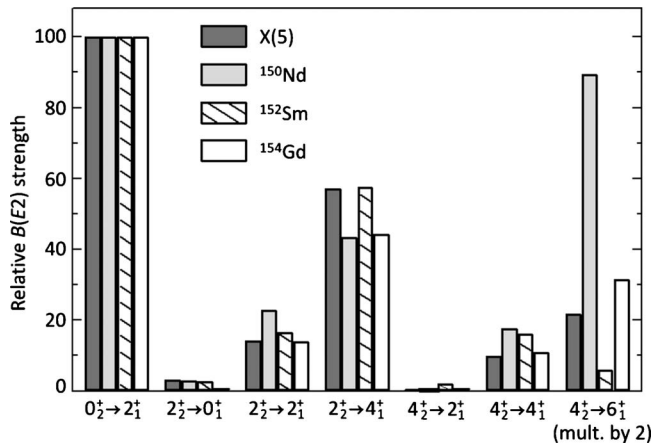


FIG. 33. Relative values of  $B(E2: L_i^+ \rightarrow L_j^+)$  for three  $N=90$  nuclei compared to X(5). The  $E2$  strengths are normalized to the  $0_2^+ \rightarrow 2_1^+$  transition. From [Casten and Zamfir, 2001](#).

Thus, one sees that X(5) correctly predicts the relative energies of yrast (quasirotational) states and intrinsic excitation modes. Moreover, the *intra*band  $B(E2)$  values connecting the yrast states are well described, and those in the excited  $0^+$  band reasonably well, although we note that there are some differences in several measurements ([Zamfir et al., 1999](#); [Kulp et al., 2004](#); [McCutchan et al., 2009](#)) regarding intra- $0_2^+$  sequence of  $B(E2)$  values.

There are, however, two glaring discrepancies in Fig. 31, concerning yrare energies and intersequence  $B(E2)$  values. The energies in the  $0_2^+$  sequence are much closer experimentally compared to X(5) and the intersequence  $B(E2)$  values are smaller experimentally than in X(5) by a factor of 4 or so. It is useful to isolate exactly the nature of those discrepancies. Figures 32 (right) and 33 show *relative* values for both observables, where the theory has been normalized to the experimental values for the  $2_2^+$  to  $0_2^+$  spacing and to the  $B(E2: 2_2^+ \rightarrow 0_1^+)$  value of 33 W.u., respectively. Seen in this way, it is clear that X(5) gives an excellent reproduction of the relative values in both cases and that the origin of the discrepancy refers to the absolute scales for both. We return to this shortly. Such predictions, given automatically in X(5), are not easy to obtain in the traditional vibrator or rotor models without invoking multiparameter mixing among nonrotational quasibands ([Zamfir et al., 1999](#)).

As successful as X(5) is, however, one cannot ignore the magnitude of the discrepancies just noted. In thinking about these, it is worth now commenting generally on the history of phenomenological models. Invariably, one starts with an utterly simple *Ansatz* (e.g., the harmonic vibrator or perfect axial rotor) and notices that the data closely resemble the simple predictions of such idealized paradigms. The next step, equally invariable, is that deviations are noted. These are useful since they help suggest refinements to the simple model; for the rotor, for example, they relate to centrifugal or pairing effects which alter the moment of inertia and cause small deviations from the  $L(L+1)$  law. However, a key point is that those deviations, and the physics they re-

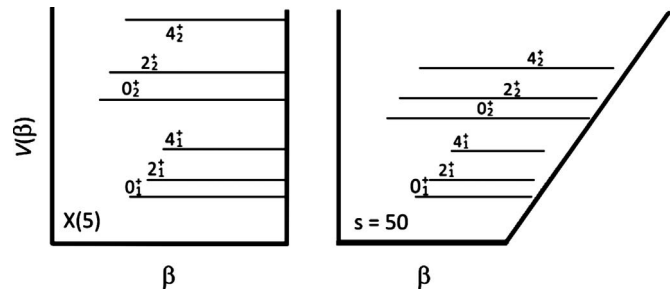


FIG. 34. Schematic comparison of yrast and higher-lying levels in a square well and in a well with sloped outer wall. Adapted from [Caprio, 2004](#).

veal, would never have been recognized were it not for the comparison to the original benchmark.

It is the same with X(5), as we now discuss. As noted, the two classes of discrepancies relate to the absolute scales of the respective observables. It is indeed possible to understand why the yrare energies in X(5) are predicted to have much larger spacings than the data and why the predicted intersequence transitions are also stronger. However, the reasons for these discrepancies turn out to be very different.

Consider first the intersequence  $B(E2)$  values. The transition  $2_2^+ \rightarrow 0_1^+$  is forbidden in the vibrator or U(5) symmetry since it represents the destruction of two phonons. Likewise it vanishes in SU(3) where it violates the  $(\lambda, \mu)$  selection rules. In between these limits, it takes on finite values. This is actually typical of many observables that are forbidden in idealized models, such as the three dynamical symmetries of the IBM-1, but not elsewhere, and therefore they peak somewhere for intermediate or transitional structures (e.g., away from the vertices of the IBM-1 triangle). We now note that the  $R_{4/2}$  ratio for <sup>152</sup>Sm is equal to 3.01, which is slightly to the rotor side of X(5) and therefore one expects the intersequence  $B(E2)$  values to be reduced relative to X(5). Naturally, similar remarks apply to the other intersequence transitions. Another recent interpretation ([Jolos and von Brentano, 2009](#)) argues that such deviations from X(5) arise due to the need for a more complicated mass tensor in the Bohr Hamiltonian or, equivalently, with a more complex quadrupole operator. Calculations in the latter scheme significantly reduce the interband transitions, giving better agreement with the data.

For the yrare energies, the problem can be related back to the X(5) assumption of an infinitely steep outer wall in the potential as a function of  $\beta$ . Clearly, real nuclei do not have such potentials and a sloped wall would obviously be a better *Ansatz*. [Caprio \(2004\)](#) investigated this. The idea is shown in Fig. 34 where it is clear that, if a sloped wall is substituted, the change in potential for the low-lying (yrast) states will be minimal but the higher states will experience a wider potential and therefore will have lower energies, as indicated. Explicit calculations validate this insight ([Caprio, 2004](#)). Note that the X(5) predictions for low-lying states do not differ significantly from those obtained for a finite potential

well (Caprio, 2002). Thus we see that the two most obvious discrepancies with X(5) give new insights into the structure of  $^{152}\text{Sm}$  and point to possible improvements in that model (albeit at the cost of additional parameters).

The  $^{150}\text{Nd}$  and  $^{154}\text{Gd}$  nuclei have also been shown to manifest X(5) quite well (Krücken *et al.*, 2002; Kulp *et al.*, 2003; Dewald *et al.*, 2004; Tonev *et al.*, 2004). Going beyond the  $N=90$  region, a number of other nuclei have been tested as candidates for X(5), including, for example,  $^{130}\text{Ce}$  (Mertz *et al.*, 2008),  $^{162}\text{Yb}$  (McCutchan *et al.*, 2004, 2006),  $^{166}\text{Hf}$  (McCutchan, Zamfir, and Casten, 2005), and  $^{178}\text{Os}$  (Dewald *et al.*, 2005). A characteristic feature is that, in each of these nuclei, some observables (e.g., yrast energies and  $E2$  strengths or intersequence  $E2$  strengths) agree well with X(5) while others do not. The nuclei  $^{226}\text{Ra}$  and  $^{226}\text{Th}$  have also been interpreted as critical point X(5)-like nuclei by Bizzeti and Bizzeti-Sona (2004, 2008) and Bonatsos, Lenis, Minkov, *et al.* (2005). These nuclei and others in this mass region which are known to exhibit octupole correlations will be discussed in terms of models that include critical point descriptions in both the quadrupole and octupole degrees of freedom in Sec. VI.A.2. A much more complete discussion of empirical manifestations of X(5), including both areas of agreement and disagreement, has been presented by Casten (2006, 2009) and McCutchan and Casten (2006). A large literature on the subject exists. We cite here, without further discussion, a number of additional references relating to these studies: Bizzeti and Bizzeti-Sona (2002), Brenner (2002), Caprio *et al.* (2002), Casten *et al.* (2003), Clark *et al.* (2003), Hutter *et al.* (2003), Dewald *et al.* (2005), McCutchan, Zamfir, and Casten (2005), and Möller *et al.* (2006).

Of course, other approaches besides X(5) have been discussed to explain the phenomenology of the shape transition region. Already before the proposal of X(5), Zamfir *et al.* (1999) showed that one could not reproduce the data on  $^{152}\text{Sm}$  by mixing pure rotational bands built on traditional  $\beta$  and  $\gamma$  bands, but if one mixes *ad hoc* quasibands, deviating from the bands of the pure rotor, one could in fact fit the data. However, they showed that this requires a large number of parameters to specify the unperturbed bands and their mixing strengths. Later Wood *et al.* (2002) argued that one could interpret the data on  $^{152}\text{Sm}$  in terms of multiband mixing of conventional  $\beta$  and  $\gamma$  bands if one included an oblate intruder band.

In a series of recent papers, Kulp and colleagues have provided much new detailed spectroscopy of  $^{152}\text{Sm}$  and  $^{154}\text{Gd}$  which led them to a sequence of alternative model interpretations. They interpreted (Kulp *et al.*, 2003, 2005) the second excited  $0^+$  state in these nuclei as a pairing isomer. The failure to find evidence for a two phonon mode of  $\beta\beta$  type led them (Kulp *et al.*, 2004, 2008) to question the traditional interpretation of the first excited  $0^+$  state (at about 685 keV) in these two nuclei as a  $\beta$  vibration. They have also disputed (Kulp *et al.*, 2007) the phase coexistence model and made a num-

ber of comparisons to other models, including the early work of Kumar (1974).

More recently Garrett *et al.* (2009) elaborated these ideas with the suggestion that the ground and  $0_2^+$  states are shape coexisting states arising from two Hilbert spaces [analogously, but here within a single major shell, to the normal and intruder states in Pb and Hg (see Sec. VI.A.3)]. The distinction between such shape coexistence and the phase coexistence underlying X(5) pictures is subtle and, as they point out, has been perhaps best discussed by Heyde *et al.* (2004). In the shape-coexistence picture both the ground and first excited  $0^+$  states act as base states for an independent spectrum of excited quasibands. The experiments reported by Garrett *et al.* (2009) characterized a number of negative-parity states. They noted a repeating pattern of states built on the ground and first excited  $0^+$  state in apparent support of a shape-coexistence picture. In this region, with no obvious cross-shell intruder mechanism, the difference between the phase- and shape-coexistence scenarios needs to be elucidated. It is of particular interest to determine if the empirical  $R_{4/2}$  values and the extensive sets of collective ( $0_2^+$  to ground-state sequence) interband  $B(E2)$  values can be reproduced in these approaches and to assess this in the context of the number of parameters required.

In the discussion of empirical consequences of the X(5) model, we have so far considered only  $0^+$ -based sequences of states. However, as seen in Eq. (5.1), the X(5) Ansatz includes a harmonic dependence on  $\gamma$ , which yields a sequence of energies for the quasi- $\gamma$  band. Predictions for the decay properties of this band can also be easily obtained, albeit at the cost of two additional parameters. One of these parameters determines the energy of the  $\gamma$  vibration and the other sets the transitions from the  $\gamma$  band to other states (Bijker *et al.*, 2003). Taking the prolate axially symmetric case corresponding to X(5), that is,  $\gamma_0=0$ , we get the solutions given before except the order of the Bessel function is now read off from Eq. (5.4) with  $K \neq 0$ , in general. We know already that the wave functions in the  $\gamma$  degree of freedom are Laguerre polynomials. The  $B(E2)$  values are obtained using the transition operator (5.8), where only the first term survives for  $\Delta K=0$  transitions (those considered above), while the second term describes  $\Delta K=2$  transitions.

Some predictions for the  $\gamma$  band are shown in Fig. 35 in comparison with data on  $^{152}\text{Sm}$  (Zamfir *et al.*, 2002b; Kulp *et al.*, 2007). A much more complete set of  $B(E2)$  values is tabulated by Bijker *et al.* (2003). The general characteristics are as follows: intra- $\gamma$ -sequence transition strengths are, of course, large, with  $\Delta L=2$  transitions dominant over  $\Delta L=1$  ones for  $L \geq 6$  and vice versa for  $L < 6$ . Relative  $B(E2)$  values to the ground-state band are largest [approximately 20% of the  $B(E2:2_1^+ \rightarrow 0_1^+)$  value] for transitions with  $\Delta L=0$  for even  $L$  initial states. Spin increasing transitions with  $\Delta L=2$  are very weak. These latter results, however, are only weak tests

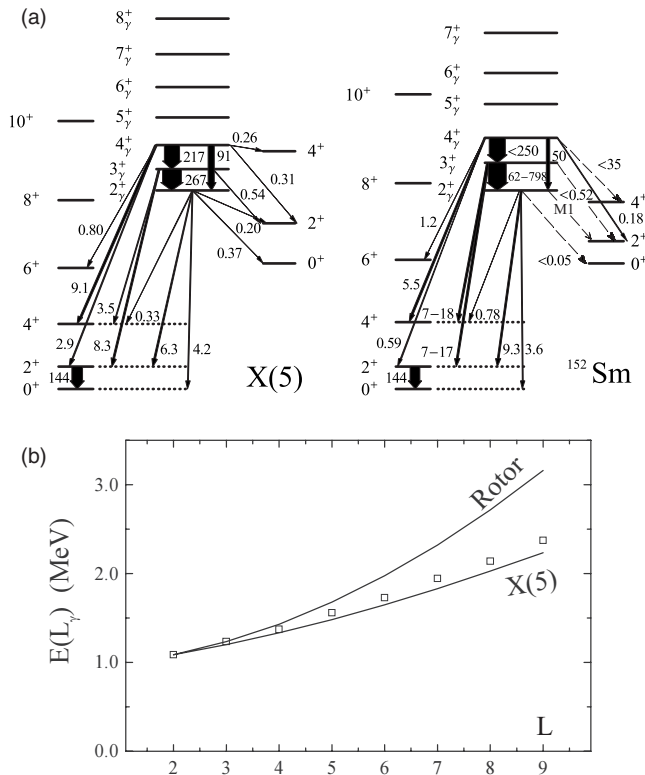


FIG. 35. X(5) description of the quasi- $\gamma$  band. Top: Comparison of the predictions of X(5) for the  $\gamma$  band with the data in  $^{152}\text{Sm}$ . Based on [Bijker et al., 2003](#) with the new results of [Kulp et al., 2007](#). Bottom: Comparison of the relative  $\gamma$ -band energies in  $^{152}\text{Sm}$  with X(5) and the rotor.

of this scheme as they are essentially the same as the Alaga rules ([Bohr and Mottelson, 1975](#)).

More characteristic of X(5) is that transitions from the  $\gamma$  band to the  $0_2^+$  sequence are weaker than those to the ground state by one to two orders of magnitude but follow similar overall trends in relative values, a reflection of the Alaga rules.

As seen in [Fig. 35](#), a comparison of these predictions to the data for  $^{152}\text{Sm}$  shows an excellent overall agreement. The absolute scale (inertial parameter) for the  $\gamma$ -sequence energies is much closer to the data than we saw for the  $0_2^+$  sequence. Also, if anything, the small deviations are actually in the opposite direction—the X(5)  $\gamma$ -band spacings are slightly smaller than the observed values. The relative energies are compared in [Fig. 35](#) (bottom). It is significant that the same scheme that reproduces the relative yrast and yrare energies gives the relative  $\gamma$ -band energies as well.

The comparison of  $E2$  strengths is good as far as it goes but it is worth stressing that, experimentally, a number of  $B(E2)$  values are only very roughly known. The  $E2$  comparison in [Fig. 35](#) has an interesting historical development as well. [Bijker et al. \(2003\)](#) gave the experimental  $B(E2:2_\gamma^+ \rightarrow 2_2^+)$  value as 27 W.u. and this was cited as the most glaring discrepancy with X(5) for the  $\gamma$  degree of freedom which predicts 0.20 W.u. in  $^{152}\text{Sm}$ . Subsequently, this transition was remeasured ([Kulp et](#)

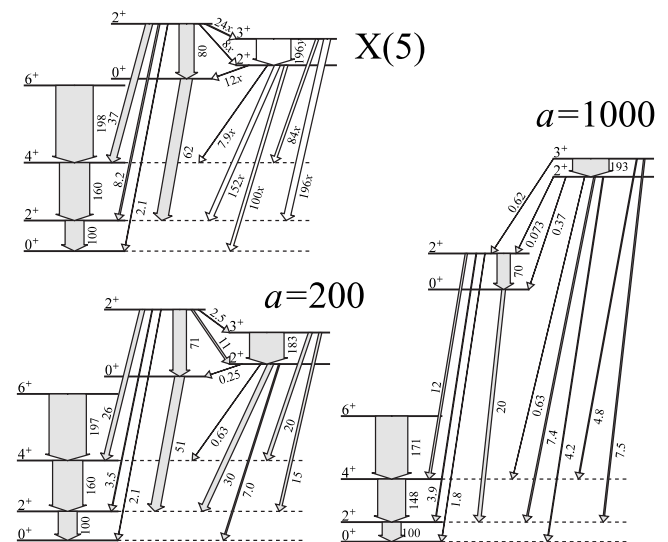


FIG. 36. Exact spectra and transition rates for the X(5) potential with two different  $\gamma$ -stiffness parameters  $a$  (see text) compared with the approximate X(5) solution assuming separability. Adapted from [Caprio, 2005](#).

[al., 2007](#)) and found to be nearly pure  $M1$  giving a nearly vanishing  $B(E2)$  in agreement with X(5).

Needless to say,  $^{152}\text{Sm}$  provides only one test case of the  $\gamma$  mode in X(5) and, moreover, the data are still incomplete despite the fact that  $^{152}\text{Sm}$  is one of the best studied atomic nuclei. Further experimental results would be useful, both more accurate  $E2$  strengths within the  $\gamma$  band for this nucleus and tests for other  $N=90$  nuclei.

Having discussed X(5), which involves the assumption of separability of the  $\beta$  and  $\gamma$  degrees of freedom, it is important to return and consider the consequences of this assumption. From [Eq. \(3.4\)](#) and our discussion at the start of [Sec. V.A.1](#) it is clear that the replacement of  $\beta$  by an average value  $\beta_0$  would be an excellent approximation if the wave function were localized in a narrow range of  $\beta$ . This is satisfied in a good rotor, but X(5) invokes in its essence a  $\beta$ -flat potential, so this approximation may be quite severe. It is further exacerbated in X(5) since  $V_2 \propto \gamma^2$  favors small  $\gamma$  (large  $1/\sin 3\gamma$ ) which makes the second term in  $T_{\text{vib}}$  large. This term is effectively a centrifugal force, pushing the wave function probability distributions outward in  $\beta$  and shifting the predictions of the  $\beta$  flat X(5) potential toward those of a fixed  $\beta$  rotor. Note that this could be ameliorated in part by incorporating a sloped wall into X(5) as well since the “outer wall” in that case is effectively softer.

[Caprio \(2005\)](#) solved the Bohr Hamiltonian without assuming separability for quadratic potentials  $V_2 = c\gamma^2$  parametrized by a dimensionless parameter  $a = 2Mc\beta_M^2/\hbar^2$  quantifying the  $\gamma$  softness. The value  $a=0$  corresponds to a completely  $\gamma$ -flat potential ( $c=0$ ) while larger  $a$  values are obtained for stiffer potentials. Results for  $a=200$  and 1000 are shown in [Fig. 36](#). One sees that the quasi- $\beta$  mode increases in energy along with  $a$  and

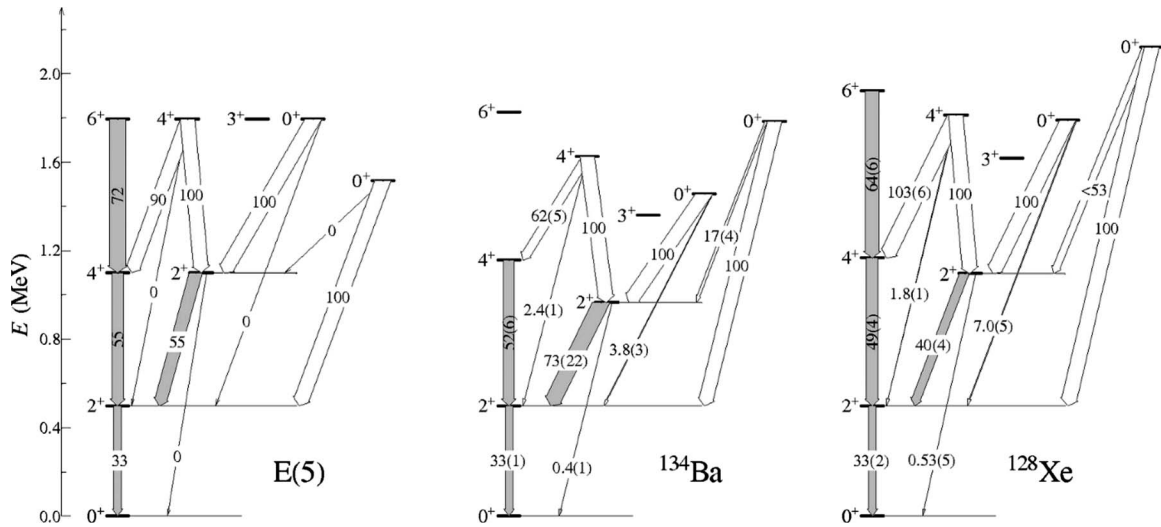


FIG. 37. Comparison of E(5) with the data for  $^{134}\text{Ba}$  and  $^{128}\text{Xe}$ . Based on [Casten and Zamfir, 2000](#), [Clark \*et al.\*, 2004](#), and [McCutchan, 2007](#).

that a number of  $B(E2)$  values change. That is, the stiffer the potential in  $\gamma$ , the larger the centrifugal effects in  $\beta$ , so that the  $\beta$  mode is squeezed and its energy increases. Assuming separability reflects an interesting conundrum, it works best for a  $\gamma$ -soft potential but X(5) invokes a stiff potential. It turns out that a value of  $a \approx 200$  best agrees with the original X(5) predictions, as shown in Fig. 36. Indeed, for that case, the overlaps of the exact solutions with the X(5) solutions are nearly unity.

### 3. The E(5) critical-point solution

We now indicate the results for an analogous critical-point solution called E(5). It invokes a CPS description of the second-order phase transition along the trajectory from a harmonic vibrator to a  $\gamma$ -soft rotor. Historically, E(5) was proposed by [Iachello \(2000\)](#) even before X(5), the name being derived from the Euclidian algebra in five dimensions. Again, an infinite square well *Ansatz* is made for the potential in  $\beta$ , while the potential in  $\gamma$  is assumed to be constant:  $V_2(\gamma)=0$ . The latter assumption makes the separation of variables  $\beta$  and  $\gamma$  exact and one again, as in the X(5) case, gets Bessel function solutions for the  $\beta$  degree of freedom. It turns out that for E(5) the order of Bessel functions is a half integer,  $\nu=\tau+3/2$ , where  $\tau$  is a phononlike O(6) quantum number (seniority) that takes integer values. For more theoretical details see [Caprio and Iachello \(2007\)](#).

The predictions for E(5) are shown on the left in Fig. 37. The levels split, as with X(5), into families labeled by a quantum number  $\zeta$  and are further classified by the quantum number  $\tau$ . The E(5) solution, of course, predicts a full set of level energies and  $B(E2)$  values. However, there is an important caveat that makes E(5) more difficult than X(5) to identify experimentally. Figure 37 appears to show distinct predictions. However, the  $\gamma$ -independent potential of E(5) carries with it an O(5) symmetry, similar to that characterizing all IBM-1 solu-

tions along the entire U(5)-O(6) leg of the symmetry triangle. Thus,  $E2$  branching ratios within a  $\zeta$  family only identify the O(5) substructure. Moreover, the degenerate multiplets are also a characteristic feature of O(5). Thus, the predictions truly unique to E(5) are the yrast energies, the relative energies of the  $\zeta$  families, and the absolute scales of  $B(E2)$  values between the different  $(\zeta, \tau)$  families.

Of course, the first signature one would look for is yrast energies consistent with E(5). The  $R_{4/2}$  value is 2.19, intermediate, as would be expected, between the harmonic vibrator ( $R_{4/2}=2.0$ ) and the  $\gamma$ -soft rotor ( $R_{4/2}=2.5$ ). Another characteristic prediction is that the  $0^+$  state with  $(\zeta, \tau)=(2, 0)$  is at 3.03 times  $E(2^+)$  and decays to the  $2^+$  state, whereas the  $0^+$  state with  $(\zeta, \tau)=(1, 3)$  is slightly higher and decays to the  $2^+$  state with a strong  $B(E2)$  value. Finally, not surprisingly,  $E2$  transitions with  $\Delta\zeta=0$  are much stronger than those with  $\Delta\zeta>1$ . Nevertheless, the relative paucity of significant transition rates has made identifications of E(5) more difficult than for X(5).

The first candidate for an empirical manifestation of E(5) was  $^{134}\text{Ba}$  ([Casten and Zamfir, 2000](#)). Comparison of the data with E(5) is shown in Fig. 37. The most obvious evidence comes from the yrast energies as well as the characteristic branching ratios from the two excited  $0^+$  states. The yrast  $E2$  strengths also agree well with E(5). While the absolute  $B(E2)$  values from the  $0^+$  state are known and in reasonable agreement with E(5), those for the  $0^+$  state are unknown and new measurements would be valuable. Another nucleus,  $^{128}\text{Xe}$ , was also discussed by [Clark \*et al.\* \(2004\)](#) and [Casten and McCutchan \(2007\)](#) as a possible example of E(5) and its level scheme is also shown in Fig. 37. Other candidates for E(5) which have also been discussed include  $^{104}\text{Ru}$ ,  $^{106,108}\text{Cd}$ ,  $^{124}\text{Te}$ , and some Pd isotopes ([Neuneyer \*et al.\*, 1996](#); [Arias, 2001](#); [Frank \*et al.\*, 2001](#); [Zamfir \*et al.\*, 2002a](#); [Zhang and Liu, 2002](#); [Zhang \*et al.\*, 2003](#); [Kirson, 2004](#); [Marginean \*et\*](#)

TABLE I. A few predictions of various CPSs (Iachello, 2000, 2001; Bonatsos *et al.*, 2004; Bonatsos, Lenis, Petrellis, *et al.*, 2005; Bonatsos, Lenis, Petrellis, *et al.*, 2006; Casten, 2006).

CPS	$R_{4/2}$	$R_{0/2}$	$E(2_{\gamma}^+)/E(2_1^+)$
X(5)	2.91	5.67	
E(5)	2.19	3.03	2.19
Y(5)	3.33		
X(3)	2.44	2.87	
Z(4)	2.23	2.95	1.77
Z(5)	2.35	3.91	1.83

*al.*, 2006). In all cases, further data are needed both in terms of experimental information in individual nuclei and in the search for other possible candidates for E(5).

Finally, we note that the relation between E(5) and the IBM-1 has been explored by García-Ramos and Arias (2008). Caprio *et al.* (2002) carried out calculations for a finite E(5)-like potential in  $\beta$  and showed that the assumption of an infinite square well in E(5) is not severe.

#### 4. Other critical-point solutions

The success of the union of the QPT and CPS concepts in the description of shape evolution in nuclei, as reflected in X(5) and E(5), has encouraged the development of many other geometric models. These models either discuss alternative critical-point solutions for various structures or they describe structural evolution en route to and from the critical points. We discuss the latter in Sec. V.B. Examples of the former are solutions such as Y(5) (Iachello, 2003), which describes a phase transition in variable  $\gamma$  (having a harmonic oscillator in  $\beta$  and a square well in  $\gamma$ ), X(3) (Bonatsos, Lenis, Petrellis, *et al.*, 2006), Z(4) (Bonatsos, Lenis, Petrellis, *et al.*, 2005), and Z(5) (Bonatsos *et al.*, 2004), which employ the same square well in  $\beta$  as in X(5) but have alternate potentials in  $\gamma$ : X(3) and Z(4) have rigid potentials in  $\gamma$ , with sharp minima at  $\gamma=0^\circ$  and  $30^\circ$ , respectively. Thus Z(4) could simulate a transition from spherical to a rigid triaxial shape. In Z(5), the  $\gamma$  potential is a harmonic oscillator centered at  $\gamma=30^\circ$  and is therefore related to a prolate-oblate transition. A few predictions of these CPSs are given in Table I.

As shown in Table I, various critical-point solutions have different features but intriguingly those with infinite square-well potentials in  $\beta$  [that is, all except Y(5)] share some remarkable uniformities due to approximate and only recently recognized properties of their Bessel function solutions (Bonatsos, McCutchan, and Casten, 2008). An example is illustrated in Fig. 38 which shows the energies of the  $0^+$  states for X(5), E(5), and Z(5). On the left, these energies are shown in the usual way, normalized to the energy of the first  $2^+$  state. However, the right side shows these same energies normalized to that of the first excited  $0^+$  state itself. Then one sees that the relative energies are virtually *identical* in all three col-

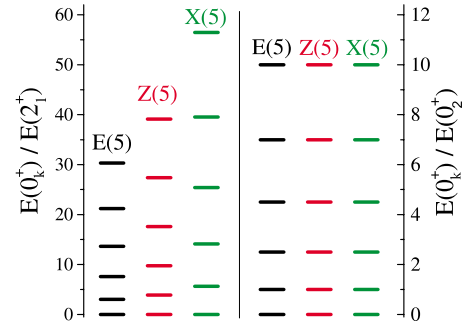


FIG. 38. (Color online) Energies of  $0^+$  states for several CPSs. Left: normalized to  $E(2_1^+)$ . Right: normalized to  $E(0_2^+)$ . Adapted from Bonatsos, McCutchan, and Casten, 2008.

umns. Moreover, these energies (relative to  $0_1^+$ ) can be expressed to high accuracy by a simple approximate formula  $E(0_{n+1}^+) \propto n(n+3)$  with  $n=1, 2, 3, \dots$ . This expression actually is an example of a more general result. If the  $0^+$  states for other infinite square-well potentials, such as X(4) or X(3), are analyzed in the same way, one finds a single universal formula for their  $0^+$  spectra given by

$$E(0_{n+1}^+) = An \left( n + \frac{D+1}{2} \right). \quad (5.9)$$

Here  $A$  is a constant depending on the model and  $D$  is the effective dimension of the system (given in the model name). That is, the relative  $0^+$  state energies depend only on the dimensionality. This formula, as noted, is only approximate, except for  $D=3$  where it is exact. Its approximate nature probably explains why it has not been discovered until recently (Bonatsos, McCutchan, and Casten, 2008). It stems from simple approximate properties of successive Bessel functions of different orders.

There have been few detailed tests of these alternate CPSs to date but they serve to illustrate the richness of possibilities following from the square-well *Ansatz*. Generally speaking, potentials that are rigid in  $\gamma$  for  $\gamma \neq 0$  have been found less useful to describe the equilibrium structure of nuclei since it is well known that, with few exceptions, axial asymmetry in even-even nuclei at low spin almost always is of the  $\gamma$ -soft variety. Since a full discussion of these issues is beyond the scope of this review, we direct the interested reader to the original literature.

#### 5. Extension to odd- $A$ nuclei

The CPS idea has also been extended (Iachello, 2005) to odd- $A$  nuclei within the E(5/4) model, which corresponds to an odd fermion in a  $j=\frac{3}{2}$  orbit coupled to an E(5) even-even core. A theoretical account of this situation was reviewed by Caprio and Iachello (2007).

Low- $j$  orbits tend to occur near the ends of major shells in heavy nuclei, which is also where  $\gamma$  softness tends to manifest itself. Unfortunately, the shell model orbits with  $j=\frac{3}{2}$  are invariably accompanied by  $j=\frac{1}{2}$  orbits as well (as in the  $p_{3/2}-p_{1/2}$  or  $d_{3/2}-s_{1/2}$  cases). How-

ever, if the excitations originating from the  $j=\frac{1}{2}$  single-particle state and those corresponding to a  $j=\frac{1}{2}$  particle coupled to an excited core can be isolated, then at least an approximate test of E(5/4) can be made. The nucleus  $^{135}\text{Ba}$  (that is,  $^{134}\text{Ba}$  plus a neutron in a  $d_{3/2}$  orbit) provides such a case if one assumes that the low-lying  $\frac{1}{2}^+$  state arises from a neutron in a nearly pure  $3s_{1/2}$  orbit (Fetea *et al.*, 2006).

We do not have space here for a detailed discussion. Suffice it to say that it is possible to plausibly associate most of the low-lying levels to corresponding states in E(5/4), that, overall, the measured  $B(E2)$  strengths are in reasonable agreement with theory, but that the energies differ very much from the predicted values. Alonso *et al.* (2007b) extended the E(5/4) model to the multi- $j$  case, with  $j=\frac{1}{2}$ ,  $\frac{3}{2}$ , and  $\frac{5}{2}$ , leading to a model called E(5/12). Analytic solutions for the excitation energies and  $B(E2)$  values are derived. Unfortunately, no comparison with experimental data is made. Clearly much more work would be needed to advance the study of odd- $A$  nuclei near critical points, including especially the incorporation of realistic combinations of shell model angular momenta. We will return to problems of odd- $A$  nuclei in Sec. VI.A.3.

## B. Calculations away from critical points

The critical-point descriptions we have been discussing describe singular situations, that is, nuclei with particular properties. Though these nuclei play crucial roles as benchmarks in structural evolution, most nuclei, of course, will not reflect these simple potentials. Therefore, one must resort to more general (and, hence, usually more complicated) models. We already discussed some predictions for the IBM-1 including the mapping of actual nuclei into the symmetry triangle. Here it is appropriate to look at a few geometric models that can relate to a wider variety of structures and which can describe particular trajectories of structural evolution. We start with some simple cases and then discuss a recent development that generalizes the capabilities to handle arbitrary potentials in a simple way. Figure 30 shows the regions of structural evolution for each of the models discussed below in the context of a geometrical structural triangle.

Since vibrational nuclei correspond to  $V(\beta) \propto \beta^2$  and the square well in  $\beta$  can be approximated by  $V(\beta) \propto (\beta/\beta_M)^{2n}$  with  $n \rightarrow \infty$ , a series of models with  $n = 1, 2, 3, \dots$  has been worked out for both the X(5) (Bonatsos, Lenis, Minkov, Raychev, and Terziev, 2004b) and E(5) (Bonatsos, Lenis, Minkov, Raychev, and Terziev, 2004a) *Ansätze* regarding the  $\gamma$  degree of freedom. These approaches simulate the transition from the vibrator up to the critical point for both  $\gamma$ -rigid and  $\gamma$ -soft cases, the corresponding models being denoted as X(5)- $\beta^{2n}$  and E(5)- $\beta^{2n}$ , respectively. Figure 39 shows level schemes and transition rates for  $n=1$  and 2. The latter case for  $V(\beta) \propto \beta^4$  was also discussed earlier by Vorov and Zelevinsky (1985). These geometrical de-

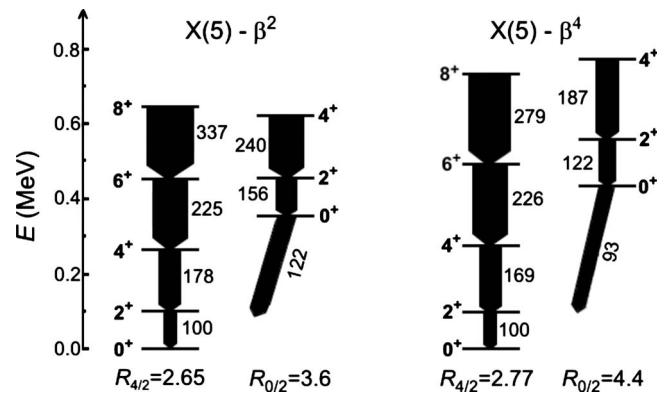


FIG. 39. Level schemes for  $\beta^2$  and  $\beta^4$  models in the X(5) framework. Adapted from Bonatsos, Lenis, Minkov, Raychev, and Terziev, 2004b.

scriptions have been compared with IBM-1 calculations for realistic boson numbers (McCutchan, Bonatsos, and Zamfir, 2006).

The structures on the deformed side of the phase transition can be described by the “moving-wall” potential,

$$V_1(\beta) = \begin{cases} 0 & \text{for } \beta \in [\beta_m, \beta_M] \\ \infty & \text{otherwise,} \end{cases} \quad (5.10)$$

proposed by Pietralla and Gorbachenko (2004). Here  $\beta_m$ , demarcating the inner edge of the square well, represents an adjustable parameter (additional to outer edge  $\beta_M$ ). For  $\beta_m=0$  we have the critical-point square-well solution. As  $\beta_m$  increases toward  $\beta_M$ , the potential describes deformed nuclei with decreasing softness in the variable  $\beta$ , hence the name confined beta soft (CBS) model. In the limit  $\beta_m \rightarrow \beta_M$ , we would get an infinitely rigid potential. Figure 40 shows examples of spectra generated by this model for various values of  $r_\beta = \beta_m/\beta_M$ . The method was originally designed for  $\gamma$ -rigid potentials of the form (5.1). A generalization to  $\gamma$ -soft cases

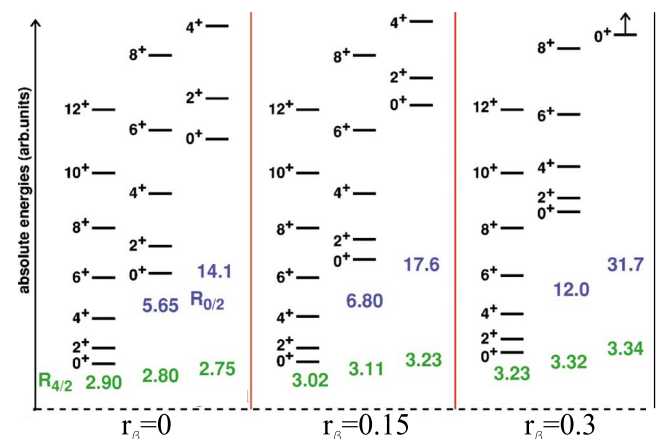


FIG. 40. (Color online) Calculations in the CBS for increasing values of the  $\beta$ -rigidity parameter  $r_\beta$ . The  $\beta$ -soft case ( $r_\beta=0$ ) coincides with X(5). Values of  $R_{4/2}=E(4_s^+)/E(2_1^+)$  and  $R_{0/2}=E(0_s^+)/E(2_1^+)$  are indicated below each band with  $s=1, 2, 3$ . From Pietralla and Gorbachenko, 2004.

was presented by [Bonatsos, Lenis, Pietralla, and Terziev \(2006\)](#). A combination of the  $\beta^{2n}$  potentials and the CBS model enables one to describe the path between the vibrator (spherical) nuclei and  $\gamma$ -rigid or  $\gamma$ -soft rotor (deformed) nuclei (see Fig. 30).

An apparent drawback of this approach is the necessity to join the two distinct models at the critical point ( $n=\infty$  and  $\beta_m=0$ ). A way to bypass this problem is to use the potential introduced by [Davidson \(1932\)](#) in the context of molecular physics. It reads as

$$V_1(\beta) = a \left( \beta^2 + \frac{\beta_0^4}{\beta^2} \right) \propto 2 + \left( \frac{\beta}{\beta_0} - \frac{\beta_0}{\beta} \right)^2, \quad (5.11)$$

where  $a$  and  $\beta_0$  are adjustable parameters. For  $\beta_0 \rightarrow 0$  one gets the harmonic oscillator, while increasing values of  $\beta_0$  move the dynamics toward the rigid-rotor case (see examples of Davidson potentials in Fig. 30). Analytic solutions of the Davidson potential are available ([Elliott et al., 1986](#); [Rowe and Bahri, 1998](#)). This potential has been compared to the critical-point solutions ([Bonatsos, Lenis, Minkov, Petrellis, et al., 2004a, 2004b](#)) and also used in the separable form (3.10) in the transitional regions ([Bonatsos, McCutchan, et al., 2007](#)). Other special forms of potentials have also been considered for transitional nuclei. Calculations spanning a variety of structures with the Davidson, Morse, and Kratzer potentials have been extensively discussed by [Boztosun et al. \(2008\)](#).

Lastly, separable potentials of the form (3.10) have been studied, for cases where  $V_2(\gamma) \propto \gamma^2$  and  $V_1(\beta)$  is either of X(5) form or of an oscillator form, as with the Davidson potential ([Bonatsos, Lenis, McCutchan, et al., 2007](#)). Studies with  $\gamma_0=0$  and with  $\gamma_0=30^\circ$  have likewise been carried out for separable Kratzer and Davidson potentials ([Fortunato, 2004](#); [Fortunato and Vitturi, 2004](#); [Fortunato et al., 2006](#)).

It is beyond the scope of this review to collect and discuss all the predictions of these models and other geometric models utilizing the Bohr Hamiltonian. These approaches incorporate important features of structural evolution, they differ substantially from one another in certain properties, like inertial behavior of quasibands or  $B(E2)$  values, while agreeing in others, e.g., behavior of  $E(0_2^+)$ . They have been discussed with many references in several recent reviews ([Casten, 2006](#); [Bonatsos, Lenis, and Petrellis, 2007](#); [Casten and McCutchan, 2007](#)). Some useful additional references are [Arias, Alonso, et al. \(2003\)](#), [Bonatsos, Lenis, Minkov, et al. \(2005\)](#), [García-Ramos, Dukelsky, and Arias \(2005\)](#), and [Bonatsos, Lenis, Petrellis, et al. \(2006\)](#).

Of course, ideally, one wants to solve the Bohr Hamiltonian for an arbitrary potential—of which the above examples would just be specific realizations. Until recently, this has been a formidable mathematical problem due to the slow convergence in the diagonalization in the traditional five-dimensional oscillator basis. However, recently an algebraic collective model has been developed which provides a major simplification by exploiting an  $SU(1,1) \times O(5)$  basis ([Rowe, 2004b, 2005](#);

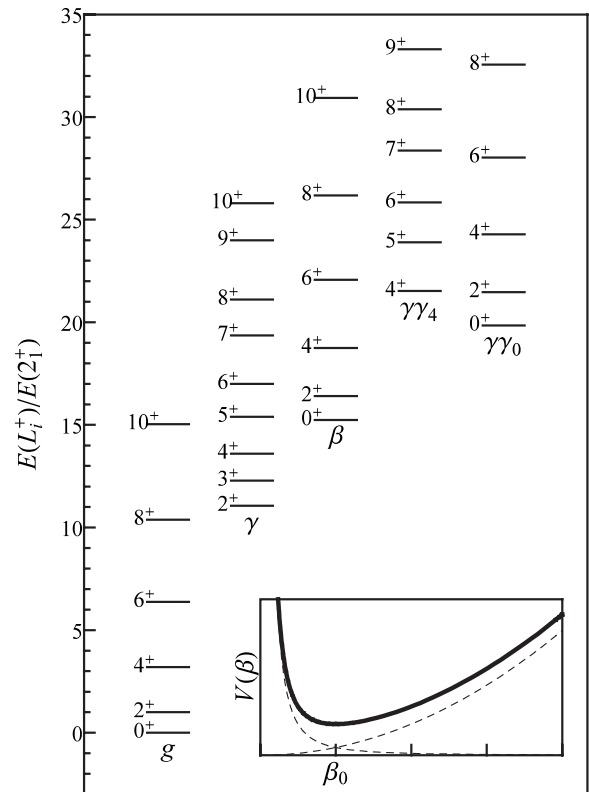


FIG. 41. Calculations by [Caprio \(2009\)](#) for the Davidson-like potential with  $\beta_0=3$  and  $\chi=5$  (see text).

[Rowe and Turner, 2005](#); [De Baerdemacker et al., 2007, 2009](#); [Caprio, 2009](#); [Rowe et al., 2009](#)). In this basis, one can solve for potentials with almost arbitrary shapes, obtaining rapid convergence and rather simple wave functions. This has recently been exemplified in calculations by [Caprio \(2009\)](#). Figure 41 shows an example for the Davidson potential from Eq. (5.11) supplemented by the term  $V_2(\gamma) \propto \chi(1 - \cos 3\gamma)$ , where the coefficient  $\chi$  quantifies the stiffness of the potential in  $\gamma$ . Clearly, one can now obtain a large variety of observables, including (though not shown) transition rates. Thus the purview of the geometrical model is now greatly expanded and rivals the richness of structure of the IBA.

## VI. FURTHER DEVELOPMENTS

This section deals with some issues exceeding the framework of the previous discussion. First, we hint at possible modifications following from specific extensions of the above-discussed models which lead to other types of shapes and transitions (Sec. VI.A). Second, we look more closely at the mechanisms underlying the critical behavior in these models (Sec. VI.B). Finally, we review new results related to nonanalytic evolutions of excited states (Sec. VI.C). In many cases, the topics discussed in this section are still open. New findings are expected, which may deepen our understanding of the QPT phenomena in general quantum systems.

## A. Extensions of models

Our attention in the preceding sections was focused entirely on the transitions within the phase diagram of Fig. 12. As emphasized, the shape phases involved in this diagram (spherical, axially symmetric prolate or oblate, and  $\gamma$  soft) represent the most important structural types of even-even nuclei. Nevertheless, other types of shape and related transitions may be relevant as well. They can be described theoretically if the models considered above are extended in various directions, e.g., by taking into account nonquadrupole excitations, by separating proton and neutron degrees of freedom, by considering higher-order interactions of bosons, etc. We now discuss some of these extensions.

### 1. Simple treatment of triaxial shapes

We saw that both GCM and IBM-1 potential energy surfaces [Eqs. (3.2) and (3.26), respectively] depend on the angle variable  $\gamma$  solely through the cubic term  $\propto \beta^3 \cos 3\gamma$ . This has an immediate consequence that the equilibrium deformed shape of a nucleus is axially symmetric, either prolate (with  $\beta > 0$  and  $\gamma = 0$ ) or oblate (with  $\beta > 0$  and  $\gamma = \pi/3$  or, equivalently,  $\beta < 0$  and  $\gamma = 0$ ), depending on the sign of the coefficient  $B$  in front of the cubic term. Nonaxial shapes, also called triaxial (all three eigenvalues of the quadrupole tensor are different, which can be represented as an ellipsoid having unequal radii along the three principal axes), do not appear in this simple description.

However, for a few nuclei triaxial deformation may be present either on the ground-state level or within the spectrum of excited (rotational) states (Nilsson and Ragnarsson, 1995). This is also supported by various microscopic calculations taking into account the  $\beta$ - $\gamma$  coupling (cf. Sec. III.C.2). To get such shapes into the basic geometric description, one simply includes in the GCM potential a sextic term  $\propto \beta^6 \cos^2 3\gamma$ , which results from a sixth-order scalar coupling of coefficients  $\alpha$  [cf. Eq. (3.1)]. A phase corresponding to triaxial shapes ( $0 < \gamma < \pi/3$ ) appears for sufficiently large values of the coefficient in front of the sextic term if it has an opposite sign than that of the cubic term, the phase transition from the axially symmetric to triaxial shapes being of second order. Such a possibility was discussed by Iachello (2003), who also introduced the associated critical-point solution Y(5) and suggested  $^{166,168}\text{Er}$  as the most likely candidates for the nuclei possessing this structure. Numerical signatures of the axial-to-triaxial transition in the geometric framework were discussed by Caprio (2009).

Can we obtain triaxial shapes also in the IBA framework? The answer is yes, and there are actually many ways how to do it. In Sec. VI.A.3 we discuss model extensions that describe the coupling of various degrees of freedom (those corresponding to protons and neutrons, paired and unpaired nucleons, normal and intruder configurations) within the IBA framework. Some of these extensions yield possible triaxial deformations. How-

ever, even the simple IBM-1 version of the model offers several possibilities for the inclusion of triaxiality.

The first one relies on recognition of finite-size effects in the IBA ground state  $\psi_0(\beta, \gamma)$  expressed in a coordinate representation (Chacón and Moshinsky, 1977). As shown by Castaños *et al.* (1984), when evaluating the mean value and rms deviation of the shape variable  $\gamma$  in the ground-state wave function, one obtains  $\langle \gamma \rangle > \sqrt{\langle \gamma^2 \rangle - \langle \gamma \rangle^2} > 0$  even for relatively large boson numbers  $N_B$ . Although this is just an effect of quantum fluctuations (which vanish as  $N_B \rightarrow \infty$ ), the interpretation in terms of an *effective* triaxial deformation can be formulated. Note the same mechanism also works for excited states and in the geometric model (Caprio, 2009). Another approach leading to similar conclusions makes use of angular momentum and seniority projection of the  $s + d$  condensate state (Dobeš, 1990).

The second path to triaxiality within the IBM-1 proceeds via introduction of higher-order interactions of bosons (Van Isacker and Chen, 1981; Van Isacker, 1999). In contrast to the first path, this allows one to produce *stable* triaxial deformation in the limit  $N_B \rightarrow \infty$ . Such a possibility was recently studied by Jolos (2004a) and Sorgunlu and Van Isacker (2008) using a simple Hamiltonian,

$$H = H_\chi(\eta) + \frac{\xi(1-\eta)}{N_B(N_B-1)} \sum_{\lambda,l} c_\lambda [[d^\dagger \times d^\dagger]^{(l)} \times d^\dagger]^{(\lambda)} \cdot [[\tilde{d} \times \tilde{d}]^{(l)} \times \tilde{d}]^{(\lambda)}, \quad (6.1)$$

where  $H_\chi(\eta)$  is the two-body Hamiltonian (3.21) and the sum represents three-body interactions between  $d$  bosons, with  $c_\lambda$  being specific constants. The parameter  $\xi > 0$ , which measures an overall strength of the three-body interaction in Eq. (6.1), appears in front of the sextic term  $\beta^6 \cos^2 3\gamma / (1 + \beta^2)^3$  in the potential-energy surface obtained from the standard coherent-state formalism (Sec. III.B.2) and hence controls the onset of triaxiality in the equilibrium shape (Van Isacker and Chen, 1981). The critical value  $\xi = \xi_c$ , where the second-order phase transition to triaxial shapes takes place, depends on the other control parameters  $\eta$  and  $\chi$ . Not surprisingly,  $\xi_c$  is close to zero in the  $\gamma$ -unstable case ( $\chi = 0$ ), while in the  $\gamma$ -rigid case the value of  $\xi_c$  grows with  $|\chi|$ . Details can be found in Jolos (2004a, 2004b).<sup>19</sup>

Finally, the third way that triaxial shapes can enter into the IBM-1 description proceeds by imposing external rotation onto the ensemble of interacting bosons (Cejnar, 2002, 2003). We stress that in this case the triaxiality does not appear in the  $0^+$  ground state but may affect the yrast states with higher angular momenta. The cranking approach originates from fermionic models of

<sup>19</sup>We stress that certain types of three-body interactions do not imply the occurrence of the triaxial phase; an example using a triple product  $\propto [[Q_0 \times Q_0]^{(2)} \times Q_0]^{(0)}$  of quadrupole operators from Eq. (3.18) was analyzed by Thiamova and Cejnar (2006).

nuclear structure, where it is commonly used to describe properties of rotating nuclei (e.g., moments of inertia). One starts from identifying the rotating-frame Hamiltonian  $H_{\text{crank}} \equiv H - \vec{\omega} \cdot \vec{L}$ , where  $H$  is the stationary Hamiltonian,  $\vec{\omega}$  is a vector of the rotational angular frequency (pointing along the rotation axis), and  $\vec{L}$  is the vector of angular-momentum operators. Minimization of the expectation value  $\langle H_{\text{crank}} \rangle \equiv \langle \Psi | H_{\text{crank}} | \Psi \rangle$  in the mean-field states  $|\Psi\rangle$  for each value of the cranking frequency yields a relation between  $\omega$  and an average angular momentum  $\langle L \rangle \equiv \langle \Psi | \vec{L} \cdot \vec{n} | \Psi \rangle$ , where  $\vec{n} \equiv \vec{\omega} / \omega$ .

For the IBA, the cranking analysis was explicitly discussed by [Dukelsky et al. \(1983\)](#), [Schaaser and Brink \(1984, 1986\)](#), [Cambiaggio et al. \(1985\)](#), and [Alonso et al. \(1996\)](#). Expectation values of  $H_{\text{crank}}$  are evaluated in condensate states of the known form (3.24) but with the *Ansatz* (3.25) replaced by one with  $a_{\pm 1} \neq 0$ . Geometric interpretation of the modified condensate states follows from evaluation of their associated expectation values  $\langle Q_\chi \rangle \equiv \langle \Psi | Q_\chi | \Psi \rangle$  of the quadrupole tensor. The spherical phase is identified with a pure *s*-boson condensate, while the deformed phase is represented by a condensate in an *s*+*d* superposition. For  $\omega=0$  one gets  $\langle L \rangle=0$ , the equilibrium shape being equivalent to that obtained from the standard analysis. As  $\omega$  increases,  $\langle L \rangle$  grows and also expectation values of the quadrupole tensor change ([Cejnar, 2002](#)). The deformed shapes for  $\omega > 0$  are triaxial as they generally show three different eigenvalues of the  $\langle Q_\chi \rangle$  matrix. It should be stressed, however, that in the cranking case there is no phase transition from axial to nonaxial deformation; the axial shape (valid for  $\omega=0$ ) smoothly changes into a triaxial shape observed at arbitrarily small value  $\omega > 0$ .

Interestingly, the IBM-1 phase diagram in the rotating frame ([Cejnar, 2003](#)) resembles a phase diagram of a superconductor in an external magnetic field. The separatrix between spherical and deformed phases (which are analogous to superconducting and normal phases, respectively) is demarcated by a curve starting at the standard (first- or second-order) critical point for  $\omega=0$  and leaning toward the U(5) limit for increasing  $\omega$ . Transition to the triaxial phase along this curve keeps the same order as at  $\omega=0$ . This indicates a possibility of a rotation-induced spherical-to-deformed phase transition, which is supported by analyses of the backbending phenomenon in a number of nuclei such as  $^{108-114}\text{Cd}$ ,  $^{108-104}\text{Pd}$ ,  $^{100,102}\text{Ru}$ , and  $^{100}\text{Mo}$  having nearly spherical ground state ([Regan et al., 2003](#); [Cejnar and Jolie, 2004](#)). Note that this kind of transition was absent in earlier non-IBA analyses performed in the cranking framework ([Levit and Alhassid, 1984](#); [Alhassid et al., 1987](#)). A numerical study of transitional signatures of the IBM-1 eigenstates with different angular momenta was presented by [Williams et al. \(2008\)](#).

## 2. Nonquadrupole degrees of freedom

A more radical departure from standard treatments of nuclear shapes follows from the inclusion of other than

quadrupole types of deformation. In this respect, the octupole deformation (leading to pearlike nuclei) is the most common possibility. Experimental observables (in particular, the presence of a negative-parity band  $1^-, 3^-, 5^-$  close to the positive-parity ground-state band  $0^+, 2^+, 4^+$  as well as certain E1 and E3 transitions) indicate the existence of stable octupole deformation in some Th and Ra isotopes ([Butler and Nazarewicz, 1996](#)). Recently anomalies in binding energies were identified just in these two regions ([Neidherr et al., 2009a, 2009b](#)).

[Scott et al. \(1979\)](#) discussed signatures of a spherical-deformed shape change for the octupole degree of freedom, noting a characteristic switch in the order of the lowest  $1^-$  and  $3^-$  states. In the vibrational regime the base octupole state is the  $3^-$  level and the  $1^-$  is a higher-lying member of a two-phonon octupole vibration multiplet. In deformed nuclei, one has a series of rotational bands with  $K=0, 1, 2, 3$ . In an RPA analysis, [Neergaard and Vogel \(1970\)](#) showed that, at the beginning of a shell, the  $K^\pi=0^-$  mode and hence a  $1^-$  bandhead should lie lowest and, in particular, below the  $3^-$  level. Such crossovers are indeed seen in the Sm and Gd nuclei around  $N=90$ . Recently [Garrett et al. \(2009\)](#) garnered extensive new data on negative-parity states in  $^{152}\text{Sm}$  which should shed light on both the role of octupole correlations in the onset of deformation and on signatures of transitional regions that they offer.

A theoretical description of octupole nuclear shapes in their full complexity is not an easy problem; this is because the octupole deformation itself has a large number of degrees of freedom and moreover must be treated in conjunction with the (dominant) quadrupole deformation. It implies extension of kinematical variables by those parametrizing the octupole shape coefficients  $\alpha_\mu^{(3)}$  (in general, one needs seven new real variables) and introduction of many additional parameters of the quadrupole-octupole Hamiltonian.

Separation of internal and external variables (describing the shape in the body-fixed frame and its orientation in the laboratory frame, respectively) is much more difficult in the octupole than in quadrupole case ([Rohozinski, 1988](#)). [Bizzeti and Bizzeti-Sona \(2004, 2008\)](#) introduced a parametrization, in which the tensor of inertia is diagonalized up to terms of first order in the quantities describing nonaxial deformations, but severe dynamical simplifications are needed to keep the problem tractable. With these simplifications, they introduced an X(5)-like two-dimensional model in quadrupole and octupole deformation parameters  $\beta_2$  and  $\beta_3$ . Similarly, [Bonatsos, Lenis, Minkov, et al. \(2005\)](#) constrained the system by requiring strict axial symmetry and investigated solutions similar to X(5) and E(5) near the critical point of the transition from dynamical octupole vibrations to static octupole deformation. Both [Bizzeti and Bizzeti-Sona \(2004, 2008\)](#) and [Bonatsos, Lenis, Minkov, et al. \(2005\)](#) applied their models to the Ra-Th region and identified  $^{226}\text{Th}$  and  $^{226}\text{Ra}$  as being close to critical or border point nuclei in both the quadrupole and octupole degrees of freedom.

Octupole modes can be treated also within the IBA description. The so-called *spdf*-IBA adds negative-parity bosons  $p$  and  $f$  with  $\lambda^\pi=1^-$  and  $3^-$ , respectively, to the familiar pair of bosons  $s$  and  $d$  (Engel and Iachello, 1985, 1987), hence also including E1 and E3 electromagnetic transitions. This model has been addressed in several works [see, e.g., Alonso *et al.* (1995)]. Recently it was applied to describe octupole collectivity in Sm isotopes (Babilon *et al.*, 2005), but its phase structure has not been fully analyzed yet.

Even a more difficult problem is the inclusion of hexadecapole ( $\lambda^\pi=4^+$ ) modes in both geometric and interacting boson models. Dynamical symmetries of the *sdg*-IBA (a version in which the  $g$  boson is added) were discussed by Iachello and Arima (1987) and its shape analysis was introduced by Devi and Kota (1990). The motivation for this extension of the IBA was not so much the existence of stable hexadecapole deformations in nuclei but rather the need to include the E4 dynamical modes. A comprehensive shape phase analysis of the *sdg* model would be in order. As in the previous case, one of the main obstacles is the large number of variables and parameters involved. The phase structure of a simplified *sdg* Hamiltonian was presented by Van Isacker *et al.* (2010).

More extensive (although still incomplete) results are available for a simpler class of IBA modifications, in which the new boson  $x=p, f, g, \dots$  substitutes the  $d$  boson instead of supplementing the  $sd$  set. Since in atomic nuclei quadrupole modes represented by the  $d$  bosons are essential, these *sx*-IBA descriptions (with  $x \neq d$ ) are not suitable for nuclear-structure physics. They are nevertheless relevant in molecular physics, where they give rise to the so-called vibron models (Frank and Van Isacker, 1994; Iachello and Levine, 1995).

The choice  $x=p$  leads to the three-dimensional (3D) vibron model used to describe rotation-vibration spectra of diatomic molecules, with U(4) being the spectrum generating group. Phase transitions in this model were considered by Van Roosmalen (1982) and recently subject to methods going beyond the mean field (Dusuel *et al.*, 2005b). The choice  $x=\tau$ , where  $\tau$  is a two-component boson (it must not be confused with a spin- $\frac{1}{2}$  particle), creates a two-dimensional (2D) vibron model based on the U(3) algebra, which can be applied to bending vibrations in polyatomic molecules (Iachello and Oss, 1996). Phase transitions in the 2D vibron model were studied by Pan, Zhang, Jin, *et al.* (2005), Iachello and Pérez-Bernal (2008), and Pérez-Bernal and Iachello (2008). General features of phase transitions between  $s$  and  $s+x$  condensates in a wider class of U(2)–U(9) models were compared and summarized by Cejnar and Iachello (2007).

### 3. Coupled boson-boson and boson-fermion systems

A number of modifications of the basic IBM-1 description follow from coupling of the Hilbert space generated by  $s^\dagger$  and  $d^\dagger$  boson operators to spaces associated with some additional degrees of freedom. A well-known

example of such coupling is provided by an extended version of the interacting boson model called IBM-2 (Iachello and Arima, 1987). In this version, proton and neutron degrees of freedom are taken into account separately by distinguishing  $s$  and  $d$  bosons associated with protons and neutrons. The corresponding operators may be denoted  $s^{\pi\dagger}, d_\mu^{\pi\dagger}$ , for the proton component, and  $s^{\nu\dagger}, d_\mu^{\nu\dagger}$ , for the neutron component, while the Hilbert space of physical states can be formally identified with  $\mathbf{H} \equiv \mathbf{H}^\pi \otimes \mathbf{H}^\nu$ , a tensor product of spaces corresponding to proton and neutron configurations.

The shape phase analysis of this model was presented simultaneously by Arias *et al.* (2004) and by Caprio and Iachello (2004) [see also Caprio and Iachello (2005)]. The Hamiltonian can be taken in the form (3.21), but with  $n_d$  replaced by  $n_d^{\pi\nu} \equiv n_d^\pi + n_d^\nu$  and  $Q_\chi$  by  $Q_{\chi_\pi \chi_\nu}^{\pi\nu} \equiv Q_{\chi_\pi}^\pi + Q_{\chi_\nu}^\nu$ , where  $n_d^\pi$  (or  $n_d^\nu$ ) and  $Q_{\chi_\pi}^\pi$  (or  $Q_{\chi_\nu}^\nu$ ) stand for the  $d$ -boson number operator and the quadrupole operator of the proton (or neutron) component, respectively. This Hamiltonian is of the form

$$H \propto H^\pi + H^\nu - 2 \frac{1-\eta}{N_B} (Q_{\chi_\pi}^\pi \cdot Q_{\chi_\nu}^\nu), \quad (6.2)$$

where the first two terms are given by Eq. (3.21) applied to both proton and neutron components (with boson numbers  $N_B^\pi + N_B^\nu = N_B$ ) and the last term, which in a general case can be denoted  $H^{\pi\nu}$ , represents an interaction between both components. Note that the proton and neutron quadrupole-operator parameters  $\chi_\pi$  and  $\chi_\nu$  may be equivalently expressed by  $\chi_S = (\chi_\pi + \chi_\nu)/2$  and  $\chi_V = (\chi_\pi - \chi_\nu)/2$ .

The coherent states exploited in the mean-field analysis of a general IBM-2 Hamiltonian read as  $|N_B^\pi, a^\pi, N_B^\nu, a^\nu\rangle = |N_B^\pi, a^\pi\rangle \otimes |N_B^\nu, a^\nu\rangle$ , where  $|N_B^x, a^x\rangle$  with  $x=\pi, \nu$  stand for proton- and neutron-boson condensate states from Eq. (3.24). The energy functional  $F = \langle \Psi | H | \Psi \rangle$  derived from these two-component condensates  $|\Psi\rangle$  contains, besides variables  $\beta^\pi, \gamma^\pi$  and  $\beta^\nu, \gamma^\nu$  characterizing shapes of both proton and neutron “fluids,” Euler angles describing the relative orientation of both intrinsic frames.

It was proved that for the Hamiltonian (6.2) the minimization in Euler angles can only lead to configurations in which both proton and neutron quadrupole deformations have the same internal axes up to reordering. Therefore, besides the phases known from the IBM-1 and their combinations, the two-component model yields also a phase in which proton and neutron fluids exhibit prolate or oblate deformations with perpendicular symmetry axes. These shapes lack axial symmetry. As in the simple treatment outlined in Sec. VI.A.1, the transition from axially symmetric to triaxial shapes has a critical character and is of the second order. The spherical-deformed phase transition is of the first order for axially symmetric deformed shapes and of the second order for triaxial or  $\gamma$ -soft deformed shapes. The phase diagram is shown in Fig. 42.

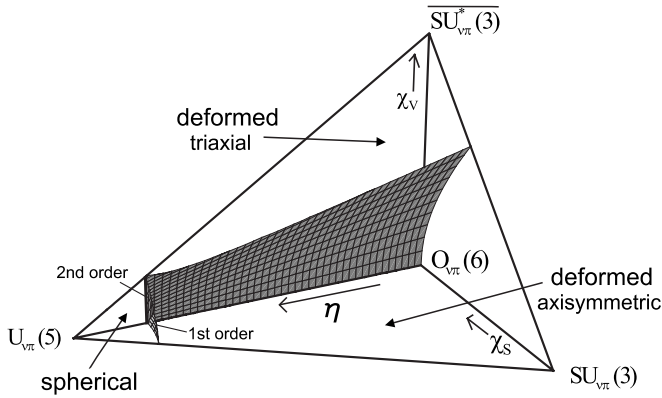


FIG. 42. The phase diagram corresponding to the IBM-2 Hamiltonian (6.2). Adapted from Caprio and Iachello, 2005.

The situation is more complex in another extension of the simple IBA description, which takes into account multiple particle-hole ( $p$ - $h$ ) excitations across the closed shell (Duval and Barrett, 1981, 1982). It is well known that such configurations may benefit from the attractive internucleon interactions so that their energy becomes comparable with normal collective excitations of the valence shell; we then talk about intruder states (Heyde *et al.*, 1983, 2004). A mean-field analysis of these excitations was given [see, e.g., Nazarewicz (1993), Reinhard *et al.* (1999), and Smirnova *et al.* (2003)], while an algebraic description in the IBA framework was developed by De Coster *et al.* (1996, 1997, 1999) and Lehman *et al.* (1997). Consider a simple example in which the valence-shell (normal) collective excitations coexist with  $2p$ - $2h$  intruder configurations. While the normal states are described by an IBM-1 Hamiltonian with a boson number  $N_B$  derived in a standard way from the occupancy of the valence shell, the intruder states can be described by another Hamiltonian with  $N_B+2$  bosons.

The Hilbert space of such an extended model can be written as a direct sum  $\mathbf{H} \equiv \mathbf{H}_1 \oplus \mathbf{H}_2$ , where  $\mathbf{H}_1$  and  $\mathbf{H}_2$  correspond to the orthogonal subspaces of normal and intruder states, respectively, with the associated projection operators denoted as  $P_1$  and  $P_2$ . The Hamiltonian takes the form

$$H = P_1 H_1 P_1 + P_2 H_2 P_2 + H_{\text{mix}}. \quad (6.3)$$

Here  $H_1$  and  $H_2$  represent IBM-1 Hamiltonians corresponding to the normal and intruder configurations, respectively, which may be associated with different equilibrium shapes. These shapes coexist within the same nucleus and become dynamically coupled due to the mixing term  $H_{\text{mix}}$ , whose action on  $\mathbf{H}_1$  yields vectors in  $\mathbf{H}_2$  and vice versa. In the  $0p$ - $0h$  plus  $2p$ - $2h$  model we can set  $H_{\text{mix}} = w_0(s^\dagger s^\dagger + ss) + w_2(d^\dagger \cdot d^\dagger + \tilde{d} \cdot \tilde{d})$ , where  $w_0, w_2$  stand for adjustable constants.

The mean-field description of Hamiltonian (6.3) was introduced by Frank *et al.* (2004) and later elaborated in the phase-transitional analysis by Frank *et al.* (2006), Hellemans *et al.* (2007, 2009), and Morales *et al.* (2008). The method can be reformulated in the following way:

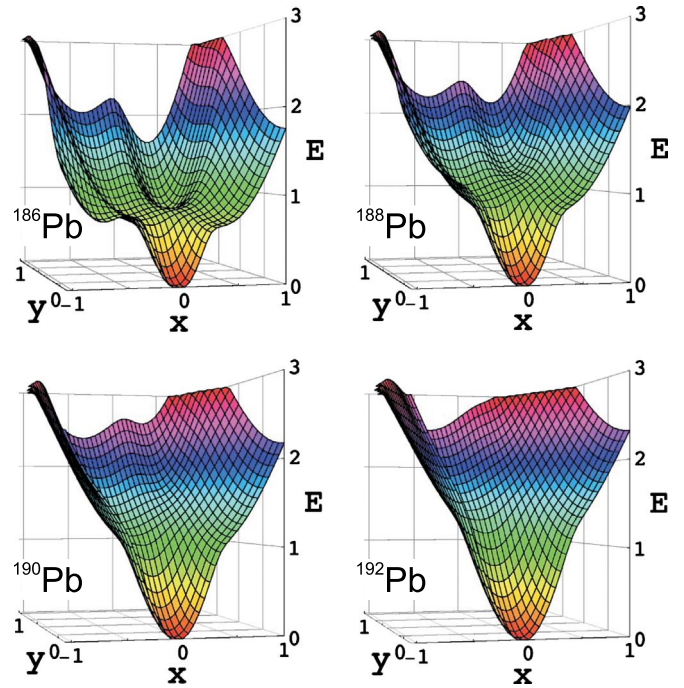


FIG. 43. (Color online) The potential-energy surface for Pb isotopes with  $A=186, 188, 190$ , and  $192$  calculated in the IBA framework including the mixing of particle-hole configurations. Here  $x = \beta \sin(\gamma + \pi/6)$  and  $y = \beta \cos(\gamma + \pi/6)$ . From Frank *et al.*, 2004.

A general wave function is written as a superposition  $|\Psi\rangle = \sum_i c_i |\Psi_i\rangle$ , with  $\sum_i |c_i|^2 = 1$  and both normalized states  $|\Psi_i\rangle \in \mathbf{H}_i$  chosen in the form of condensate states (3.24). The condensates differ in the numbers of bosons, but they are assumed to have the same set of shape parameters  $\beta, \gamma$ . In the  $0p$ - $0h$  plus  $2p$ - $2h$  case we have  $|\Psi_1\rangle = |N_B, a\rangle$  and  $|\Psi_2\rangle = |N_B+2, a\rangle$ . The energy functional  $F \equiv \langle \Psi | H | \Psi \rangle$  depends on shape parameters  $\beta, \gamma$  as well as on coefficients  $\{c_i\}$ , so in search of the form of the ground state it has to be minimized in both these sets of variables. Since the energy functional can be written as

$$F = (c_1^*, c_2^*) \begin{pmatrix} \langle \Psi_1 | H_1 | \Psi_1 \rangle & \langle \Psi_1 | H_{\text{mix}} | \Psi_2 \rangle \\ \langle \Psi_2 | H_{\text{mix}} | \Psi_1 \rangle & \langle \Psi_2 | H_2 | \Psi_2 \rangle \end{pmatrix} \begin{pmatrix} c_1 \\ c_2 \end{pmatrix}, \quad (6.4)$$

the task can be reduced to the minimization of the lower eigenvalue of the middle  $2 \times 2$  matrix in variables  $\beta, \gamma$ . Indeed, the lower eigenvalue represents the minimal energy achievable by a mixing of the two configurations (the  $0p$ - $0h$  and  $2p$ - $2h$  amplitudes in the ground-state wave function being determined by the eigenvector components  $c_1$  and  $c_2$ , respectively). The upper eigenvalue, in turn, represents the maximal energy and corresponds to an excited mean-field state.

Examples of the potential energy surface calculated for four even-even Pb isotopes are shown in Fig. 43. These calculations take into account  $0p$ - $0h$ ,  $2p$ - $2h$ , and  $4p$ - $4h$  configurations, hence generalize the above-outlined approach to three-dimensional matrices. All cases shown have a spherical ground state, but as seen,

the surfaces in the lighter Pb isotopes go beyond the simple forms following from the IBA description without configuration mixing.

A comprehensive phase analysis has been so far performed only for two-dimensional cases, with  $H_1$  and  $H_2$  corresponding to spherical and deformed configurations (Frank *et al.*, 2006; Hellemans *et al.*, 2007) as well as to two different deformed shapes (Morales *et al.*, 2008; Hellemans *et al.*, 2009). In general, a rather complex phase structure is obtained, showing first- or second-order phase transitions between spherical and prolate- or oblate-deformed shapes localized in the domains that sensitively depend on the Hamiltonian internal parameters. The studies performed to date have excluded the phase corresponding to a stable triaxial deformation.

As the last type of coupling in the IBA framework we discuss the interacting boson-fermion model (IBFM) which describes odd- $A$  nuclei in terms of an interacting system of bosons and one fermion (Iachello and Scholten, 1979; Iachello and Van Isacker, 1991). A detailed analysis of this case is of general interest since the influence of an odd fermion on the QPT in a bosonic core may be relevant also in other quantum systems.

The IBFM Hilbert space can be written as a tensor product of the bosonic and fermionic spaces,  $\mathbf{H} \equiv \mathbf{H}_B \otimes \mathbf{H}_F$ , while the Hamiltonian consists of parts describing bosons alone ( $H^B$ ), the odd fermion ( $H^F$ ), and the mutual boson-fermion interaction ( $H^{BF}$ ). As a simple example, consider a fermion on a single-particle shell with angular momentum  $j$  interacting with the bosonic core via a quadrupole-quadrupole coupling

$$H = H^B + H^F - \kappa(Q_\chi^B \cdot \underbrace{[a_j^\dagger \times \tilde{a}_j]^{(2)}}_{Q_j^F}), \quad (6.5)$$

where  $Q_\chi^B \equiv Q_\chi$  stands for the IBM-1 quadrupole operator (3.18), while  $Q_j^F$  is its fermionic analog composed of creation and annihilation operators  $a_{jm}^\dagger$  and  $a_{jm} = (-)^{j+m} \tilde{a}_{j-m}$  for angular momentum projection  $m$ . In a wider context, this interaction can be taken as a part of an IBFM Hamiltonian of the type (3.21), where  $n_d \equiv n_d^B$  is replaced by  $n^{BF} = n_d^B + n_j^F$  (with  $n_j^F$  standing for the fermion number operator) and  $Q_\chi^B$  by  $Q_\chi^{BF} = Q_\chi^B + Q_j^F$ . (Note that the  $Q_j^F \cdot Q_j^F$  term does not count for states with a single fermion.) As in Eq. (6.2), the interaction strength  $\kappa$  is then rewritten as a function of  $\eta$ .

In a realistic case, the Hilbert space of the odd particle should be created by several fermionic orbitals coming from the valence shell of a nucleus, e.g., by the orbitals with angular momenta  $j = \frac{1}{2}, \frac{3}{2}, \frac{5}{2}$  (cf. Sec. V.A.5). This situation was considered in the first phase-transitional study for odd nuclei by Jolie, Heinze, *et al.* (2004) as well as in subsequent analyses of Alonso *et al.* (2007a, 2007b, 2009). In Fig. 44, we show as an example the evolution of IBFM states with the total angular momentum  $L = \frac{1}{2}$  across the prolate-oblate transition. This case, investigated numerically by Jolie, Heinze, *et al.* (2004), indicates that the phase-transitional behavior of the even-even core remains present if an odd fermion is

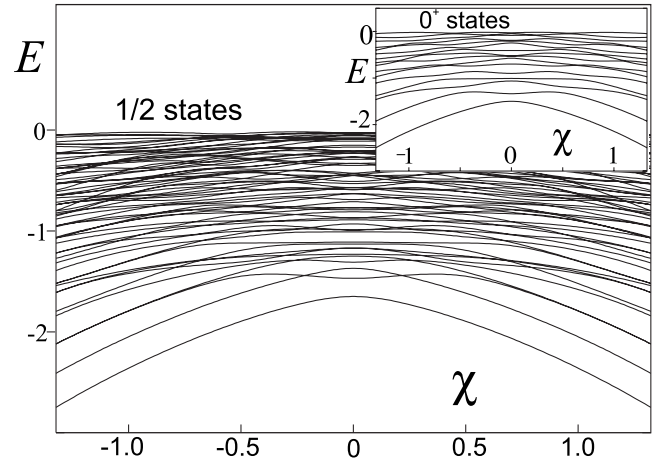


FIG. 44. Level dynamics of the  $L = \frac{1}{2}$  spectrum across the prolate-oblate transition in the IBFM with  $N_B = 10$  bosons and a single fermion with  $j = \frac{1}{2}, \frac{3}{2}, \frac{5}{2}$ . The inset shows the corresponding dynamics of  $L = 0$  states of the bosonic core (cf. Fig. 18). Adapted from Jolie, Heinze, *et al.*, 2004.

introduced. For pedagogical purposes, in order to illustrate the influence of the odd particle on the bosonic core, we now analyze a simpler schematic case with a single  $j$ , namely,  $j = \frac{3}{2}$ , which represents a minimal model in which the boson-fermion interaction from Eq. (6.5) does not vanish (Alonso *et al.*, 2005, 2006; Liu, 2007).

The trial mean-field state can be written in the form  $|\Psi\rangle = |N_B, a\rangle \otimes (\sum_m c_m a_{jm}^\dagger |0\rangle)$ , where the first part stands for the familiar boson condensate (3.24) and the second one represents a single-fermion state in the subshell  $j$  (with  $\sum_m |c_m|^2 = 1$ ). The energy functional  $F \equiv \langle \Psi | H | \Psi \rangle$  must be minimized in both sets of variables  $\beta, \gamma$  (characterizing the bosonic core) and  $\{c_m\}$  (characterizing the odd fermion). Equivalently, one may write down the Hamiltonian matrix expressed in the orthogonal set of states  $|N_B, a\rangle \otimes a_{jm}^\dagger |0\rangle$  and minimize its lowest eigenvalue in variables  $\beta, \gamma$ . For the Hamiltonian (6.5) the second method leads to the following function to be minimized:

$$\frac{F}{N_B} = \frac{F^B}{N_B} - \frac{|\kappa|}{\sqrt{5}} \sqrt{\frac{\beta^2 - \bar{\chi} \beta^3 \cos 3\gamma + \bar{\chi}^2 \beta^4 / 4}{(1 + \beta^2)^2}}, \quad (6.6)$$

where we skipped an unimportant energy shift and introduced notation  $\bar{\chi} = \sqrt{2/7} \chi$ . The term  $F^B/N_B$  stands for the known potential energy surface of the boson Hamiltonian  $H^B$  given by Eq. (3.26) while the square-root term represents the contribution of the boson-fermion interaction.

The phase structure of the model can be read out from Eq. (6.6). Since  $\partial F / \partial \beta|_{\beta=0} \neq 0$  for  $\kappa \neq 0$ , the quadrupole-quadrupole interaction with an odd fermion always generates a deformation of the bosonic core. The spherical-deformed transition of this type does not have a critical character.

The evolution of the deformed shape with increasing value of the interaction strength  $|\kappa|$  depends on interrelation of the coefficient  $B$  from Eq. (3.26) and the parameter  $\chi$  in the boson-fermion interaction (6.5). If  $B$

$\neq 0$  and  $\chi$  have the same sign, the deformation remains axially symmetric (prolate for  $B < 0$  or oblate for  $B > 0$ ) and its  $\gamma$  rigidity  $G \propto \partial^2 F / \partial \gamma^2|_{\beta_0, \gamma_0}$  increases with  $|\kappa|$ . For  $B = 0$ , the type of axial deformation is determined by the sign of  $\chi$ , the point  $\chi = B = 0$  demarcating the prolate-oblate transition (cf. Fig. 44). However, if  $B \neq 0$  has the opposite sign than  $\chi$  (that is, if the boson-fermion interaction drives the bosonic core to the opposite type of deformation than the boson-boson interaction), the increase of  $|\kappa|$  can lead to phase transitions changing the deformation, e.g., from prolate to triaxial and eventually from triaxial to oblate. Critical values of  $|\kappa|$  for these transitions depend on coefficients  $A$ ,  $B$ , and  $C$  from Eq. (3.26).

We conclude by noting that a comprehensive analysis of the phase structure for realistic IBFM Hamiltonians is an important task for the future. This is so not only because of the need to treat the shape evolution in odd nuclei but also because interacting boson-fermion systems are of great interest in a broader physical context.

## B. Mechanism of critical phenomena

In this section, we turn attention to more theoretical aspects of structural phase transitions related to the origin of such phenomena in general quantum systems. In particular, we ask what in the fundamental description of the system converts a smooth transition (crossover) observed in the finite-size case to a nonanalytic phase transition in the infinite-size limit and how it decides whether the transition will be of the first order or continuous. These questions are still open, but some promising clues have been suggested.

### 1. Critical-point scaling properties

As pointed out above (see Sec. IV.A), phase transitions do not typically appear in finite systems. In a finite system, the variation of the ground-state properties with changing control parameters is locally smoothed by quantum fluctuations. This was demonstrated in both the IBM-1 and GCM, whose infinite-size and semiclassical limits are synonymous; therefore, the absence of the zero-point motion in the infinite case drives the ground state to evolve along a sharp (possibly nonanalytic) trajectory of the potential minimum. In a finite case, however, the smeared form of the wave function prohibits a nonanalytic change of the ground-state properties.

Nevertheless, it has been argued (Fisher and Berker, 1982) that the use of the term phase transition makes good sense even in finite cases. The key observation is that at the critical point the scaling of some quantities with the system's size becomes singular, i.e., different from elsewhere in the parameter space. For instance, if the number of IBM-1 bosons  $N_B$  is increasing to asymptotic values, the Hamiltonians (3.21) and (3.22) yield an energy gap  $\Delta = E(2_1^+) - E(0_1^+)$  between the ground state and the first excited state of order  $\Delta(N_B) \sim \mathcal{O}(1)$  everywhere except at the critical curves of the phase diagram in Fig. 13. At these curves the gap de-

creases to zero with  $N_B \rightarrow \infty$ , the type of the critical dependence  $\Delta_c(N_B)$  being specific for the first- and second-order phase transitions present in the symmetry triangle.<sup>20</sup>

Scaling properties of various observables in the IBM-1 and the related Lipkin and vibron models were studied by Dusuel *et al.* (2005a, 2005b), Vidal *et al.* (2006), Arias *et al.* (2007), and Pérez-Bernal and Iachello (2008) with the aid of sophisticated methods going beyond the mean-field (coherent-state) approximation. These analyses showed, for example, that the critical behavior of the gap between the ground state and the first excited state is  $\Delta_c \sim N_B^{-1/3}$  in the second-order ( $\chi = 0$ ) spherical-deformed transition and  $\Delta_c \sim \exp(-aN_B)$  (with  $a > 0$  depending on  $\chi$ ) in the first-order transition. Scaling for some other quantities can be found in the above references.

Rowe (2004a) presented a simple reasoning for the algebraic scaling at the *second-order* critical point. At this point, the IBM-1 Hamiltonian in an appropriate coordinate transcription has the form of a five-dimensional quartic oscillator. In particular, for  $N_B \gg 1$  and  $\beta \approx 0$  (the region near the potential minimum) one can write

$$H_c \approx \frac{1}{2\mathcal{M}N_B} \nabla_\beta^2 + \mathcal{C}N_B\beta^4, \quad (6.7)$$

where  $\nabla_\beta^2$  is the Laplace operator in a five-dimensional space and  $\mathcal{M}$  and  $\mathcal{C}$  are constants depending on the specific parametrization of the Hamiltonian. After rescaling the coordinates according to  $\tilde{\beta} = N_B^{1/3}\beta$ , the dependence of Eq. (6.7) on  $N_B$  is expressed by an overall factor  $N_B^{-1/3}$  in front of the whole Hamiltonian. Note that an equivalent argument holds in an extended family of interacting boson models, i.e., also in the Lipkin and vibron models. Closely related scaling properties of the spectrum at the second-order critical point are also valid in the GCM with the basic potential (3.2) [see Turner and Rowe (2005)]. As discussed by Arias, Alonso, *et al.* (2003) and García-Ramos, Dukelsky, and Arias (2005), the fact that the IBM-1 spectrum at the second-order critical point converges with  $N_B \rightarrow \infty$  to the spectrum of a quartic oscillator is in contrast to the *Ansatz* of the E(5) critical-point solution used in the GCM framework.

The above-mentioned result on the scaling in the *first-order* transition has been obtained within an extended Lipkin model (Vidal *et al.*, 2006). This model can be transformed into a one-dimensional problem with a potential

$$V = \frac{Ax^2 + Bx^3 + Cx^4}{(1+x^2)^2}, \quad (6.8)$$

which is analogous to the GCM and IBM-1 potentials in Eqs. (3.2) and (3.26). In the spinodal region around the

<sup>20</sup>Scaling laws in the form of power-law dependences are introduced for second-order critical points. In the present context, another type of scaling is also applied in first-order transitions.

first-order QPT, the potential (6.8) has a double-well form, the two minima being symmetric at the transitional point. At this point, the low-energy spectrum is formed by nearly degenerate pairs of levels, whose wave functions yield the same weight for the localization in both minima, having symmetric and antisymmetric forms with respect to the exchange of minima. For a decreasing value of  $\hbar \sim N_B^{-1}$ , the tunneling amplitude between the two wells quenches, which exponentially reduces the separation of the levels within the doublets and therefore also the gap  $\Delta_c$  between the ground state and the first excited state.

To numerically analyze scaling properties of the first-order transition in the IBM-1 (Rowe, 2004a; Rosensteel and Rowe, 2005), gets trickier because of the difficulty to access large values of  $N_B$  for a general IBM-1 Hamiltonian.<sup>21</sup> Unfortunately, the first-order critical Hamiltonian obtained from Eqs. (3.21) and (3.22) or from similar parametrizations exhibits a small energy barrier between the coexisting wells (Jolie *et al.*, 1999). To get a sufficient part of the spectrum below the barrier would require extremely large values of  $N_B$ . A way to produce a first-order IBM-1 Hamiltonian with a larger barrier was described by Leviatan (2006, 2007). Nevertheless, a comprehensive analysis of the IBM-1 scaling properties for the first-order phase transition is not yet available.

## 2. Relation to thermal phase transitions

Critical-point scaling properties are closely related to the mechanisms underlying the first- and second-order phase transitions in general quantum systems. It turns out that these mechanisms can be formulated in parallel to standard phase transitions in thermodynamics, although the actual physical contents are different in both cases.

A direct analogy between quantum and thermal phase transitions follows from a formal association of the ground-state energy  $E_0(\xi)$  as a function of the control parameter  $\xi$  with the thermodynamic equilibrium free energy  $F_0(T)$  as a function of temperature  $T$ . The Ehrenfest classification of QPTs is based on this analogy. Such an approach enables one to define a direct QPT analog of the specific heat (Cejnar *et al.*, 2003, 2005), namely,  $c_1 = -d^2 E_0 / d\xi^2$ , which behaves exactly as ordinary spe-

cific heat in thermal phase transitions of the respective order (omitting an unimportant  $T$ -dependent scaling factor). Examples of the  $c_1$  dependence for the IBM-1 first- and second-order phase transitions were shown in the insets of Fig. 18 for increasing boson numbers  $N_B$ . Note that some other possible definitions of the QPT “specific heat” were discussed by Cejnar *et al.* (2001, 2003).

A more sophisticated link between QPTs and classical thermodynamics can be elaborated using a fundamental approach to thermal phase transitions proposed by Yang and Lee (1952). It proceeds by extending the temperature (or another thermodynamic control parameter) into the complex plane  $\tilde{T} = T + iT'$  and analyzing the system's partition function  $Z(\tilde{T}) \equiv \tilde{Z}$  in this plane. By definition, the value of  $\tilde{Z}$  cannot vanish at the real axis, but it can be zero at some places with  $T' \neq 0$ . In finite systems, these places form isolated points which may appear at an arbitrarily small distance from the real axis. If the  $\tilde{Z}=0$  points with an increasing size of the system accumulate infinitesimally close to  $\tilde{T}_c = T_c + i0$ , one encounters a thermodynamic singularity (phase transition) at temperature  $T = T_c$  in the infinite-size limit. The degree of accumulation (the asymptotic density of zeros close to  $\tilde{T}_c$ ) determines the type and order of the phase transition (Grossmann and Rosenhauer, 1967; Borrmann *et al.*, 2000).

A similar mechanism to the one described above was shown to also be applicable to quantum phase transitions (Heiss, 1988; Heiss and Sannino, 1991; Cejnar *et al.*, 2005, 2007; Heiss *et al.*, 2005). Since the temperature is zero in the QPT case, the parameter to be extended to complex values is identified with the interaction strength  $\xi$  driving the system through the transition. We assume here a general linear Hamiltonian

$$H = H_0 + \xi H', \quad [H_0, H'] \neq 0, \quad (6.9)$$

where  $\xi$  is a real number and  $H_0, H'$  are two incompatible Hermitian operators, and consider its extension to  $\tilde{\xi} = \xi + i\xi'$ . The Hamiltonian  $\tilde{H} = H_0 + \tilde{\xi} H'$  is non-Hermitian, i.e., has complex eigenvalues  $\tilde{E}_i$ . The places where two (or more) eigenvalues are equal ( $\tilde{E}_i = \tilde{E}_j$ ) form isolated points in the plane  $\tilde{\xi}$  and may be called non-Hermitian degeneracies (Zirnbauer *et al.*, 1983; Berry, 2004).

The degeneracies can in general be sorted to the so-called diabolic points and exceptional (or branch) points (Kato, 1966; Berry and Wilkinson, 1984).<sup>22</sup> The diabolic

<sup>21</sup>The large- $N_B$  calculations along the U(5)-O(6) side of the symmetry triangle make use of the fact that in absence of the SU(3) term in the decomposition (3.15) the IBM-1 Hamiltonian is invariant under the transformations of the underlying group O(5). As a consequence, seniority  $\tau$  is a good quantum number along the whole transitional path and the Hamiltonian remains integrable all the way. The determination of the spectrum for large boson numbers can then be performed using approaches such as Richardson equations (Arias, Dukelsky, and García-Ramos, 2003), the continuous unitary transformation technique (Dusuel *et al.*, 2005b) or with the aid of large-size diagonalization (Cejnar *et al.*, 2007; Pan *et al.*, 2008; Williams *et al.*, 2008).

<sup>22</sup>This distinction concerns the local behavior of the difference  $\tilde{\Delta}_{ij} = \tilde{E}_i - \tilde{E}_j$  as a function of  $\tilde{\delta} = \tilde{\xi} - \tilde{\xi}_0$  close to the degeneracy at  $\tilde{\xi}_0$ . While in a diabolic point the behavior of  $\tilde{\Delta}_{ij}$  is essentially linear in  $\tilde{\delta}$  (the local dependence of energies has a conical topology), in the branch point it is proportional to  $\sqrt{\tilde{\delta}}$ , which implies that the  $\tilde{E}_i$  and  $\tilde{E}_j$  Riemann sheets are mutually entangled by the square-root singularity.

point is the only type of degeneracy in the Hermitian case, i.e., at real  $\tilde{\xi}$ . However, since we consider here only the sets of levels with the same symmetry quantum numbers, the Hermitian degeneracies (crossings of levels in variable  $\xi$ ) are forbidden (von Neumann and Wigner, 1929). On the other hand, the degeneracies in complex  $\tilde{\xi}$  are always present. They are generically of the branch-point type and form  $n(n-1)/2$  conjugate pairs in the complex plane, where  $n$  is the dimension of the Hilbert space (Zirnbauer *et al.*, 1983). Whenever a non-Hermitian degeneracy comes close to the real axis, one observes an avoided crossing of the corresponding real levels.

As shown by Cejnar *et al.* (2005, 2007), the non-Hermitian degeneracies play an analogous role in the QPTs as do the complex zeros of  $\tilde{Z}$  in thermal phase transitions. In particular, a cumulation of the degeneracies near  $\tilde{\xi}_c = \xi_c + i0$  in the infinite-size limit of the system leads to a quantum phase transition at  $\xi = \xi_c$ . Similarly as in the thermodynamical case, the type (order) of this transition depends on the asymptotic density of the degeneracies near  $\tilde{\xi}_c$ . There is, however, one important difference between these cases. While the thermodynamic system at any  $\tilde{T}$  yields a unique value  $\tilde{Z}$ , the quantum system is characterized by a multivalued function  $\tilde{E}_i(\tilde{\xi})$ . It is useful to think about this function as a single-valued function living on a system of  $n$  interconnected Riemann sheets (Heiss, 1988; Heiss and Sannino, 1991). These sheets can be enumerated according to the ordering of energy levels at real  $\tilde{\xi}$ . Only the degeneracies affecting the Riemann sheet connected with the lowest level are relevant for the ground-state phase transitions.

Extension of the ideas indicated above led to the following redefinition of the QPT specific heat:

$$c_2 = \frac{1}{n-1} \frac{d^2}{d\xi^2} \sum_{i>0} \underbrace{\ln|E_i - E_0|}_{-\tilde{U}_0} \quad (6.10)$$

where the sum  $U_0$  replaces the ground-state energy  $E_0$  from the expression of  $c_1$  given above. Equation (6.10) can be derived from a similarity relation between the partition function  $\tilde{Z}$  and a suitable power of the product  $\tilde{D}_0 = \prod_{i>0} (\tilde{E}_i - \tilde{E}_0)$  (Cejnar *et al.*, 2005). Such a relation captures the above-postulated analogy of the  $\tilde{Z}=0$  and  $\tilde{E}_i = \tilde{E}_0 (\tilde{D}_0=0)$  points, although the actual partition function of the system is of course not given by  $\tilde{D}_0$ .<sup>23</sup> Note that Eq. (6.10) is independent of the energy scale and

<sup>23</sup>Alternatively, Eq. (6.10) can be derived (Cejnar *et al.*, 2007) as a suitable measure of an overall proximity of the relevant branch points to  $\tilde{\xi} = \xi + i0$ , exploiting fictitious association of the branch points on the ground-state Riemann sheet with a two-dimensional gas of charged particles (then  $c_2$  represents a gradient of the “field intensity”).

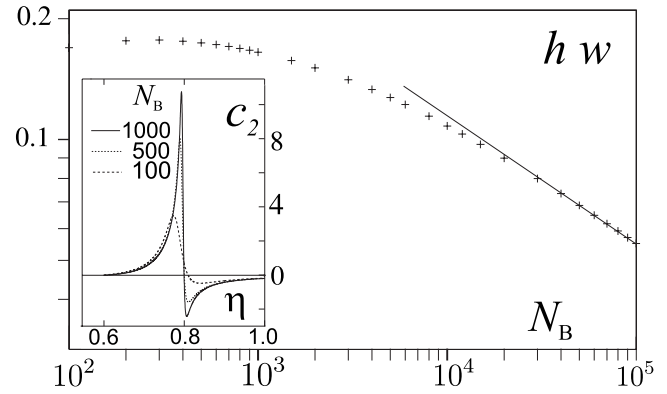


FIG. 45. Features of the “specific heat”  $c_2$  from Eq. (6.10) around the second-order critical point of the IBM-1 Hamiltonian (3.21) scaled by an extra factor  $N_B^{-1}$ . Inset: The dependence of  $c_2$  on  $\eta$  for various boson numbers  $N_B$ . The main panel: The  $N_B$  dependence of the product  $hw$ , where  $h$  is the height of the peak in  $c_2$  and  $w$  its width at half maximum. The  $hw \sim N_B^{-1/3}$  decrease indicates that the “latent heat”  $q_2=0$  (Cejnar *et al.*, 2007).

that the prefactor ensures a proper normalization with increasing size of the system (dimension  $n$  of the Hilbert space).

It turns out that in case of a first-order QPT, an asymptotic form of the quantity in Eq. (6.10) exhibits a  $\delta$ -functional or stronger type of singularity with a non-zero (finite or infinite) value of the “latent heat”  $q_2 = \lim_{\varepsilon \rightarrow 0} \int_{\xi_c - \varepsilon}^{\xi_c + \varepsilon} c_2 d\xi$ . This is always connected with a non-zero asymptotic density of complex degeneracies at the point  $\xi_c$  of the real axis. In second- and higher-order transitions (as well as in continuous phase transitions having no Ehrenfest order), the infinite-size limit of  $c_2$  still shows a singular peak, but with  $q_2=0$ . Such singularities are caused by distributions of complex degeneracies which come infinitely close to the real axis with a density vanishing at  $\xi_c$ .

The latent heat  $q_2$  at the critical point can be estimated from the asymptotic-size behavior of the height  $h$  and width  $w$  of the peak in  $c_2(\xi)$ . Results for the IBM-1 second-order phase transition, namely, for the Hamiltonian (3.21) with  $\eta = \eta_c = \frac{4}{5}$  and  $\chi=0$ , are shown as a function of the boson number in Fig. 45. Note that only the states with spin  $L=0$  and seniority  $\tau=0$  are taken into account and that the whole energy spectrum is multiplied by an extra factor  $N_B^{-1}$  (i.e., is expressed as energy per boson). One observes a roughly linear decrease of the product  $hw$  with  $N_B$  in the log-log scale for  $N_B > 10^4$ , which indicates an asymptotic power-law dependence  $(h \cdot w) \propto N_B^{-k}$ , with the exponent very close to  $k \approx \frac{1}{3}$ . This is tightly connected with the above-discussed scaling of the spectrum at the second-order critical point (Sec. VI.B.1). The density of low-energy levels of the critical Hamiltonian (in the energy-per-boson form) grows  $\rho \propto N_B^{4/3}$ , and the same scaling affects also the density of degeneracies on the ground-state Riemann sheet near the critical point. The convergence implies  $q_2=0$ ,

which indicates that density of degeneracies at  $\eta = \eta_c + i0$  remains zero in the asymptotic-size limit, in agreement with the second-order character of the transition.

We point out that a similar numerical study of the first-order transition has not been performed yet. Progress in this direction is hindered by the above-mentioned difficulty to access large values of  $N_B$  for a general IBM-1 Hamiltonian. A partial analysis (Cejnar and Stránský, 2010) of simpler cases (like a one-dimensional Schrödinger equation with a double-well potential) indicates that the first-order QPT can be locally described as a sharp avoided crossing of just two levels: the ground state and the first excited state [cf. Zamfir *et al.* (2002) and Arias, Dukelsky, and García-Ramos (2003)]. This leads to a much stronger singularity in the dependence  $c_2(\xi)$ , which in some cases produces even infinite values of the latent heat. In contrast, the second-order transition is a “collective” phenomenon, connected with a larger number of levels coming close together in the asymptotic-size regime due to a flat (e.g., quartic) form of the potential.

### C. Quantum phase transitions for excited states

Since quantum phase transitions occur at zero temperature, it is clear that their rigorous definition is restricted merely to the ground state. Nevertheless, as we discussed above, low-lying excited states reflect the change of the ground state in a variety of ways. But how far in the spectrum is the QPT felt? In solid-state physics, the finite-temperature (canonical) approach is standardly applied to answer this question, showing that the  $T=0$  QPT usually extends to the  $T>0$  domain in the form of a thermal phase transition (Sachdev, 1999; Vojta, 2003).<sup>24</sup> However, in the case of a finite quantum system (such as an atomic nucleus) the microcanonical approach is more convenient. It is based on considering individual excited states rather than a thermal population of the whole ensemble of states. As shown below, even with this approach one may observe nonanalytic properties accompanying the ground-state QPT up to very high excitation energies. The relation of these properties to known features of thermal phase transitions is not yet completely analyzed, but the present class of models offers a suitable tool for related research.

Excited-state quantum phase transitions (ESQPTs) can be observed in the “dynamics” of energy levels with variable control parameter, as well as in the dependence of the level density on excitation energy. It turns out that in a vicinity of the first- and second-order QPTs the spectrum of excited states develops some characteristic singularities in both these signatures. A simple example is given in Fig. 46, where we show level dynamics around

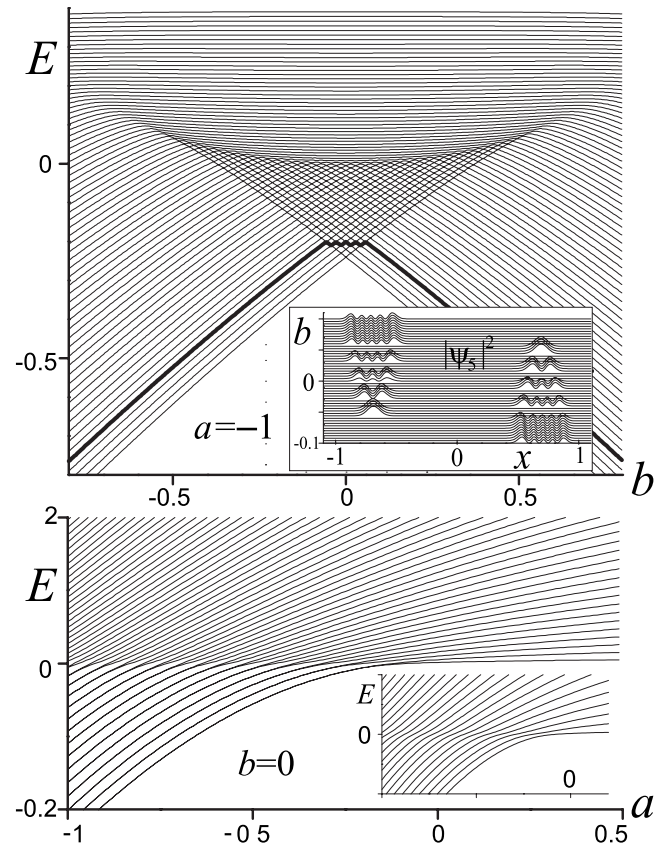


FIG. 46. Level dynamics of the cusp Hamiltonian (6.11) with a finite value of mass parameter  $M$  around the first-order (upper panel) and second-order (lower panel) QPTs. The upper inset shows the evolution of the fifth-state squared wave function, while the lower one depicts the dynamics of positive parity states. Adapted from Cejnar and Stránský, 2008.

ground-state QPTs for a one-dimensional Hamiltonian

$$H = -\frac{\hbar^2}{2M} \frac{d^2}{dx^2} + x^4 + ax^2 + bx \quad (6.11)$$

with the so-called cusp potential (referring to terminology of the catastrophe theory). This Hamiltonian is a prototype for (a) first-order and (b) second-order quantum phase transitions, which are achieved (a) for  $a < 0$  and  $b$  variable (the critical point at  $b_c = 0$ , where two coexisting minima of the potential swap) and (b) for  $b = 0$  and  $a$  variable (the critical point at  $a_c = 0$ , where the potential changes from a degenerate double-well to a single-well form). The dynamics of excited levels close to these critical points is shown in the upper and lower panels of Fig. 46.

We know that the ground-state transitions for the Hamiltonian (6.11) become truly discontinuous only in the infinite-size limit  $M \rightarrow \infty$ . In this limit, the first-order QPT is accompanied by singularities forming a  $\nabla$ -shaped region, which can be observed in the upper panel of Fig. 46 (the leftmost and rightmost limits of this region coincide with the spinodal and antispinodal points of the potential). The lower two sides of this triangle correspond to the first-order ESQPT: the slope of individual

<sup>24</sup>Note that in the context of solid-state physics models a more important issue than the QPT-related thermal (classical) phase transitions is the existence of a  $0 < T < T_{\text{up}}$  quantum critical region (with  $T_{\text{up}}$  a certain cutoff temperature) where quantum and thermal fluctuations compete (Vojta, 2003).

level energies changes abruptly as the level enters the  $\nabla$  region and the level density jumps to a higher value. The upper side of the  $\nabla$  region represents a continuous ESQPT (with no Ehrenfest classification), where the level density develops a singular peak. The inset shows a squared wave function of the fifth level (thick curve in the main panel) as an illustration of a changing structure of eigenstates passing the transitional region.

The second-order ground-state transition, on the other hand, induces a chain of ESQPTs along the line  $E=0$ ,  $a < 0$ , which is seen in the lower panel of Fig. 46. In this case, similarly as for the upper side of the  $\nabla$  region, the transitions are continuous with no Ehrenfest order. Note that for  $b=0$  parity can be assigned to all eigenstates and the lower inset shows a subset with  $\pi=+$ .

The cusp Hamiltonian is also closely connected with the Lipkin model including, in general, parity-breaking terms (Vidal *et al.*, 2006). Moreover, the case with  $b=0$  is related to the subset of IBM-1 states with  $L=0$  along the U(5)-O(6) transition [vanishing admixture of the SU(3) Casimir invariant] as well as to the U(2)-O(3) and U(3)-O(4) transitions in the 2D and 3D vibron models, respectively. Although the use of the coherent-state formalism in these models leads to potentials that replace the linear term of the cusp potential by a cubic one [cf. Eq. (6.8)], the link between both forms is possible with the aid of suitable transformations (Cejnar and Iachello, 2007). The mass parameter in the cusp Hamiltonian is given by  $\propto N_B^2$  in the bosonic models (in the energy-per-boson scaling of the Hamiltonian), although in the latter case the kinetic terms are generally more complicated.

Instead of parity, which needs to be taken into account in the reflection-symmetric ( $b=0$ ) cusp and Lipkin models, the U( $n$ )-O( $n+1$ ) transitions in the IBM-1 and vibron models are characterized by generalized angular momentum quantum numbers associated with the underlying algebra O( $n$ ). Along the U(5)-O(6) transition in the IBM-1 all states with O(3) angular momentum  $L=0$  are sorted by the O(5) quantum number (seniority) into groups that behave differently with respect to the phase transition. Specifically, it can be shown that the ESQPT signatures fade away with increasing seniority, the scaling being described by variable  $\tau/N_B$  (Cejnar *et al.*, 2006). Note that in the lower panel of Fig. 18 we showed the dynamics of  $L=0$  states with all allowed seniorities. The  $E \approx 0$  level bunching pattern that can be seen in this figure is an analog of the ESQPT structure in the lower panel of Fig. 46.

The excited-state phase transition in the Lipkin model (the parity conserving version) was first noticed by Leyvraz and Heiss (2005), although probably an equivalent result had been derived in the finite-temperature formalism already by Gilmore and Feng (1978). The same phenomenon was independently analyzed in the IBM-1 (Cejnar *et al.*, 2006; Heinze *et al.*, 2006; Macek *et al.*, 2006) and later also in the 2D vibron model (Pérez-Bernal and Iachello, 2008). The latter examples exploited a close relation of the ESQPT in two-dimensional cases with the existence of the so-called

monodromy in the phase space of the corresponding classical system.<sup>25</sup> It was shown that rather similar transitions exist in a much wider class of many-body models with a second-order QPT (Caprio *et al.*, 2008). Recent work by Relaño *et al.* (2008) and Pérez-Fernández *et al.* (2009) demonstrated the general importance of ESQPT effects in quantum dynamics of coupled quantum systems.

Concerning the ESQPT structures accompanying the first-order ground-state QPT, the results are much scarcer. Cejnar and Stránský (2008) analyzed the one-dimensional cusp case (upper panel of Fig. 46) as well as a two-dimensional model closely related to the GCM with  $L=0$ . It turns out that the role of dimension is crucial. An increase of dimension generically leads to quenching of the ESQPT signatures, although a larger sample of model examples is needed to verify this conclusion. Excited-state structures along the first-order phase-transitional path in the IBM-1 await an analysis.

Finite-size precursors of excited-state phase transitions should be sought in nuclear spectra, but in view of the relatively high excitation energies where the ESQPT predictions become relevant we have to wait for a significant extension of experimental results. In molecules, on the other hand, the sudden density changes of high-energy spectra predicted by the vibron and related models can be observed with the aid of present day technology. Similar effects probably exist in many other finite quantum systems, forming an analog of thermal phase transitions in macroscopic systems. One may therefore expect rapid progress in this field.

## VII. SUMMARY

The study of ground-state or quantum phase transitions in atomic nuclei was proposed in the late 1970s within the framework of the interacting boson approximation. During the last decade, the subject has undergone a real revival which we have reviewed here. Essential thereby were, on the one hand, the elaboration of critical-point solutions and the discussion of  $N=90$  isotones as examples of the X(5) description and, on the other hand, the systematic numerical studies using the interacting boson model.

We have highlighted in Sec. II the empirical evidence that the shape of an atomic nucleus is an important attribute. The key experimental signatures of collective behavior, nuclear shapes, and their variations for extended regions of the nuclear chart have been presented. From these data, two essential classes of even-even nuclei emerged: spherical nuclei that exhibit vibrational

<sup>25</sup>Monodromy is a certain topological anomaly in the phase space of a classical integrable system of dimension two, which shows up as a point defect in the spectrum of quantum states (Cushman and Bates, 1997). For one-dimensional systems, a similar anomaly may result from the presence of a phase-space separatrix. These nonanalytic structures represent specific classical counterparts of the ESQPT (Caprio *et al.*, 2008).

collective excitations and deformed nuclei, showing both rotational and vibrational features, for which the deformed shapes can be either prolate, oblate, or  $\gamma$  soft (i.e., unstable against the onset of triaxiality). Of course, many nuclei are intermediate between these classes, including the phase-transitional nuclei that are the focus of this review.

In Sec. III, the geometrical collective model and interacting boson model were presented and interrelated via the formalism of coherent states. The role of dynamical symmetries, which yield benchmarks of nuclear shapes, was presented as well as the so-called consistent- $Q$  Hamiltonian and the associated symmetry triangle. Two first-order phase transitions were found, a spherical-deformed one and a prolate-oblate one, as well as an isolated second-order phase transition at the intersection of both. A connection to Landau theory of continuous phase transitions could be established both for the interacting boson model and for the geometric collective model. The results obtained in these simple models are reflected by a number of studies of shape-phase transitions in more microscopically oriented models, which translate the findings of the simpler models to language at the level of nucleons and their interactions. This is typical for research in nuclear structure, where the complexity of the many-body problem can only be attacked by a clever mix of phenomenological and microscopic descriptions.

In Sec. IV, the shape phase transitions in the interacting boson model were studied and compared to experimental data. The effects of the finite number of bosons (associated with pairs of valence nucleons or holes) are of particular interest here, as they smooth the signatures of phase transitions. Several regions of the nuclear chart were compared to the predictions of the model. Clear examples of both types of the first-order phase transition could be identified, as well as candidates indicating the second-order phase transition. We have highlighted the relation between phases of a many-body system and the underlying symmetries using the concept of the quasidynamical symmetry.

In Sec. V, we presented the X(5), E(5), and some other critical-point solutions of the geometric collective model. These represent special forms of the potential  $V(\beta, \gamma)$  which, when introduced into the Bohr Hamiltonian, allow for semianalytic descriptions of spectra at the critical points of shape-phase transitions. The X(5) predictions were compared in detail with data on  $^{152}\text{Sm}$  and candidates for E(5) were also discussed. In addition, models incorporating ranges of structures, e.g., between the vibrator and X(5) or between X(5) and the axial rotor, have been reviewed. One very positive outcome of the shape phase transitions is a real revival of the use of the geometric collective model.

In Sec. VI, the most important extensions of the above-discussed models to more complex systems were outlined. These extensions deal with new degrees of freedom, allowing, e.g., the treatment of nuclei with an odd number of nucleons. Research in this field, so far mostly theoretical, is important not only because of its

potential relevance for actual nuclear systems but also because it provides a valuable insight into the nature of quantum phase-transitional phenomena in general. It was argued that the models of nuclear collective motion, apart from their empirical content, represent a useful laboratory for testing and even inventing new theoretical descriptions of various types of critical phenomena in quantum many-body systems.

## ACKNOWLEDGMENTS

We are grateful to many colleagues for fruitful collaborations and numerous important discussions related to the topic of this review, in particular Y. Alhassid, C. E. Alonso, J. M. Arias, R. Bijker, D. Bonatsos, D. S. Brenner, R. B. Cakirli, M. Caprio, O. Castaños, S. De Baerdemacker, A. Dewald, J. Dobeš, J. Dukelsky, M. Fetea, A. Frank, J. E. García-Ramos, S. Heinze, V. Hellemans, K. L. G. Heyde, F. Iachello, R. V. Jolos, A. Leviatan, M. Macek, E. A. McCutchan, W. Nazarewicz, Y. Oktem, F. Pérez-Bernal, N. Pietralla, S. Pittel, P. Regan, D. Rowe, P. Stránský, G. Thiamová, P. Van Isacker, P. von Brentano, D. D. Warner, V. Werner, N. V. Zamfir, and V. Zelevinsky. We thank M. Caprio, K. L. G. Heyde, F. Iachello, and M. Vojta for useful comments on the paper and R. B. Cakirli, R. Casperson, P. Farnsworth, and M. Spousta for their help in the preparation of figures. This work was supported by the Czech Science Foundation (Grant No. 202/09/0084), the Czech Ministry of Education (Contract No. 0021620859), the Deutsche Forschungsgemeinschaft (Grants No. JO391/5-1 and No. Ko.142/112-1), and the U.S. Department of Energy (Grant No. DE-FG02-91EE-40609).

## REFERENCES

- Åberg, S., H. Flocard, and W. Nazarewicz, 1990, *Annu. Rev. Nucl. Part. Sci.* **40**, 439.
- Alhassid, Y., and N. Whelan, 1991, *Phys. Rev. Lett.* **67**, 816.
- Alhassid, Y., J. Zingmann, and S. Levit, 1987, *Nucl. Phys. A* **469**, 205.
- Alonso, C. A., J. M. Arias, L. Fortunato, and A. Vitturi, 2009, *Phys. Rev. C* **79**, 014306.
- Alonso, C. A., J. M. Arias, H. M. Sofia, and A. Vitturi, 1996, *Nucl. Phys. A* **604**, 53.
- Alonso, C. E., J. M. Arias, L. Fortunato, and A. Vitturi, 2005, *Phys. Rev. C* **72**, 061302(R).
- Alonso, C. E., J. M. Arias, A. Frank, H. M. Sofia, S. M. Lenzi, and A. Vitturi, 1995, *Nucl. Phys. A* **586**, 100.
- Alonso, C. E., J. M. Arias, and A. Vitturi, 2006, *Phys. Rev. C* **74**, 027301.
- Alonso, C. E., J. M. Arias, and A. Vitturi, 2007a, *Phys. Rev. C* **75**, 064316.
- Alonso, C. E., J. M. Arias, and A. Vitturi, 2007b, *Phys. Rev. Lett.* **98**, 052501.
- Arias, J. M., 2001, *Phys. Rev. C* **63**, 034308.
- Arias, J. M., C. E. Alonso, A. Vitturi, J. E. García-Ramos, J. Dukelsky, and A. Frank, 2003, *Phys. Rev. C* **68**, 041302(R).
- Arias, J. M., J. Dukelsky, and J. E. García-Ramos, 2003, *Phys. Rev. Lett.* **91**, 162502.
- Arias, J. M., J. Dukelsky, J. E. García-Ramos, and J. Vidal,

- 2007, *Phys. Rev. C* **75**, 014301.
- Arias, J. M., J. E. García-Ramos, and J. Dukelsky, 2004, *Phys. Rev. Lett.* **93**, 212501.
- Arima, A., and F. Iachello, 1975, *Phys. Rev. Lett.* **35**, 1069.
- Arima, A., and F. Iachello, 1976, *Ann. Phys. (N.Y.)* **99**, 253.
- Arima, A., and F. Iachello, 1978, *Ann. Phys. (N.Y.)* **111**, 201.
- Arima, A., and F. Iachello, 1979, *Ann. Phys. (N.Y.)* **123**, 468.
- Arima, A., T. Otsuka, F. Iachello, and I. Talmi, 1977, *Phys. Lett.* **66B**, 205.
- Audi, G., A. H. Wapstra, and C. Thibault, 2003, *Nucl. Phys. A* **729**, 337.
- Babilon, M., N. V. Zamfir, D. Kusnezov, E. A. McCutchan, and A. Zilges, 2005, *Phys. Rev. C* **72**, 064302.
- Bahri, C., D. J. Rowe, and W. Wijesundera, 1998, *Phys. Rev. C* **58**, 1539.
- Bender, M., P.-H. Heenen, and P.-G. Reinhard, 2003, *Rev. Mod. Phys.* **75**, 121.
- Berry, M. V., 2004, *Czech. J. Phys.* **54**, 1039.
- Berry, M. V., and M. Wilkinson, 1984, *Proc. R. Soc. London, Ser. A* **392**, 15.
- Bijker, R., R. F. Casten, N. V. Zamfir, and E. A. McCutchan, 2003, *Phys. Rev. C* **68**, 064304.
- Bizzeti, P. G., and A. M. Bizzeti-Sona, 2002, *Phys. Rev. C* **66**, 031301(R).
- Bizzeti, P. G., and A. M. Bizzeti-Sona, 2004, *Phys. Rev. C* **70**, 064319.
- Bizzeti, P. G., and A. M. Bizzeti-Sona, 2008, *Phys. Rev. C* **77**, 024320.
- Bjerrregaard, J. H., *et al.*, 1966, *Nucl. Phys.* **86**, 145.
- Blaizot, J. P., and E. R. Marshalek, 1978, *Nucl. Phys. A* **309**, 453.
- Bohm, A., Y. Ne'eman, and A. O. Barut, 1988, Eds., *Dynamical Groups and Spectrum Generating Algebras* (World Scientific, Singapore).
- Bohr, A., 1952, K. Dan. Vidensk. Selsk. Mat. Fys. Medd. **26**, 14.
- Bohr, A., and B. R. Mottelson, 1975, *Nuclear Structure* (Benjamin, New York).
- Bohr, A., and B. R. Mottelson, 1980, *Phys. Scr.* **22**, 468.
- Bonatsos, D., 1988, *Interacting Boson Models of Nuclear Structure* (Oxford University Press, Oxford).
- Bonatsos, D., D. Lenis, E. A. McCutchan, D. Petrellis, and I. Yigitoglu, 2007, *Phys. Lett. B* **649**, 394.
- Bonatsos, D., D. Lenis, N. Minkov, D. Petrellis, P. P. Raychev, and P. A. Terziev, 2004a, *Phys. Rev. C* **70**, 024305.
- Bonatsos, D., D. Lenis, N. Minkov, D. Petrellis, P. P. Raychev, and P. P. Terziev, 2004b, *Phys. Lett. B* **584**, 40.
- Bonatsos, D., D. Lenis, N. Minkov, D. Petrellis, and P. Yotov, 2005, *Phys. Rev. C* **71**, 064309.
- Bonatsos, D., D. Lenis, N. Minkov, P. P. Raychev, and P. A. Terziev, 2004a, *Phys. Rev. C* **69**, 044316.
- Bonatsos, D., D. Lenis, N. Minkov, P. P. Raychev, and P. A. Terziev, 2004b, *Phys. Rev. C* **69**, 014302.
- Bonatsos, D., D. Lenis, and D. Petrellis, 2007, *Rom. Rep. Phys.* **59**, 273.
- Bonatsos, D., D. Lenis, D. Petrellis, and P. A. Terziev, 2004, *Phys. Lett. B* **588**, 172.
- Bonatsos, D., D. Lenis, D. Petrellis, P. A. Terziev, and I. Yigitoglu, 2005, *Phys. Lett. B* **621**, 102.
- Bonatsos, D., D. Lenis, D. Petrellis, P. A. Terziev, and I. Yigitoglu, 2006, *Phys. Lett. B* **632**, 238.
- Bonatsos, D., D. Lenis, N. Pietralla, and P. A. Terziev, 2006, *Phys. Rev. C* **74**, 044306.
- Bonatsos, D., E. A. McCutchan, and R. F. Casten, 2008, *Phys. Rev. Lett.* **101**, 022501.
- Bonatsos, D., E. A. McCutchan, and R. F. Casten, 2010, *Phys. Rev. Lett.* **104**, 022502.
- Bonatsos, D., E. A. McCutchan, R. F. Casten, and R. J. Casperson, 2008, *Phys. Rev. Lett.* **100**, 142501.
- Bonatsos, D., E. A. McCutchan, N. Minkov, R. F. Casten, P. Yotov, D. Lenis, D. Petrellis, and I. Yigitoglu, 2007, *Phys. Rev. C* **76**, 064312.
- Borrmann, P., O. Mülken, and J. Harting, 2000, *Phys. Rev. Lett.* **84**, 3511.
- Boztosun, I., D. Bonatsos, and I. Inci, 2008, *Phys. Rev. C* **77**, 044302.
- Brenner, D. S., 2002, in *Mapping the Triangle*, edited by A. Aprahamian, J. A. Cizewski, S. Pittel, and N. V. Zamfir, AIP Conf. Proc. No. 638 (AIP, Melville, NY), p. 223.
- Buchinger, F., *et al.*, 1990, *Phys. Rev. C* **41**, 2883.
- Butler, P. A., and W. Nazarewicz, 1996, *Rev. Mod. Phys.* **68**, 349.
- Cakirli, R. B., and R. F. Casten, 2006, *Phys. Rev. Lett.* **96**, 132501.
- Cakirli, R. B., and R. F. Casten, 2008, *Phys. Rev. C* **78**, 041301(R).
- Cakirli, R. B., R. F. Casten, R. Winkler, K. Blaum, and M. Kowalska, 2009, *Phys. Rev. Lett.* **102**, 082501.
- Cambiaggio, M. C., J. Dukelsky, and G. R. Zemba, 1985, *Phys. Lett.* **162B**, 203.
- Caprio, M. A., 2002, *Phys. Rev. C* **65**, 031304(R).
- Caprio, M. A., 2003, *Phys. Rev. C* **68**, 054303.
- Caprio, M. A., 2004, *Phys. Rev. C* **69**, 044307.
- Caprio, M. A., 2005, *Phys. Rev. C* **72**, 054323.
- Caprio, M. A., 2009, *Phys. Lett. B* **672**, 396.
- Caprio, M. A., P. Cejnar, and F. Iachello, 2008, *Ann. Phys. (N.Y.)* **323**, 1106.
- Caprio, M. A., and F. Iachello, 2004, *Phys. Rev. Lett.* **93**, 242502.
- Caprio, M. A., and F. Iachello, 2005, *Ann. Phys. (N.Y.)* **318**, 454.
- Caprio, M. A., and F. Iachello, 2007, *Nucl. Phys. A* **781**, 26.
- Caprio, M. A., *et al.*, 2002, *Phys. Rev. C* **66**, 054310.
- Cardman, L. S., 2006, *Eur. Phys. J. A* **28**, 7.
- Castañón, O., A. Frank, and P. Van Isacker, 1984, *Phys. Rev. Lett.* **52**, 263.
- Casten, R. F., 1981, in *Interacting Bose-Fermi Systems in Nuclei*, edited by F. Iachello (Plenum, New York), p. 1.
- Casten, R. F., 2000, *Nuclear Structure from a Simple Perspective* (Oxford University Press, Oxford).
- Casten, R. F., 2006, *Nat. Phys.* **2**, 811.
- Casten, R. F., 2009, *Prog. Part. Nucl. Phys.* **62**, 183.
- Casten, R. F., D. S. Brenner, and P. E. Haustein, 1987, *Phys. Rev. Lett.* **58**, 658.
- Casten, R. F., D. Kusnezov, and N. V. Zamfir, 1999, *Phys. Rev. Lett.* **82**, 5000.
- Casten, R. F., and E. A. McCutchan, 2007, *J. Phys. G* **34**, R285.
- Casten, R. F., and D. D. Warner, 1988, *Rev. Mod. Phys.* **60**, 389.
- Casten, R. F., D. D. Warner, D. S. Brenner, and R. L. Gill, 1981, *Phys. Rev. Lett.* **47**, 1433.
- Casten, R. F., M. Wilhelm, E. Radermacher, N. V. Zamfir, and P. von Brentano, 1998, *Phys. Rev. C* **57**, R1553.
- Casten, R. F., and N. V. Zamfir, 2000, *Phys. Rev. Lett.* **85**, 3584.
- Casten, R. F., and N. V. Zamfir, 2001, *Phys. Rev. Lett.* **87**, 052503.
- Casten, R. F., N. V. Zamfir, and D. S. Brenner, 1993, *Phys. Rev.*

- Lett.* **71**, 227.
- Casten, R. F., N. V. Zamfir, and R. Krücken, 2003, *Phys. Rev. C* **68**, 059801.
- Caurier, E., G. Martínez-Pinedo, F. Nowacki, A. Poves, and A. P. Zuker, 2005, *Rev. Mod. Phys.* **77**, 427.
- Cejnar, P., 2002, *Phys. Rev. C* **65**, 044312.
- Cejnar, P., 2003, *Phys. Rev. Lett.* **90**, 112501.
- Cejnar, P., and H. B. Geyer, 2001, *Phys. Rev. C* **64**, 034307.
- Cejnar, P., S. Heinze, and J. Dobeš, 2005, *Phys. Rev. C* **71**, 011304(R).
- Cejnar, P., S. Heinze, and J. Jolie, 2003, *Phys. Rev. C* **68**, 034326.
- Cejnar, P., S. Heinze, and M. Macek, 2007, *Phys. Rev. Lett.* **99**, 100601.
- Cejnar, P., and F. Iachello, 2007, *J. Phys. A* **40**, 581.
- Cejnar, P., and J. Jolie, 1998a, *Phys. Lett. B* **420**, 241.
- Cejnar, P., and J. Jolie, 1998b, *Phys. Rev. E* **58**, 387.
- Cejnar, P., and J. Jolie, 2000, *Phys. Rev. E* **61**, 6237.
- Cejnar, P., and J. Jolie, 2004, *Phys. Rev. C* **69**, 011301(R).
- Cejnar, P., and J. Jolie, 2009, *Prog. Part. Nucl. Phys.* **62**, 210.
- Cejnar, P., M. Macek, S. Heinze, J. Jolie, and J. Dobeš, 2006, *J. Phys. A* **39**, L515.
- Cejnar, P., and P. Stránský, 2008, *Phys. Rev. E* **78**, 031130.
- Cejnar, P., and P. Stránský, 2010, unpublished.
- Cejnar, P., V. Zelevinsky, and V. V. Sokolov, 2001, *Phys. Rev. E* **63**, 036127.
- Chacón, E., and M. Moshinsky, 1977, *J. Math. Phys.* **18**, 870.
- Charlwood, F. C., K. Baczyńska, J. Billowes, P. Campbell, B. Cheal, T. Eronen, D. H. Forest, and A. Jokinen, 2009, *Phys. Lett. B* **674**, 23.
- Chen, H., J. R. Brownstein, and D. J. Rowe, 1990, *Phys. Rev. C* **42**, 1422.
- Chou, W.-T., Gh. Cata-Danil, N. V. Zamfir, R. F. Casten, and N. Pietralla, 2001, *Phys. Rev. C* **64**, 057301.
- Chou, W.-T., N. V. Zamfir, and R. F. Casten, 1997, *Phys. Rev. C* **56**, 829.
- Clark, R. M., R. F. Casten, L. Bettermann, R. Winkler, 2009, *Phys. Rev. C* **80**, 011303(R).
- Clark, R. M., *et al.*, 2003, *Phys. Rev. C* **68**, 037301.
- Clark, R. M., *et al.*, 2004, *Phys. Rev. C* **69**, 064322.
- Cushman, R. H., and L. Bates, 1997, *Global Aspects of Classical Integrable Systems* (Birkhäuser, Basel).
- Davidson, P. M., 1932, *Proc. R. Soc. London* **135**, 459.
- Davis, E. D., and W. D. Heiss, 1986, *J. Phys. G* **12**, 805.
- De Baerdemacker, S., K. L. G. Heyde, and V. Hellemans, 2007, *J. Phys. A* **40**, 2733.
- De Baerdemacker, S., K. L. G. Heyde, and V. Hellemans, 2009, *Phys. Rev. C* **79**, 034305.
- De Coster, C., B. Decroix, K. L. G. Heyde, P. Van Isacker, J. Jolie, H. Lehmann, and J. L. Wood, 1999, *Nucl. Phys. A* **651**, 31.
- De Coster, C., K. L. G. Heyde, B. Decroix, P. Van Isacker, J. Jolie, H. Lehmann, and J. L. Wood, 1996, *Nucl. Phys. A* **600**, 251.
- De Coster, C., K. L. G. Heyde, B. Decroix, J. L. Wood, J. Jolie, and H. Lehmann, 1997, *Nucl. Phys. A* **621**, 802.
- de-Shalit, A., and M. Goldhaber, 1953, *Phys. Rev.* **92**, 1211.
- de-Shalit, A., and I. Talmi, 1963, *Nuclear Shell Theory* (Academic, New York).
- Devi, Y. D., and V. K. B. Kota, 1990, *Z. Phys. A* **337**, 15.
- Dewald, A., *et al.*, 2004, *Eur. Phys. J. A* **20**, 173.
- Dewald, A., *et al.*, 2005, *J. Phys. G* **31**, S1427.
- Dieperink, A. E. L., and O. Scholten, 1980, *Nucl. Phys. A* **346**, 125.
- Dieperink, A. E. L., O. Scholten, and F. Iachello, 1980, *Phys. Rev. Lett.* **44**, 1747.
- Dobaczewski, J., W. Nazarewicz, J. Skalski, and T. Werner, 1988, *Phys. Rev. Lett.* **60**, 2254.
- Dobeš, J., 1985, *Phys. Lett.* **158B**, 97.
- Dobeš, J., 1990, *Phys. Rev. C* **42**, 2023.
- Dukelsky, J., G. G. Dussel, R. P. J. Perazzo, and H. M. Sofia, 1983, *Phys. Lett.* **130B**, 123.
- Dukelsky, J., and S. Pittel, 2001, *Phys. Rev. Lett.* **86**, 4791.
- Dusuel, S., J. Vidal, J. M. Arias, J. Dukelsky, and J. E. García-Ramos, 2005a, *Phys. Rev. C* **72**, 011301(R).
- Dusuel, S., J. Vidal, J. M. Arias, J. Dukelsky, and J. E. García-Ramos, 2005b, *Phys. Rev. C* **72**, 064332.
- Duval, P. D., and B. R. Barrett, 1981, *Phys. Lett.* **100B**, 223.
- Duval, P. D., and B. R. Barrett, 1982, *Nucl. Phys. A* **376**, 213.
- Ehrenfest, P., 1933, *Supplement No. 75b zu den Mitteilungen aus dem Kamerlingh Onnes Instituut* (Kamerlingh Onnes Instituut, Leiden).
- Elliott, J. P., J. A. Evans, and P. Park, 1986, *Phys. Lett.* **169B**, 309.
- Engel, J., and F. Iachello, 1985, *Phys. Rev. Lett.* **54**, 1126.
- Engel, J., and F. Iachello, 1987, *Nucl. Phys. A* **472**, 61.
- Epelbaum, E., H.-W. Hammer, and U.-G. Meissner, 2009, *Rev. Mod. Phys.* **81**, 1773.
- Federman, P., and S. Pittel, 1977, *Phys. Lett.* **69B**, 385.
- Federman, P., and S. Pittel, 1979, *Phys. Rev. C* **20**, 820.
- Federman, P., S. Pittel, and R. Campos, 1979, *Phys. Lett.* **82B**, 9.
- Feng, D. H., R. Gilmore, and S. R. Deans, 1981, *Phys. Rev. C* **23**, 1254.
- Fetea, M., *et al.*, 2006, *Phys. Rev. C* **73**, 051301(R).
- Fisher, M. E., and A. N. Berker, 1982, *Phys. Rev. B* **26**, 2507.
- Fleming, D. G., *et al.*, 1971, *Phys. Rev. Lett.* **27**, 1235.
- Fleming, D. G., *et al.*, 1973, *Phys. Rev. C* **8**, 806.
- Fortunato, L., 2004, *Phys. Rev. C* **70**, 011302(R).
- Fortunato, L., 2005, *Eur. Phys. J. A* **26**, 1.
- Fortunato, L., S. De Baerdemacker, and K. L. G. Heyde, 2006, *Phys. Rev. C* **74**, 014310.
- Fortunato, L., and A. Vitturi, 2004, *J. Phys. G* **30**, 627.
- Fossion, R., C. E. Alonso, J. M. Arias, L. Fortunato, and A. Vitturi, 2007, *Phys. Rev. C* **76**, 014316.
- Fossion, R., D. Bonatsos, and G. A. Lalazissis, 2006, *Phys. Rev. C* **73**, 044310.
- Fossion, R., C. De Coster, J. E. García-Ramos, T. Werner, and K. L. G. Heyde, 2002, *Nucl. Phys. A* **697**, 703.
- Frank, A., 1989, *Phys. Rev. C* **39**, 652.
- Frank, A., C. E. Alonso, and J. M. Arias, 2001, *Phys. Rev. C* **65**, 014301.
- Frank, A., and P. Van Isacker, 1994, *Algebraic Methods in Molecular & Nuclear Structure Physics* (Wiley, New York).
- Frank, A., P. Van Isacker, and F. Iachello, 2006, *Phys. Rev. C* **73**, 061302(R).
- Frank, A., P. Van Isacker, and C. E. Vargas, 2004, *Phys. Rev. C* **69**, 034323.
- García-Ramos, J. E., and J. M. Arias, 2008, *Phys. Rev. C* **77**, 054307.
- García-Ramos, J. E., J. M. Arias, J. Barea, and A. Frank, 2003, *Phys. Rev. C* **68**, 024307.
- García-Ramos, J. E., C. De Coster, R. Fossion, and K. L. G. Heyde, 2001, *Nucl. Phys. A* **688**, 735.
- García-Ramos, J. E., J. Dukelsky, and J. M. Arias, 2005, *Phys. Rev. C* **72**, 037301.

- García-Ramos, J. E., K. L. G. Heyde, R. Fossion, V. Hellemans, and S. De Baerdemacker, 2005, *Eur. Phys. J. A* **26**, 221.
- Garrett, P. E., *et al.*, 2009, *Phys. Rev. Lett.* **103**, 062501.
- Geyer, H. B., and S. Y. Lee, 1982, *Phys. Rev. C* **26**, 642.
- Gilmore, R., 1979, *J. Math. Phys.* **20**, 891.
- Gilmore, R., 1981, *Catastrophe Theory for Scientists and Engineers* (Wiley, New York).
- Gilmore, R., and D. H. Feng, 1978, *Nucl. Phys. A* **301**, 189.
- Ginocchio, J. N., 1980, *Ann. Phys. (N.Y.)* **126**, 234.
- Ginocchio, J. N., and M. W. Kirson, 1980a, *Phys. Rev. Lett.* **44**, 1744.
- Ginocchio, J. N., and M. W. Kirson, 1980b, *Nucl. Phys. A* **350**, 31.
- Gneuss, G., U. Mosel, and W. Greiner, 1969, *Phys. Lett.* **30B**, 397.
- Grossmann, S. and W. Rosenhauer, 1967, *Z. Phys.* **207**, 138.
- Harder, M. K., and K. T. Tang, 1996, *Phys. Lett. B* **369**, 1.
- Hatch, R. L., and S. Levit, 1982, *Phys. Rev. C* **25**, 614.
- Haxel, O., J. H. D. Jensen, and H. E. Suess, 1950, *Z. Phys.* **128**, 295.
- Heinze, S., P. Cejnar, J. Jolie, and M. Macek, 2006, *Phys. Rev. C* **73**, 014306.
- Heiss, W. D., 1988, *Z. Phys. A* **329**, 133.
- Heiss, W. D., and A. L. Sannino, 1991, *Phys. Rev. A* **43**, 4159.
- Heiss, W. D., F. G. Scholtz, and H. B. Geyer, 2005, *J. Phys. A* **38**, 1843.
- Hellemans, V., P. Van Isacker, S. De Baerdemacker, and K. L. G. Heyde, 2007, *Nucl. Phys. A* **789**, 164.
- Hellemans, V., P. Van Isacker, S. De Baerdemacker, and K. L. G. Heyde, 2009, *Nucl. Phys. A* **819**, 11.
- Hertz, J., 1976, *Phys. Rev. B* **14**, 1165.
- Heyde, K. L. G., 1989, *Int. J. Mod. Phys. A* **4**, 2063.
- Heyde, K. L. G., 2004, *Basic Ideas and Concepts in Nuclear Physics: An Introductory Approach* (Taylor & Francis, Bristol).
- Heyde, K. L. G., J. Jolie, R. Fossion, S. De Baerdemacker, and V. Hellemans, 2004, *Phys. Rev. C* **69**, 054304.
- Heyde, K. L. G., P. Van Isacker, R. F. Casten, and J. L. Wood, 1985, *Phys. Lett.* **155B**, 303.
- Heyde, K. L. G., P. Van Isacker, M. Waroquier, J. L. Wood, and R. A. Meyer, 1983, *Phys. Rep.* **102**, 291.
- Hinds, S., *et al.*, 1965, *Phys. Lett.* **14B**, 48.
- Hutter, C., *et al.*, 2003, *Phys. Rev. C* **67**, 054315.
- Iachello, F., 1979, in *Group Theoretical Methods in Physics*, edited by A. Bohm *et al.* (Springer, Berlin).
- Iachello, F., 2000, *Phys. Rev. Lett.* **85**, 3580.
- Iachello, F., 2001, *Phys. Rev. Lett.* **87**, 052502.
- Iachello, F., 2003, *Phys. Rev. Lett.* **91**, 132502.
- Iachello, F., 2005, *Phys. Rev. Lett.* **95**, 052503.
- Iachello, F., 2006, *Lie Algebras and Applications*, Lecture Notes in Physics Vol. 708 (Springer, Berlin).
- Iachello, F., and A. Arima, 1987, *The Interacting Boson Model* (Cambridge University Press, Cambridge, U.K.).
- Iachello, F., and R. D. Levine, 1995, *Algebraic Theory of Molecules* (Oxford University Press, Oxford).
- Iachello, F., and S. Oss, 1996, *J. Chem. Phys.* **104**, 6956.
- Iachello, F., and F. Pérez-Bernal, 2008, *Mol. Phys.* **106**, 223.
- Iachello, F., and O. Scholten, 1979, *Phys. Rev. Lett.* **43**, 679.
- Iachello, F., and P. Van Isacker, 1991, *The Interacting Boson Fermion Model* (Cambridge University Press, Cambridge, U.K.).
- Iachello, F., and N. V. Zamfir, 2004, *Phys. Rev. Lett.* **92**, 212501.
- Iachello, F., N. V. Zamfir, and R. F. Casten, 1998, *Phys. Rev. Lett.* **81**, 1191.
- Ising, E., 1925, *Z. Phys.* **31**, 253.
- Jahn, H. A., and E. Teller, 1937, *Proc. R. Soc. London, Ser. A* **161**, 220.
- Janssen, D., R. V. Jolos, and F. Dönau, 1974, *Nucl. Phys. A* **224**, 93.
- Janssens, R. V. F., 2005, *Nature (London)* **435**, 897.
- Johnson, C. W., G. F. Bertsch, and D. J. Dean, 1998, *Phys. Rev. Lett.* **80**, 2749.
- Jolie, J., R. F. Casten, P. Cejnar, S. Heinze, E. A. McCutchan, and N. V. Zamfir, 2004, *Phys. Rev. Lett.* **93**, 132501.
- Jolie, J., R. F. Casten, P. von Brentano, and V. Werner, 2001, *Phys. Rev. Lett.* **87**, 162501.
- Jolie, J., P. Cejnar, R. F. Casten, S. Heinze, A. Linnemann, and V. Werner, 2002, *Phys. Rev. Lett.* **89**, 182502.
- Jolie, J., P. Cejnar, and J. Dobeš, 1999, *Phys. Rev. C* **60**, 061303(R).
- Jolie, J., S. Heinze, P. Van Isacker, and R. F. Casten, 2004, *Phys. Rev. C* **70**, 011305(R).
- Jolie, J., and A. Linnemann, 2003, *Phys. Rev. C* **68**, 031301.
- Jolos, R. V., 2004a, *Phys. At. Nucl.* **67**, 931.
- Jolos, R. V., 2004b, *Phys. Part. Nucl.* **35**, 225.
- Jolos, R. V., and P. von Brentano, 2009, *Phys. Rev. C* **80**, 034308.
- Kato, T., 1966, *Perturbation Theory of Linear Operators* (Springer, New York).
- Kim, G. K., and C. M. Vincent, 1987, *Phys. Rev. C* **35**, 1517.
- Kirson, M. W., 2004, *Phys. Rev. C* **70**, 049801.
- Klein, A., C.-T. Li, and M. Vallieres, 1982, *Phys. Rev. C* **25**, 2733.
- Klein, A., and E. R. Marshalek, 1991, *Rev. Mod. Phys.* **63**, 375.
- Klug, T., A. Dewald, P. von Brentano, and R. F. Casten, 2000, *Phys. Lett. B* **495**, 55.
- Krücken, R., *et al.*, 2002, *Phys. Rev. Lett.* **88**, 232501.
- Kulp, W. D., J. L. Wood, K. S. Krane, J. Loats, P. Schmelzenbach, C. J. Stapels, R.-M. Larimer, and E. B. Norman, 2003, *Phys. Rev. Lett.* **91**, 102501.
- Kulp, W. D., J. L. Wood, K. S. Krane, J. Loats, P. Schmelzenbach, C. J. Stapels, R.-M. Larimer, and E. B. Norman, 2004, *Phys. Rev. C* **69**, 064309.
- Kulp, W. D., *et al.*, 2005, *Phys. Rev. C* **71**, 041303.
- Kulp, W. D., *et al.*, 2007, *Phys. Rev. C* **76**, 034319.
- Kulp, W. D., *et al.*, 2008, *Phys. Rev. C* **77**, 061301.
- Kumar, K., 1974, *Nucl. Phys. A* **231**, 189.
- Kusnezov, D., 1997, *Phys. Rev. Lett.* **79**, 537.
- Kuyucak, S., and I. Morrison, 1988, *Ann. Phys. (N.Y.)* **181**, 79.
- Landau, L., 1937, *Phys. Z. Sowjetunion* **11**, 545; reprinted in 1965, *Collected Papers of L. D. Landau* (Pergamon, Oxford), p. 193.
- Laubacher, D. B., Y. Tanaka, R. M. Steffen, E. B. Shera, and M. V. Hoehn, 1983, *Phys. Rev. C* **27**, 1772.
- Lehmann, H., J. Jolie, C. De Coster, K. L. G. Heyde, B. Decroix, and J. L. Wood, 1997, *Nucl. Phys. A* **621**, 767.
- Leviatan, A., 1987, *Nonlinear Anal. Theory, Methods Appl.* **179**, 201.
- Leviatan, A., 1996, *Phys. Rev. Lett.* **77**, 818.
- Leviatan, A., 2005, *Phys. Rev. C* **72**, 031305(R).
- Leviatan, A., 2006, *Phys. Rev. C* **74**, 051301(R).
- Leviatan, A., 2007, *Phys. Rev. Lett.* **98**, 242502.
- Leviatan, A., and J. N. Ginocchio, 2003, *Phys. Rev. Lett.* **90**, 212501.
- Levit, S., and Y. Alhassid, 1984, *Nucl. Phys. A* **413**, 439.
- Leyvraz, F., and W. D. Heiss, 2005, *Phys. Rev. Lett.* **95**, 050402.

- Li, Z. P., T. Nikšić, D. Vretenar, J. Meng, G. A. Lalazissis, and P. Ring, 2009, *Phys. Rev. C* **79**, 054301.
- Lievens, P., *et al.*, 1991, *Phys. Lett. B* **256**, 141.
- Lipas, P. O., P. Toivonen, and D. D. Warner, 1985, *Phys. Lett.* **155B**, 295.
- Lipkin, H. J., N. Meshkov, and A. J. Glick, 1965, *Nucl. Phys.* **62**, 188.
- Liu, M. L., 2007, *Phys. Rev. C* **76**, 054304.
- López-Moreno, E., and O. Castaños, 1996, *Phys. Rev. C* **54**, 2374.
- Macek, M., P. Cejnar, J. Jolie, and S. Heinze, 2006, *Phys. Rev. C* **73**, 014307.
- Macek, M., J. Dobeš, and P. Cejnar, 2009, *Phys. Rev. C* **80**, 014319.
- Macek, M., P. Stránský, P. Cejnar, S. Heinze, J. Jolie, and J. Dobeš, 2007, *Phys. Rev. C* **75**, 064318.
- Marginean, N., *et al.*, 2006, *Phys. Lett. B* **633**, 696.
- Marshalek, E. R., 2006, *Phys. Rev. C* **74**, 044307.
- Maxwell, J. R., G. M. Reynolds, and N. M. Hintz, 1966, *Phys. Rev.* **151**, 1000.
- Mayer, M. G., 1950, *Phys. Rev.* **78**, 16.
- McCutchan, E. A., D. Bonatsos, and N. V. Zamfir, 2006, *Phys. Rev. C* **74**, 034306.
- McCutchan, E. A., R. F. Casten, 2006, *Phys. Rev. C* **74**, 057302.
- McCutchan, E. A., R. F. Casten, and N. V. Zamfir, 2005, *Phys. Rev. C* **71**, 061301(R).
- McCutchan, E. A., N. V. Zamfir, 2005, *Phys. Rev. C* **71**, 054306.
- McCutchan, E. A., N. V. Zamfir, R. F. Casten, 2004, *Phys. Rev. C* **69**, 064306.
- McCutchan, E. A., N. V. Zamfir, and R. F. Casten, 2005, *Phys. Rev. C* **71**, 034309.
- McCutchan, E. A. *et al.*, 2004, *Phys. Rev. C* **69**, 024308.
- McCutchan, E. A., *et al.*, 2006, *Phys. Rev. C* **73**, 034303.
- McCutchan, E. A., *et al.*, 2009, private communication.
- Meng, J., W. Zhang, S. G. Zhou, H. Toki, and L. S. Geng, 2005, *Eur. Phys. J. A* **25**, 23.
- Mertz, A. F., *et al.*, 2008, *Phys. Rev. C* **77**, 014307.
- Meyer, D. A., *et al.*, 2006, *Phys. Lett. B* **638**, 44.
- Mihai, C., *et al.*, 2007, *Phys. Rev. C* **75**, 044302.
- Möller, O., *et al.*, 2006, *Phys. Rev. C* **74**, 024313.
- Morales, I. O., A. Frank, C. E. Vargas, and P. Van Isacker, 2008, *Phys. Rev. C* **78**, 024303.
- Navrátil, P., S. Quaglioni, I. Stetcu, and B. R. Barrett, 2009, *J. Phys. G* **36**, 083101.
- Nazarewicz, W., 1992, *Prog. Part. Nucl. Phys.* **28**, 307.
- Nazarewicz, W., 1993, *Phys. Lett. B* **305**, 195.
- Nazarewicz, W., 1994, *Nucl. Phys. A* **574**, 27c.
- Neergaard, K., and P. Vogel, 1970, *Nucl. Phys. A* **145**, 33.
- Neidherr, D., *et al.*, 2009a, *Phys. Rev. Lett.* **102**, 112501.
- Neidherr, D., *et al.*, 2009b, *Phys. Rev. C* **80**, 044323.
- Neuneyer, U., *et al.*, 1996, *Nucl. Phys. A* **607**, 299.
- Nikšić, T., Z. P. Li, D. Vretenar, L. Próchniak, J. Meng, and P. Ring, 2009, *Phys. Rev. C* **79**, 034303.
- Nikšić, T., D. Vretenar, G. A. Lalazissis, and P. Ring, 2007, *Phys. Rev. Lett.* **99**, 092502.
- Nilsson, S. G., and I. Ragnarsson, 1995, *Shapes and Shells in Nuclear Structure* (Cambridge University Press, Cambridge).
- Noack, C. C., 1968, *Nucl. Phys. A* **108**, 493.
- Nomura, K., N. Shimizu, and T. Otsuka, 2008, *Phys. Rev. Lett.* **101**, 142501.
- Omnès, R., 1992, *Rev. Mod. Phys.* **64**, 339.
- Othoudt, M. A., and N. M. Hintz, 1973, *Nucl. Phys. A* **213**, 221.
- Otsuka, T., A. Arima, and F. Iachello, 1978, *Nucl. Phys. A* **309**, 1.
- Pan, F., J. P. Draayer, and Y. Luo, 2003, *Phys. Lett. B* **576**, 297.
- Pan, F., T. Wang, Y.-S. Huo, and J. P. Draayer, 2008, *J. Phys. G* **35**, 125105.
- Pan, F., Y. Zhang, J. P. Draayer, 2005, *J. Phys. G* **31**, 1039.
- Pan, F., Y. Zhang, S. Jin, J. P. Draayer, M. L. Ge, and J. L. Birman, 2005, *Phys. Lett. A* **341**, 291.
- Pérez-Bernal, F., and F. Iachello, 2008, *Phys. Rev. A* **77**, 032115.
- Pérez-Fernández, P., A. Relaño, J. M. Arias, J. Dukelsky, and J. E. García-Ramos, 2009, *Phys. Rev. A* **80**, 032111.
- Pieper, S. C., K. Varga, and R. B. Wiringa, 2002, *Phys. Rev. C* **66**, 044310.
- Pietralla, N., and O. M. Gorbachenko, 2004, *Phys. Rev. C* **70**, 011304(R).
- Regan, P. H. *et al.*, 2003, *Phys. Rev. Lett.* **90**, 152502.
- Reinhard, P.-G., D. J. Dean, W. Nazarewicz, J. Dobaczewski, J. A. Maruhn, and M. R. Strayer, 1999, *Phys. Rev. C* **60**, 014316.
- Reinhard, P.-G., and E. W. Otten, 1984, *Nucl. Phys. A* **420**, 173.
- Relaño, A., J. M. Arias, J. Dukelsky, J. E. García-Ramos, and P. Pérez-Fernández, 2008, *Phys. Rev. A* **78**, 060102(R).
- Robledo, L. M., R. R. Rodríguez-Guzmán, and P. Sarriguren, 2008, *Phys. Rev. C* **78**, 034314.
- Rodríguez, T. R., and J. L. Egido, 2008, *Phys. Lett. B* **663**, 49.
- Rohozinski, S. G., 1988, *Rep. Prog. Phys.* **51**, 541.
- Rosensteel, G., and D. J. Rowe, 2005, *Nucl. Phys. A* **759**, 92.
- Rowe, D. J., 2004a, *Phys. Rev. Lett.* **93**, 122502.
- Rowe, D. J., 2004b, *Nucl. Phys. A* **735**, 372.
- Rowe, D. J., 2004c, *Nucl. Phys. A* **745**, 47.
- Rowe, D. J., 2005, *J. Phys. A* **38**, 10181.
- Rowe, D. J., and C. Bahri, 1998, *J. Phys. A* **31**, 4947.
- Rowe, D. J., C. Bahri, and W. Wijesundera, 1998, *Phys. Rev. Lett.* **80**, 4394.
- Rowe, D. J., P. Rochford, and J. Repka, 1988, *J. Math. Phys.* **29**, 572.
- Rowe, D. J., and P. S. Turner, 2005, *Nucl. Phys. A* **753**, 94.
- Rowe, D. J., P. S. Turner, and G. Rosensteel, 2004, *Phys. Rev. Lett.* **93**, 232502.
- Rowe, D. J., T. A. Welsh, and M. A. Caprio, 2009, *Phys. Rev. C* **79**, 054304.
- Sachdev, S., 1999, *Quantum Phase Transitions* (Cambridge University Press, Cambridge, U.K.).
- Schaaser, H., and D. M. Brink, 1984, *Phys. Lett.* **143**, 269.
- Schaaser, H., and D. M. Brink, 1986, *Nucl. Phys. A* **452**, 1.
- Scholten, O., F. Iachello, and A. Arima, 1978, *Ann. Phys. (N.Y.)* **115**, 325.
- Scott, S. M., D. D. Warner, W. D. Hamilton, G. Jung, K. D. Wunsch, and B. Pfeiffer, 1979, *J. Phys. G* **5**, L187.
- Sheng, Z. Q., and J. Y. Guo, 2005, *Mod. Phys. Lett. A* **20**, 2711.
- Shimizu, N., T. Otsuka, T. Mizusaki, and M. Honma, 2001, *Phys. Rev. Lett.* **86**, 1171.
- Shirokov, A. M., N. A. Smirnova, and Yu. F. Smirnov, 1998, *Phys. Lett. B* **434**, 237.
- Smirnova, N. A., P.-H. Heenen, and G. Neyens, 2003, *Phys. Lett. B* **569**, 151.
- Sorgunlu, B., and P. Van Isacker, 2008, *Nucl. Phys. A* **808**, 27.
- Stachel, J., P. Van Isacker, and K. L. G. Heyde, 1982, *Phys. Rev. C* **25**, 650.
- Stewart, I., 1982, *Rep. Prog. Phys.* **45**, 185.
- Stoitsov, M. V., R. B. Cakirli, R. F. Casten, W. Nazarewicz, and W. Satula, 2007, *Phys. Rev. Lett.* **98**, 132502.
- Stoitsov, M. V., J. Dobaczewski, W. Nazarewicz, S. Pittel, and

- D. J. Dean, 2003, *Phys. Rev. C* **68**, 054312.
- Stránský, P., P. Hruška, and P. Cejnar, 2009a, *Phys. Rev. E* **79**, 046202.
- Stránský, P., P. Hruška, and P. Cejnar, 2009b, *Phys. Rev. E* **79**, 066201.
- Talmi, I., 1962, *Rev. Mod. Phys.* **34**, 704.
- Thiamova, G., and P. Cejnar, 2006, *Nucl. Phys. A* **765**, 97.
- Thouless, D. J., 1960, *Nucl. Phys.* **21**, 225.
- Thouless, D. J., 1961, *Nucl. Phys.* **22**, 78.
- Tonev, D., *et al.*, 2004, *Phys. Rev. C* **69**, 034334.
- Turner, P. S., and D. J. Rowe, 2005, *Nucl. Phys. A* **756**, 333.
- Van Isacker, P., 1999, *Phys. Rev. Lett.* **83**, 4269.
- Van Isacker, P., A. Bouldjedri, and S. Zerguine, 2010, *Nucl. Phys. A* **836**, 225.
- Van Isacker, P., and J. Q. Chen, 1981, *Phys. Rev. C* **24**, 684.
- Van Isacker, P., A. Frank, and J. Dukelsky, 1985, *Phys. Rev. C* **31**, 671.
- Van Roosmalen, O. S., 1982, Ph.D. thesis (Rijksuniversiteit Groningen).
- Vidal, J., J. M. Arias, J. Dukelsky, and J. E. García-Ramos, 2006, *Phys. Rev. C* **73**, 054305.
- Vojta M., 2003, *Rep. Prog. Phys.* **66**, 2069.
- von Brentano, P., V. Werner, R. F. Casten, C. Scholl, E. A. McCutchan, R. Krücken, and J. Jolie, 2004, *Phys. Rev. Lett.* **93**, 152502.
- von Neumann, J., and E. Wigner, 1929, *Phys. Z.* **30**, 467.
- Vorov, O. K., and V. G. Zelevinsky, 1985, *Nucl. Phys. A* **439**, 207.
- Warner, D. D., and R. F. Casten, 1982, *Phys. Rev. Lett.* **48**, 1385.
- Werner, T. R., J. Dobaczewski, M. V. Guidry, W. Nazarewicz, and J. A. Sheikh, 1994, *Nucl. Phys. A* **578**, 1.
- Werner, V., N. Pietralla, P. von Brentano, R. F. Casten, and R. V. Jolos, 2000, *Phys. Rev. C* **61**, 021301(R).
- Werner, V., P. von Brentano, R. F. Casten, and J. Jolie, 2002, *Phys. Lett. B* **527**, 55.
- Werner, V., E. Williams, R. J. Casperson, R. F. Casten, C. Scholl, and P. von Brentano, 2008, *Phys. Rev. C* **78**, 051303(R).
- Whelan, N., and Y. Alhassid, 1993, *Nucl. Phys. A* **556**, 42.
- Wilets, J., and M. Jean, 1956, *Phys. Rev.* **102**, 788.
- Wilets, L., D. L. Hill, and K. W. Ford, 1953, *Phys. Rev.* **91**, 1488.
- Williams, E., R. J. Casperson, and V. Werner, 2008, *Phys. Rev. C* **77**, 061302(R).
- Wimmer, K., *et al.*, 2009, in *Capture Gamma-Ray Spectroscopy and Related Topics*, edited by A. Blazhev, J. Jolie, N. Warr, and A. Zilges, AIP Conf. Proc. No. 1090 (AIP, Melville, NY), p. 539.
- Wood, J. L., W. D. Kulp, K. S. Krane, J. Loats, P. Schmelzenbach, C. J. Stapels, R.-M. Larimer, and E. B. Norman, 2002, *Bull. Am. Phys. Soc.* **47**, 81.
- Wood, J. L., E. F. Zganjar, C. De Coster, and K. L. G. Heyde, 1999, *Nucl. Phys. A* **651**, 323.
- Wu, C.-L., D. H. Feng, X.-G. Chen, J.-Q. Chen, and M. V. Guidry, 1986, *Phys. Lett.* **168B**, 313.
- Yang, C. N., and T. D. Lee, 1952, *Phys. Rev.* **87**, 410.
- Yu, M., P. F. Zhang, T. N. Ruan, and J. Y. Guo, 2006, *Int. J. Mod. Phys. E* **15**, 939.
- Zamfir, N. V., P. von Brentano, R. F. Casten, and J. Jolie, 2002, *Phys. Rev. C* **66**, 021304(R).
- Zamfir, N. V., *et al.*, 1999, *Phys. Rev. C* **60**, 054312.
- Zamfir, N. V., *et al.*, 2002a, *Phys. Rev. C* **65**, 044325.
- Zamfir, N. V., *et al.*, 2002b, *Phys. Rev. C* **65**, 067305.
- Zhang, D., and Y. Liu, 2002, *Phys. Rev. C* **65**, 057301.
- Zhang, D., and Y. Liu, 2003, *Chin. Phys. Lett.* **20**, 1028.
- Zhang, J., G. Long, Y. Sun, S. Zhu, F. Liu, and Y. Jia, 2003, *Chin. Phys. Lett.* **20**, 1231.
- Zhang, J.-y., M. A. Caprio, N. V. Zamfir, and R. F. Casten, 1999, *Phys. Rev. C* **60**, 061304.
- Zhang, J.-y., R. F. Casten, and N. V. Zamfir, 1997, *Phys. Lett. B* **407**, 201.
- Zhang, W.-M., D. H. Feng, and R. Gilmore, 1990, *Rev. Mod. Phys.* **62**, 867.
- Zhang, W.-M., D. H. Feng, and J. N. Ginocchio, 1988, *Phys. Rev. C* **37**, 1281.
- Zhang, W.-M., C.-L. Wu, D. H. Feng, J. N. Ginocchio, and M. V. Guidry, 1988, *Phys. Rev. C* **38**, 1475.
- Zhang, Y., Z. F. Hou, and Y. X. Liu, 2007, *Phys. Rev. C* **76**, 011305(R).
- Zirnbauer, M. R., J. J. M. Verbaaschot, and H. A. Weidenmüller, 1983, *Nucl. Phys. A* **411**, 161.